CHARACTERIZATION OF SPECIATED ATMOSPHERIC MERCURY CONCENTRATION MEASUREMENTS IN NORTHERN UTAH

by

Melissa May Maestas

A thesis submitted to the faculty of
The University of Utah
in partial fulfillment of the requirements for the degree of

Master of Science

Department of Atmospheric Sciences

The University of Utah

December 2011

The University of Utah Graduate School

STATEMENT OF THESIS APPROVAL

The thesis of **Melissa May Maestas**

has been approved by the following supervisory committee members:

Kevin Perry	, Chair	**10/03/2011** Date Approved
John Horel	, Member	**10/03/2011** Date Approved
JoAnn Lighty	, Member	**10/03/2011** Date Approved

and by **Kevin Perry** , Chair of

the Department of **Atmospheric Sciences**

and by Charles A. Wight, Dean of The Graduate School.

ABSTRACT

Two years of speciated atmospheric mercury data in the Intermountain West are examined for annual, seasonal, and diurnal patterns, as well as influences of precipitation. Mercury is a pollutant in the atmosphere that occurs as three species: gaseous elemental mercury (GEM), particulate-bound mercury (PBM), and gaseous oxidized mercury (GOM). Mercury can enter ecosystems from the atmosphere via wet and dry deposition. In aquatic ecosystems, it can convert to the neurotoxin methylmercury, which has prompted consumption advisories for both fish and waterfowl. A Tekran ambient air mercury monitor was deployed at a site (UT96) near the Great Salt Lake, Utah as part of the Atmospheric Mercury Network (AMNet). UT96 has the only such detector in continuous operation in Utah with two years of data (July 2009 - June 2011).

All three mercury species exhibit right-skewed distributions and vary in concentration over multiple orders of magnitude. GEM is the dominant species with a median concentration of 1.58 ng m^{-3} (range 0.25 - 64.47 ng m^{-3}). PBM has a median concentration of 5.7 pg m^{-3} (range 0 - 803.2 pg m^{-3}), while GOM has a median concentration of 2.6 pg m^{-3} (range 0 - 225.6 pg m^{-3}). The sporadic nature of the extremely high GEM and PBM events suggest that they primarily result from local/regional emissions. In contrast, extremely high GOM events depend strongly on time of day and season, suggesting a connection to meteorological conditions.

All three species exhibit statistically significant seasonal and diurnal patterns. GOM exhibits the strongest seasonal pattern, peaking during summer with median summer concentrations a factor of six greater than median winter concentrations. GEM and PBM peak during winter. All three species exhibit statistically significant diurnal patterns for at least

part of the year. GOM has the most pronounced diurnal cycle, particularly during summer. Median concentrations of GOM during the afternoons of summer months are greater than 20 pg m^{-3}, while median concentrations overnight are below 5 pg m^{-3}. GEM and PBM both exhibit minima in concentrations during the afternoons, and both exhibit the largest diurnal variation amplitude during summer. Neither GEM nor PBM exhibit a statistically significant diurnal pattern during winter.

An examination of the influences of precipitation on mercury concentrations indicates that precipitation scavenges GOM more efficiently than PBM, and that the scavenging increases as the amount of precipitation increases. Mixed precipitation scavenges PBM better than either rain or snow alone. The median GOM concentration during rain, snow, and mixed precipitation were all below the method detection limit (MDL), and could not be distinguished. There are some indications in the data that rain may promote slightly elevated concentrations of GEM.

TABLE OF CONTENTS

ACKNOWLEDGMENTS

I would like to thank my advisor Dr. Kevin Perry for his insight into mercury dynamics and for his guidance and patience through the writing process. I would like to thank the members of my thesis committee, Dr. John Horel and Dr. JoAnn Lighty for their insights and assistance in writing and editing of this thesis. I would like to thank Dr. Mark Olson for his advise on the Tekran equipment. I would like to acknowledge Tekran Instruments for providing a schematic of the Tekran system as well as the plot of impactor cut point vs. actual flow rate. I would also like to acknowledge MesoWest and the Utah Division of Air Quality for providing meteorological data. I would like to thank the Center for High Performance Computing at the University of Utah for providing computer support. I would like to thank Brad O'Brien and Sheena Mugavin of the University of Utah Writing Center for their assistance in the editing process. I would like to thank Joel Lisonbee for creating the majority of the quality assurance code. I would like to thank my friends throughout the Department of Atmospheric Sciences for making graduate school in general, and the lunch hour in particular, a pleasure. I would especially like to thank Clint Schmidt for his seemingly endless patience and encouragement.

This research was funded through a grant from the Environmental Protection Agency.

CHAPTER 1

INTRODUCTION

In 1997, the U.S. Environmental Protection Agency (EPA) provided evidence of a "plausible link between anthropogenic releases of mercury [Hg] from industrial and combustion sources in the United States and methylmercury in fish" (EPA, 1997a). "Human exposure to monomethylmercury (MMHg) through the consumption of freshwater and marine fish is the principal public health concern with Hg in the environment" (Fitzgerald et al., 1998). Understanding mercury deposition is important because "Elevated levels of mercury in aquatic environments remote from industrial sources have been broadly attributed to long-range atmospheric transport and deposition of anthropogenic Hg" (Fitzgerald et al., 1998). Mercury in aquatic ecosystems, including wetland areas, can convert into the neurotoxin methylmercury, which is hazardous to both humans and wildlife (EPA, 1997a,d; Furl et al., 2010). Methylmercury also accumulates in the food chain by more than a million-fold (Schroeder and Munthe, 1998). Mercury contamination in lakes and rivers has prompted all states in the U.S. to issue fish consumption advisories (EPA, 2011a). Furthermore, Utah was the first state to issue waterfowl consumption advisories due to mercury contamination (UDEQ, 2009). In addition to affecting aquatic ecosystems, plants can accumulate mercury during the growing season (Ericksen et al., 2003).

In this chapter, properties of the three dominant species of atmospheric mercury will be introduced, including characteristics such as water solubility and atmospheric lifetime (Section 1.1). Sources, conversions, and sinks of atmospheric mercury will be discussed in Section 1.2. Observed concentrations and seasonality at various locations will be described

in Section 1.3. Finally, the objectives of this thesis are described in Section 1.4.

1.1 Properties of Atmospheric Mercury

The three primary species of atmospheric mercury are gaseous elemental mercury (GEM), particulate-bound mercury (PBM), and gaseous oxidized mercury (GOM). GOM is also commonly referred to as reactive gaseous mercury (RGM) (e.g., Lindberg et al., 2007; Abbott et al., 2008; Liu et al., 2010). GEM constituted more than 98% of total atmospheric mercury (TAM) during a year-long study of speciated atmospheric mercury in Canada (Poissant et al., 2005).

1.1.1 Properties of GEM

GEM is highly volatile with low water solubility and consequently is removed relatively slowly from the atmosphere via wet and dry deposition (Lindberg et al., 2007; Fain et al., 2009; Liu et al., 2010). GEM can react with ozone (O_3), the hydroxyl radical (OH), bromine (Br), hypobromite (BrO), and chlorine (Cl_2). Some of these reactions can occur relatively rapidly in a laboratory setting, but it is unclear how quickly such reactions proceed in the ambient atmosphere (Lindberg et al., 2007).

The atmospheric lifetime of GEM is not a fixed value because it can vary significantly by season, latitude, and the ambient concentration of atmospheric oxidants (Lindberg et al., 2007). Estimates of the atmospheric lifetime of GEM, however, range between 0.5 to 2 years (Sakata and Asakura, 2007; Fain et al., 2009). Because GEM can stay in the atmosphere so long, it is subject to both regional and global transport (Liu et al., 2010). The atmospheric lifetime of GEM is thought to be much shorter in polar regions, marine boundary layers, and the upper troposphere (Lindberg et al., 2007). The lifetime of GEM in the marine boundary layer is thought to be about ten days under typical summer conditions on the basis of model calculations (Sakata and Asakura, 2007). It has been suggested that in the marine boundary layer, GEM, sunlight, low temperatures, sea-salt halogens, and water-soluble particles combine to produce rapid oxidation of GEM and subsequent deposition to

the water surface (Lindberg et al., 2007).

GEM concentrations tend to be higher when PBM concentrations, relative humidity (RH), and dewpoint temperature are higher. Conversely, GEM concentrations tend to be lower when GOM concentrations, ozone, ambient temperature, solar radiation, and wind speed are higher (Weiss-Penzias et al., 2009). Little vertical gradient in GEM concentration has been observed in the lower troposphere (Swartzendruber et al., 2006).

1.1.2 Properties of PBM

PBM consists of mercury associated with airborne dust, soot, sea-salt aerosols, and ice crystals (Lu and Schroeder, 2004). The majority of PBM exists in the form of fine particles with aerodynamic diameters $\leq 2\mu\mathrm{m}$. Fine particulate matter can spread over a large spatial area due to its low gravitational settling velocity (Seinfeld, 1986). PBM has a typical lifetime less than ten days (Fain et al., 2009), but the lifetime is particle-size dependent (EPA, 1997c). Both GEM and GOM can adsorb to particulate matter where heterogeneous reactions can occur (Lindberg et al., 1999).

1.1.3 Properties of GOM

GOM is five orders of magnitude more water soluble than GEM, and is sequestered by rain or cloud droplets (Schroeder and Munthe, 1998; Lindberg et al., 2007). Concentrations of GOM are also strongly affected by relative humidity. Fain et al. (2009) found that the relationship of relative humidity to GOM was stronger than with either water vapor or temperature. High GOM concentrations were only observed at Storm Peak Laboratory, Colorado while RH < 50%, and Fain et al. (2009) concluded that a build up of high concentrations of GOM requires dry air. GOM may be scavenged by particles when RH > 50% due to increases in the total particle surface area (Fain et al., 2009). Abbott et al. (2008) and Liu et al. (2010) also observed an anti-correlation of GOM concentrations with RH. GOM concentrations have been observed to follow solar radiation, temperature, mixing height, and ozone (Lynam and Keeler, 2005; Abbott et al., 2008; Liu et al., 2010). Abbott

et al. (2008) observed pronounced summertime diurnal cycles of GOM that correlated with ozone concentrations, and suggested that photochemistry plays a role in the production of GOM.

GOM is removed from the atmosphere relatively quickly compared to GEM because of its high solubility and reactivity with surfaces (Lindberg et al., 2007; Liu et al., 2010). GOM is estimated to have a typical lifetime of 1-7 days, but some estimates are as long as 16 days (Fain et al., 2009). GOM may have of a lifetime of 16 days in the free troposphere (Selin et al., 2007). The most probable compounds comprising GOM are $\mathrm{HgCl_2}$ and $\mathrm{HgBr_2}$ (Schroeder and Munthe, 1998; Fain et al., 2009). However, the temporal and spatial variations are highly uncertain.

1.2 Sources, Conversions and Sinks of Atmospheric Mercury

"The dynamics for the three mercury species are very complex, suggesting that the source profiles are multi-factorial" (Lynam and Keeler, 2005). Mercury enters the atmosphere from both natural and anthropogenic sources. It has been suggested that perhaps one-third of the global atmospheric pool of mercury is from new point-source emissions, another third is from natural emissions from both land and ocean, and the final third is Earth-surface recycling of anthropogenic mercury (Lindberg et al., 2007). Mercury can convert from one form to another while in the atmosphere. Conversion between types of mercury constitutes a source for one type of mercury while being a sink for another type. PBM and GOM concentrations in air depend on direct emissions from local and regional sources as well as in situ formation in the atmosphere (Sakata and Asakura, 2007). Finally, mercury can be removed from the atmosphere via dry deposition or scavenging by precipitation. Mercury deposition in rural areas is usually lower than in urban areas because local urban emissions are attenuated by deposition and dilution as the distance from the urban source increases (Guentzel et al., 2001).

1.2.1 Natural Sources

The average annual global natural mercury emissions to the atmosphere are estimated to be between 1.6 x 10^6 kg and 4.0 x 10^6 kg (Fitzgerald et al., 1998). The dominant natural sources of mercury include wildfires (Friedli et al., 2003), volcanoes and geothermal areas (Schuster et al., 2002; Engle et al., 2006), naturally enriched substrates (Engle et al., 2001), and the ocean (Mason and Sheu, 2002). Most natural mercury emissions are in the form of GEM (Gustin et al., 2000; Engle et al., 2001; Mason and Sheu, 2002).

Friedli et al. (2003) used a combination of laboratory and airborne measurements to determine that both plant material and surface soils emit mercury during wildfires, primarily in the form of GEM. Generally, more than 90% of the mercury emitted was in the form of GEM, depending on the type of plant material. The rest of the mercury was in the form of PBM, while GOM concentrations were below detectable limits. Friedli et al. (2003) calculated an emission factor for the fire they observed to be 112$\pm$17 g Hg per kg of fuel (dry mass). Caldwell et al. (2006) observed a nearly 12-fold increase of PBM when an air mass influenced by a wildfire passed over their detector in south central New Mexico.

Volcanoes and geothermal areas are natural sources of mercury (Schuster et al., 2002; Engle et al., 2006). An ice core study in Wyoming concluded that >6% of atmospheric deposition of mercury over 270 years (ending in 1998) was due to volcanoes (Schuster et al., 2002). This is a lower bound estimate because it only includes the three largest volcanic eruptions to impact Wyoming over the 270 year period: Mount St. Helens, Krakatau, and Tambora. It is also possible that not all of the mercury deposited by the volcanoes stayed in the ice (elution processes). The mercury concentration of the volcanic plume of the Krakatau eruption was estimated to be 2.44 x 10^5 ng m^{-3} (Schuster et al., 2002), while the maximum observed concentration of the fumarole gas and steam from hot springs in Yellowstone is 3.0 x 10^4 ng m^{-3} (Engle et al., 2006). Typical ambient concentrations are < 3 ng m^{-3} (e.g. Fain et al., 2009; Weiss-Penzias et al., 2009; Liu et al., 2010).

"Naturally Hg-enriched substrate is found associated with plate tectonic boundaries;

areas of high crustal heat flow; precious and base metal mineralization; Hg mineralization; recent volcanism; and organic rich sedimentary rocks" (Rasmussen, 1994; Engle et al., 2001). Sources of mercury to soils also include atmospheric deposition and contamination from mining activities (Lindberg et al., 1999). Volatilization of soil mercury is an important contributor to the global mercury cycle (Lindberg et al., 1999). Soils enriched with mercury typically have concentrations of 10^0 to 10^2 μg g^{-1}, while background soils contain less than 0.5 μg g^{-1} (Lindberg et al., 1999).

There are several factors that influence volatilization of soil mercury. These factors include soil temperature, mercury speciation, humidity, solar radiation, soil moisture, and rainfall effects (Lindberg et al., 1999). Several forms of mercury in soil (particularly elemental mercury) exhibit relatively high elevated vapor pressures at ambient temperatures (Lindberg et al., 1999). The relationship between soil temperature and volatilization of soil mercury is exponential (Lindberg et al., 1999). Mercury emission from soil can be increased with increases in light and soil moisture, and elevated soil mercury concentrations can also contribute to elevated mercury emissions from soil (Engle et al., 2001). Mercury emissions from soil follow a diurnal pattern, with the highest emissions around noon (local time), with deposition at night (Engle et al., 2001). Increases in GEM flux have also been observed from relatively dry soils following simulated precipitation in a laboratory setting (Song and Heyst, 2005).

Soils in parts of Nevada have unusually high concentrations of mercury (Engle et al., 2001). The average flux from the Ivanhoe Mining District in north-central Nevada (586 km^2), for example, is 17.1 ng m^{-2} h^{-1} (Engle et al., 2001). The mercury in soils in Nevada is thought to be 30-50% elemental mercury (Lindberg et al., 1999). The Nevada soils that Lindberg et al. (1999) studied contained 1.4 to 4.7 μg g^{-1} mercury.

Lindberg et al. (1999) observed that atmospheric mercury concentrations inside flux chambers increased after both rain and irrigation with low-mercury distilled water compared to before-wet conditions. Prior to the rain event, the mercury concentrations inside

the flux chambers rose from 7.6 ± 9.3 ng m^{-3} prior to the rain to 31 ± 25 ng m^{-3} after the rain. It is important to note that the study was conducted over mercury-enriched soils in Nevada. That Lindberg et al. (1999) were able to observe the same effect via irrigation with low-mercury distilled water suggests the mercury is not coming from the precipitation water. Lindberg et al. (1999) suggest that the following mechanisms are the dominant causes for the increase in mercury emissions from the soil: 1) physical displacement of Hg-enriched soil gas by the percolating water, 2) exchange of elemental mercury adsorbed on dry soil particle surfaces with water molecules (essentially soil "sticks" to water better than mercury, so the soil releases mercury), and 3) desorption of GOM adsorbed on soil solid particle surfaces and its subsequent reduction. The increased emissions in the Nevada soil represent $\ll 0.1\%$ of the total mercury in the upper 2 cm of the soil. Lindberg et al. (1999) conducted similar lab studies on soils from Tennessee with similar results. Meanwhile, irrigating with methanol, which is less polar than water, did not increase mercury emissions.

In the global budget, the ocean is a sink for mercury. However, important exchanges of mercury occur between the ocean and atmosphere. Approximately 5.4 $\mu\mathrm{g}\ \mathrm{m}^{-2}\ \mathrm{yr}^{-1}$ of mercury are deposited to the ocean via wet deposition and dry deposition of PBM. The ocean emits ~7.2 $\mu\mathrm{g}\ \mathrm{m}^{-2}\ \mathrm{yr}^{-1}$ GEM, of which ~3.1 $\mu\mathrm{g}\ \mathrm{m}^{-2}\ \mathrm{yr}^{-1}$ are converted into GOM and dry deposited back to the ocean (Mason and Sheu, 2002).

1.2.2 Anthropogenic Sources

U.S. anthropogenic emissions of mercury have declined substantially in recent years, dropping from 220 tons in 1990 to 115 tons in 1999 (EPA, 2011b). High temperature waste and fossil fuel combustion are the most significant sources of anthropogenic mercury emissions (EPA, 1997b). Anthropogenic sources of atmospheric mercury include combustion, manufacturing, refineries, agricultural burning, mobile sources, utility coal boilers, industrial boilers, and both municipal and medical combustion (EPA, 1997b). Mercury is also a

common byproduct in gold mining operations (EPA, 1997b). It has even been noted that farming activities that disturb soil can resuspend PBM, increasing mercury emissions from the soil (Engle et al., 2001; Poissant et al., 2005).

Mason et al. (1997) concluded that PBM in the Chesapeake Bay area is predominantly coming from coal combustion because of its association with sulfur (S). Most of those particles are less than 1 μm in size with only 10% larger than 2.5 μm. Other co-pollutants with mercury include sulfur dioxide (SO_2), nitrous oxide (NO_x), and particulate matter ($PM_{2.5}$) (Liu et al., 2010).

The primary anthropogenic sources of RGM in southern Florida are municipal solid and medical waste incinerators, and are responsible for less than half of the RGM in the southern Florida airshed (2.5 ± 0.5 kg day^{-1}) with a combined PBM and RGM load of 2.6 to 4.0 kg day^{-1} (Guentzel et al., 2001).

Major sources of mercury in Japan are equipped with wet scrubbers that remove GOM but not GEM, so that only 5-17% of the total mercury emitted by coal- and oil-fired power plants is in the form of GOM (Sakata and Asakura, 2007). A mercury speciation study on the emissions from six coal-fired power plants in China found that between 66% and 94% of mercury emitted was in the form of GEM, depending on the composition of the coal used as well as the type of emissions control equipment used (Wang et al., 2010). Nearly all PBM can be removed with the use of certain emissions control equipment (e.g., electrostatic precipitators).

1.2.3 Conversions

Atmospheric mercury can convert from one form to another through oxidation and/or photochemistry, adsorption, and reduction (Fig. 1.1).

1.2.3.1 Oxidation/Photochemistry

Correlations of GOM with meteorological variables suggests the role of photochemistry in its production (Abbott et al., 2008). GEM can also be converted to GOM through

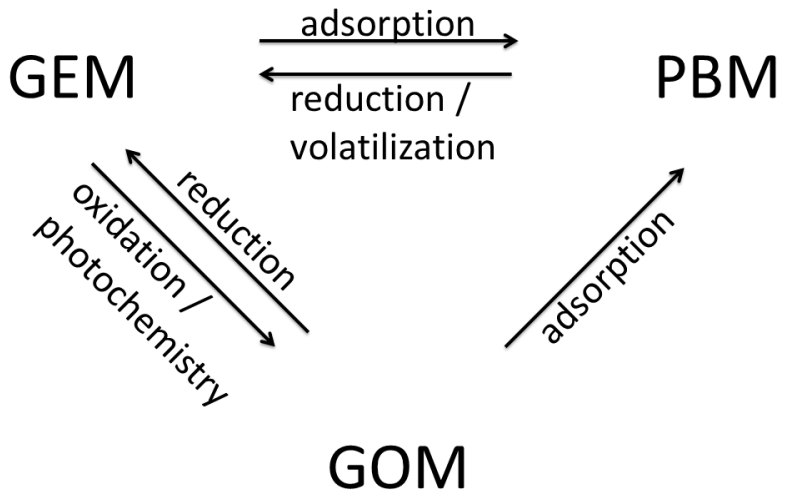

Figure 1.1: Schematic of conversions among atmospheric mercury species (based on references in Section 1.2.3).

oxidation by O_3 and OH radicals in gas and/or aqueous phases (Sakata and Asakura, 2007). Such reactions may involve O_3, the OH, H_2O_2, NO_3 and reactive halogens in both gaseous and aqueous phase, and the reactions may be photochemical in nature (Lin et al., 2006). The conversion of GEM to GOM via O_3 is thought to be slow (Poissant et al., 2005). This conversion is favored during warm seasons due to the higher air temperature, solar radiation intensity, and higher concentrations of atmospheric O_3 (Sakata and Asakura, 2007). Given a one-year residence time of GEM in the atmosphere, Guentzel et al. (2001) estimated a daily increase in GOM of 3-5 $\mathrm{pg\ m^{-3}}$ via O_3 oxidation if there is no precipitation. In situ oxidation of GEM to GOM may also be responsible for 8% of the daily RGM burden in the boundary layer in southern Florida Guentzel et al. (2001). Relatively low concentrations of GEM in the free troposphere are thought to be due to conversion of GEM into GOM (Swartzendruber et al., 2006).

Atmospheric Mercury Depletion Events (AMDEs) occur during rapid oxidation reactions of GEM. AMDEs reduce the concentration of GEM while increasing the concentrations of GOM and PBM. AMDEs lead to elevated deposition of GOM and PBM, and are

most noted to occur at the poles during spring (Lindberg et al., 2007). As will be shown in Chapter 3, depletion events occur in Utah as well.

Fain et al. (2009) concluded that high concentrations of GOM were related to oxidation of tropospheric GEM by halogens, possibly from sea-salt over the ocean, though they observed a lack of mass balance. Only ~10% of the depletion in GEM was explained by an increase in GOM concentration, and the rest was attributed to deposition and scavenging, possibly over the Pacific Ocean. The conversion of GEM to GOM is thought to occur both in the free troposphere and over the ocean. While Fain et al. (2009) observed no correlation between O_3 and GOM at Storm Peak Laboratory, Colorado, the oxidation of GEM in the upper troposphere and lower stratosphere is thought to occur with O_3, OH, and other oxidation mechanisms (Swartzendruber et al., 2006). The GOM-enriched air is then brought to the surface via deep convective mixing (Swartzendruber et al., 2006) and subsidence of free-tropospheric air (Sillman et al., 2007; Selin and Jacob, 2008). Multi-day enhancements in GOM concentrations were observed at Storm Peak Laboratory, and seven of the eight such events were found to have a statistically significant negative correlation with GEM concentration (Fain et al., 2009).

Stutz et al. (2002) concluded that "reactive halogens are mobilized from salt on the flats around the Great Salt Lake, Utah." Stutz et al. (2002) observed 15 ± 2 pmoles/mole-air of chlorine oxide (ClO) and 6 ± 0.4 pmoles/mole-air of bromine oxide (BrO) in the vicinity of the Great Salt Lake, Utah. In addition, there are a number of chlorine sources in the vicinity of the Great Salt Lake, the largest being U.S. Magnesium on the western side of the basin (EPA, 2011c).

1.2.3.2 Adsorption

GEM and GOM are thought to be converted to PBM via temperature dependent physical adsorption onto atmospheric particles and is favored at low temperatures (Sakata and Asakura, 2007; Lindberg et al., 2007). GOM can adhere to particles rapidly (Liu et al.,

2010). GOM may be scavenged by particles when the relative humidity is above 50% due to an increase in the total particle surface area (Fain et al., 2009).

1.2.3.3 Reduction

The reduction of PBM and GOM can produce GEM (Gratz et al., 2009). GOM readily converts to GEM after deposition, though the exact mechanism is unknown (Lindberg et al., 2007). It has been suggested that between 5% and 40% of the deposited GOM is re-emitted as GEM (Lindberg et al., 2007).

1.2.4 Deposition in General

PBM and GOM can be deposited relatively near emission sources (Schroeder and Munthe, 1998). GOM is thought to deposit relatively close to its source (order of 10-100 km), while PBM may be transported further (order of 100-1000 km) (Schroeder and Munthe, 1998). Elevated mercury concentrations in an urban environment "may substantially increase Hg Levels in dry and wet deposition, as well as urban runoff, thus ultimately impacting the water quality in its surrounding area" (Liu et al., 2010).

It has been estimated from lake-sediment records that there has been approximately a three-fold increase in deposition since preindustrial times (Lindberg et al., 2007). In lakes in Minnesota and Wisconsin, recent deposition of mercury to lake sediments is about 12.5 $\mu\mathrm{g\ m^{-2}\ yr^{-1}}$, while preindustrial deposition was about 3.7 $\mu\mathrm{g\ m^{-2}\ yr^{-1}}$ (Fitzgerald et al., 1998). It has been calculated that 84% of the mercury entering Lake Michigan was from the atmosphere (Lynam and Keeler, 2005). Model estimates of annual mercury deposition in Idaho suggest that the total deposition is 11.9 $\mu g\ m^{-2} \pm 3.3\ \mu g\ m^{-2}$, 2/3 of which is dry deposition, but this does not account for an upward flux of mercury from the soil (Abbott et al., 2008).

1.2.4.1 Dry Deposition

All three forms of atmospheric mercury can dry deposit (Lindberg et al., 2007). Dry

deposition is a function of atmospheric mercury concentrations, atmospheric stability, and terrain (Schroeder and Munthe, 1998; Seinfeld and Pandis, 1998). Dry deposition is enhanced by the presence of vegetation and is also influenced by temperature, surface wetness and windspeed (Seinfeld and Pandis, 1998; Lindberg et al., 2007). Mercury fluxes on bare soils (deposition and emission) can be influenced by radiation and atmospheric oxidants such as O_3 (Engle et al., 2005; Xin and Gustin, 2007). The deposition velocity of GOM is one and two orders of magnitude higher than PBM and GEM, respectively, and hence GOM does not survive long-range transport (Liu et al., 2010).

1.2.4.2 Wet Deposition

Both cloud droplets and hydrometeors efficiently scavenge reactive forms of atmospheric mercury (Schroeder and Munthe, 1998). GEM has a low water solubility, so it is thought that GEM is oxidized in clouds by O_3 and OH before scavenging occurs (Sakata and Asakura, 2007; Lindberg et al., 2007). Wet deposition is a function of atmospheric mercury concentrations, rainfall rates, and aqueous mercury concentrations (Guentzel et al., 2001; Abbott et al., 2008). Larger particles are more efficiently scavenged by wet deposition (Seinfeld and Pandis, 1998), and Lynam and Keeler (2005) observed that days with precipitation and dew formation had reduced concentrations of GOM relative to days without in Michigan. PBM can be removed from the upper troposphere and lower stratosphere during deep convective storms (Lindberg et al., 2007).

The Mercury Deposition Network (MDN) provides longterm records of mercury wet deposition in the United States and Canada (MDN, 2011). The MDN consists of 169 sites in North America, two of which are in Mexico, 14 in Canada, and the rest in the United States, though some are no longer active (MDN, 2011). Japan also has a network observing mercury wet deposition consisting of 10 sites (Sakata and Asakura, 2007).

The annual mercury wet deposition fluxes were 5.8 to 18.0 $\mu g\ m^{-2}\ yr^{-1}$ at 10 sites in Japan (Sakata and Asakura, 2007). Regional and seasonal variations in mercury wet

deposition are observed in Japan (Sakata and Asakura, 2007). Sakata and Asakura (2007) found that $26 \pm 11\%$ of wet deposition of mercury was due to PBM (i.e., their wet deposition is dominated by GOM). Sakata and Asakura (2007) also found a significant correlation between annual wet deposition flux of mercury and annual amount of precipitation, and they concluded that GOM mainly originates from in situ oxidation in the atmosphere.

The Florida Atmospheric Mercury Study (FAMS) study was initiated in 1992 (Guentzel et al., 2001). FAMS operated 10 sites in Florida on 15 m towers, as well as two ground-based sites. They measured the monthly bulk and wet-only deposition for 2-5 years, depending on the site. Guentzel et al. (2001) hypothesize that long-range transport of RGM coupled with strong convective thunderstorm activity is responsible for more than 50% of the mercury deposition in southern Florida. Local anthropogenic PBM and RGM could be responsible for 30-46% of the summertime rainfall deposition in southern Florida (Guentzel et al., 2001). Mercury concentrations in precipitation water in southern Florida ranged from 14 ± 2 to 16 ± 2 ng L^{-1} while the flux of mercury due to precipitation was 20 ± 3 to 23 ± 3 μg m^{-2} yr^{-1} (Guentzel et al., 2001). The annual rainfall in southern Florida is 102-213 cm, 70% of which falls during May-October (Guentzel et al., 2001). 70-90% of the mercury deposition occurs during May-October (Guentzel et al., 2001). Mercury deposition in southern Florida is greater than in northern and central Florida, while marine sites had the lowest mercury deposition (Guentzel et al., 2001).

Mason et al. (1997) concluded that "rain effectively scavenges particles from the atmosphere within the initial storm period with little washout later in the rain event." Mason et al. (1997) measured wet deposition of mercury at two sites near the Chesapeake Bay by collecting precipitation water and testing it for Hg. They also made measurements of atmospheric mercury by using a vacuum pump to draw air over filters and then analyzing the filters. They found that Hg concentrations in precipitation water varied between 10 pM - 400 pM, with most samples below 150 pM. They also found that MMHg comprised less than 1% of the mercury in precipitation water. Mason et al. (1997) concluded

that both particulate scavenging and in-cloud conversion of elemental mercury contribute to wet deposition as scavenging of particulate mercury appears to explain only 40% of the mercury in precipitation water. High concentrations of mercury only occurred in precipitation water for small precipitation events while low mercury concentrations were observed in conjunction with large precipitation events.

Gratz et al. (2009) found that "The highest concentrations were typically observed with low precipitation amounts, suggesting that at this remote site most of the mercury was removed during the onset of precipitation, and additional precipitation acted to dilute samples throughout the remainder of the event," and this relationship was observed regardless of precipitation type. They studied wet deposition of mercury and categorized precipitation events by type (rain, snow, and mixed) in Underhill, Vermont. The largest wet deposition events were associated with winds coming from the midwest and east coast of the U.S. and temperatures between $4.9°$C and $27°$C with precipitation in the form of rain. The lowest wet deposition events were associated with winds coming from the northwest or southeast with temperatures between $-22.4°$C and $6.7°$C in the form of snow and mixed precipitation. Gratz et al. (2009) observed more wet deposition during warmer months than colder months, with a three-fold or more difference between summer and winter. They only included precipitation samples $\geq$0.10 cm in their analysis.

Fain et al. (2009) found that the "occurrence of precipitation leads to very strong and immediate drops of RGM to levels close to the detection limit of the analyzer." They also noted that high concentrations of RGM in the Rocky Mountains could be a significant source of mercury to snowpacks via wet deposition.

1.3 Observed Concentrations and Seasonality

1.3.1 Observed Concentrations and Seasonality of GEM

The northern hemisphere atmospheric pool of GEM (i.e., the sea-level atmospheric concentration at remote sites) is ~1.5-1.7 $\mathrm{ng\ m^{-3}}$ (Lindberg et al., 2007). The observed

concentration of GEM at 22 sites in the northern hemisphere is 1.7 ± 0.3 ng m^{-3} (Valente et al., 2007). The average total gaseous mercury at 211 sites in Japan was 2.2 ± 0.5 ng m^{-3} for 2004, and the average O_3 concentration was 0.032 ± 0.005 ppmv (Sakata and Asakura, 2007). The average concentration of GEM at Storm Peak Laboratory, Colorado from 28 April to 1 July 2008 was 1.6 ng m^{-3} (Fain et al., 2009).

Liu et al. (2010) observed slightly higher concentrations of GEM during the summer compared to other seasons at both urban and rural settings in Michigan. Abbott et al. (2008) also observed the highest concentrations of GEM during the summer in south-central Idaho. Fall had the second-highest concentrations, followed by spring then winter (Abbott et al., 2008). Converse et al. (2010) observed the highest mean GEM concentration during winter in Shenandoah National Park, Virginia.

1.3.2 Observed Concentrations and Seasonality of PBM

Mean concentrations of PBM observed at various rural locations in the U.S. are generally below 10 pg m^{-3} (e.g., Caldwell et al., 2006; Abbott et al., 2008; Liu et al., 2010). The average PBM concentrations at 10 sites in Japan ranged between 4.9 and 59.4 pg m^{-3} (Sakata and Asakura, 2007). The weekly integrated PBM concentrations in southern Florida ranged from 2.0 to 9.3 pg m^{-3} and did not exhibit strong seasonal variability (Guentzel et al., 2001).

Sakata and Asakura (2007) observed more PBM during winter than summer in Japan, and they provide two explanations. First, clean air masses entering Japan from the Pacific Ocean during the summer dilute atmospheric mercury. However, that does not explain all of the seasonality when PBM is compared to other trace elements. Second, PBM is formed by temperature-dependent adsorption or condensation of GOM and GEM onto atmospheric particles. Relatively high concentrations of PBM were observed during winter in Detroit, which was attributed to "increased production of electricity from coal and heating activities in the region" (Liu et al., 2010). In addition, PBM concentrations were negatively

correlated with temperature (Liu et al., 2010). Mason et al. (1997) found the average concentration of PBM near the Chesapeake Bay to be 16 ± 15 pg m^{-3} during summer with 60% of all samples below 10 pg m^{-3}, and the average wintertime concentration was 21 ± 20 pg m^{-3} with 30% of all samples below 10 pg m^{-3}. Fain et al. (2009) observed an average PBM concentration of 9 pg m^{-3} from 28 April to 1 July 2008 at Storm Peak Laboratory, Colorado. Data from the lower stratosphere indicate significant PBM enrichment (Murphy et al., 2006). PBM is the dominant form of mercury near the tropopause (Lindberg et al., 2007).

1.3.3 Observed Concentrations and Seasonality of GOM

Mean concentrations of GOM observed at various rural locations in the U.S. are generally below 10 pg m^{-3} (e.g., Caldwell et al., 2006; Abbott et al., 2008; Liu et al., 2010). Significantly higher concentrations of GOM have been observed in the free troposphere (Lindberg et al., 2007). Guentzel et al. (2001) used ion-exchange filter packs to measure RGM. This technique is known to underestimate mercury concentrations relative to a mist chamber technique or relative to KCl-coated annular denuders (Guentzel et al., 2001). Guentzel et al. (2001) measured 5 pg m^{-3} during winter and 30 pg m^{-3} during the summer in southern Florida. Florida has a wet season from May to October characterized by strong southeast and easterly winds and deep (12-16 km) convective thunderstorm clouds, enabling scavenging of mercury from the middle and upper troposphere in addition to the boundary layer (Guentzel et al., 2001). Aircraft measurements (800 - 2600 m) of RGM east of Miami yielded 50 - 340 pg m^{-3} during late summer (Guentzel et al., 2001).

The mean concentration of GOM measured during 28 April to 1 July 2008 at Storm Peak Laboratory was 20 pg m^{-3}, and the maximum concentration was 137 pg m^{-3} (Fain et al., 2009). The GOM concentration peaked slightly around 1500 LT.

Relatively high concentrations of GOM were observed during the summer in Detroit, which was attributed to photochemical reactions converting GEM to GOM via O_3 and other

oxidants (Liu et al., 2010). In addition, GOM concentration is positively correlated with temperature (Liu et al., 2010). GEM was weakly negatively correlated with O_3 while GOM and O_3 had a weak positive correlation (Liu et al., 2010).

In south-central Idaho, the highest concentrations of GOM were observed during summer, and the lowest during fall and winter (Abbott et al., 2008). A daytime high and nighttime low diurnal pattern has been observed during summer in both Idaho and Nevada (Abbott et al., 2008; Weiss-Penzias et al., 2009). Weiss-Penzias et al. (2009) suggested that the decline in GOM could be due, at least in part, to deposition after formation. In addition, the free troposphere can have high concentrations of GOM, which may act as a source to the boundary layer (e.g., Swartzendruber et al., 2006; Fain et al., 2009; Weiss-Penzias et al., 2009).

"Long-range transport of RGM from the free troposphere is a potentially important component of Hg input to rural areas of the western United States" (Weiss-Penzias et al., 2009). GOM concentrations up to 600 pg m^{-3} have been observed in the free troposphere (Swartzendruber et al., 2006). Weiss-Penzias et al. (2009) observed that relatively high GOM concentrations were associated with dry air from above the boundary layer. Swartzendruber et al. (2006) found that the highest quartile data observed at Mount Bachelor, OR generally had back-trajectories to the free troposphere of the middle-latitudes above the Pacific Ocean, while the lowest quartile had back-trajectories from the boundary layer over land.

1.4 Thesis Outline

The goals of this thesis are to analyze the first two years of speciated atmospheric mercury data measured at the UT96 site and to explore the influence of precipitation on speciated atmospheric mercury. The UT96 site will be described in Chapter 2 as well as the instrumentation used. As will be shown in Chapter 3, Gaussian statistics cannot be used to adequately describe the speciated atmospheric mercury data. Therefore, nonparametric

statistics will be discussed in Chapter 2. Chapter 3 introduces the speciated atmospheric mercury data set, including summary statistics as well as the temporal patterns observed on timescales of annual to diurnal. Extreme events will also be discussed. The effects of precipitation on atmospheric mercury are explored in Chapter 4. Finally, Chapter 5 describes the conclusions of this work and includes ideas for future work.

CHAPTER 2

SITE, INSTRUMENTATION, AND STATISTICAL METHODOLOGY

Chapter 2 will provide a description of the UT96 site including location, meteorology, and instrumentation. In addition, the nonparametric statistical descriptors and tests used to analyze the mercury data will be described.

2.1 Site Description

UT96 is an Atmospheric Mercury Network (AMNet) dry deposition monitoring site located on the eastern shore of the Great Salt Lake. AMNet was created to measure atmospheric mercury fractions that contribute to dry and total mercury deposition (AMNet, 2011b). UT96 has collected 2 years of continuous data, and represents the only such data set in the Intermountain Western U.S. An additional Tekran mercury speciation system has been placed at the UT97 AMNet site in West Valley, UT, but does not run continuously. UT97 does measure wet deposition. The next closest sites are along the coast of California and eastern Oklahoma, see Figure 2.1 (AMNet, 2011b). UT96 is co-located with a Utah Division of Air Quality Weather Station adjacent to the entrance to Antelope Island State Park approximately 37 kilometers from Salt Lake City, Utah, USA. West of the site is the Great Salt Lake (GSL). The Wasatch mountains are to the east with primarily urban areas between the mountains and the site (Fig. 2.2).

Local wind patterns are influenced by the land/lake breeze due to the presence of the GSL and by upslope/downslope mountain flows due to the proximity of the Wasatch Moun-

Figure 2.1: Map of AMNet sites (AMNet, 2011b).

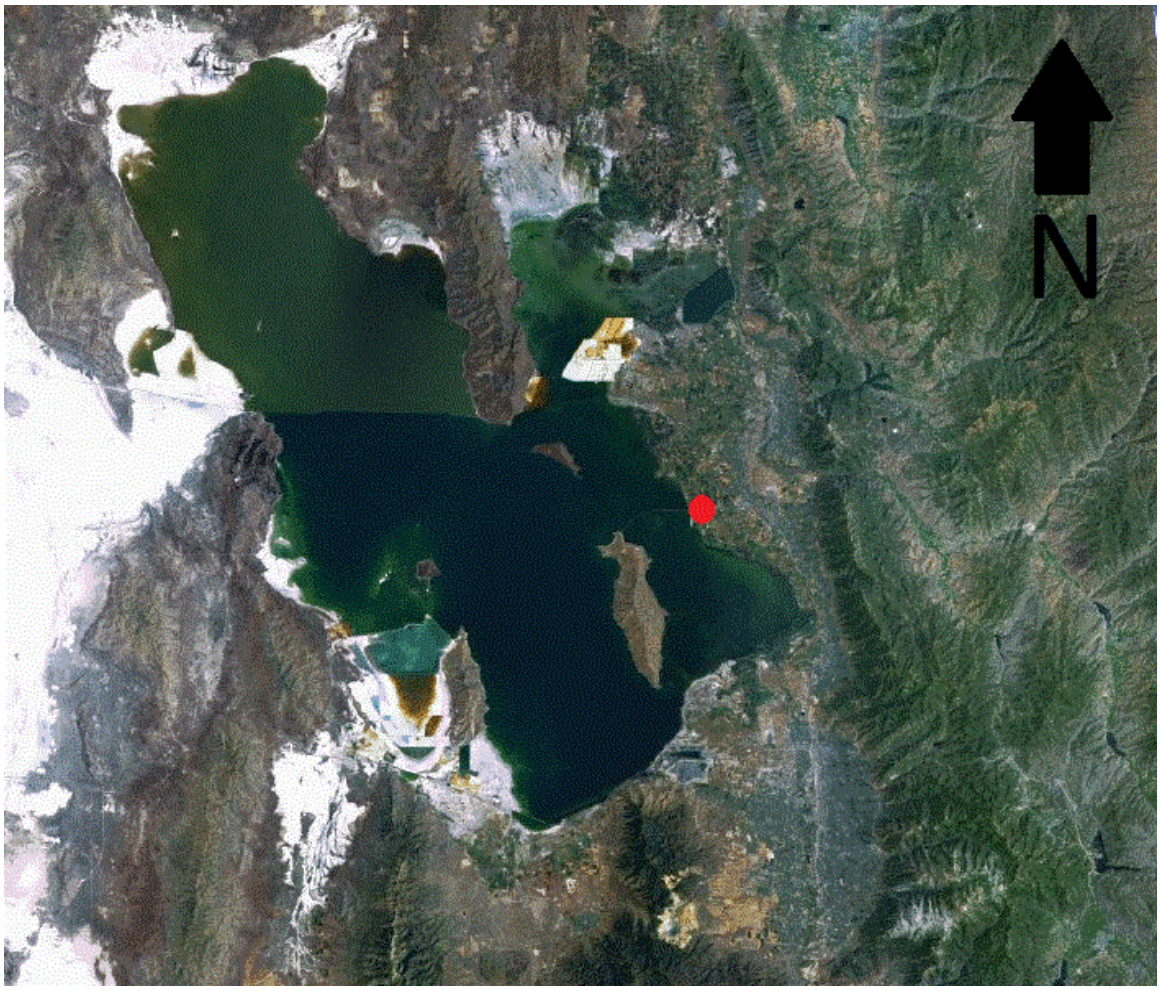

Figure 2.2: Map (USGS, 1984) showing the location of the UT96 AMNet site (red circle). The Great Salt Lake is west of UT96 and the Wasatch Mountains are to the east.

tains. Figure 2.3 shows the wind rose by season for UT96 from 1 July 2009 through 30 June 2011. Figures 2.4-2.5 show the diurnal wind pattern at UT96. Overnight winds at UT96 tend to be either from the north or east. The northerly winds likely represent synoptic forcing while the easterly winds represent downslope flows from the Wasatch Mountains and the land breeze. Afternoon winds tend to be westerly due to the lake breeze. Figure 2.6 shows histograms of the primary meteorological variables measured at UT96 (temperature, relative humidity, solar radiation, and dew point), which will be used in Chapter 3 to compare typical weather at UT96 to the weather occurring during unusually high or low mercury concentrations.

2.2 Instrumentation Description

The UT96 site employs a Tekran ambient air mercury analyzer system which measures GEM, PBM, and GOM (Fig. 2.7). The Tekran system consists of a Model 2537B cold vapor atomic fluorescence spectroscopy mercury analyzer, a Model 1130 oxidized mercury speciation module, and a Model 1135 particulate mercury module. Ambient air is pulled in through an air intake located at a height of ~4 m. Particles in the air with an effective diameter larger than the cutpoint impact the impactor frit and are removed from the airstream and discarded. The Tekran system is designed to have a flow rate of 10 L m^{-1} and a 50% cutpoint of 2.5 μm. However, due to the altitude of UT96, the system pump only pulls approximately 8.5 L m^{-1}. Weiss-Penzias et al. (2009) also had lower flow in their Tekran system in Nevada. The low flow leads to a 50% cutpoint of approximately 2.7 μm aerodynamic diameter (Fig. 2.8). This could lead to PBM concentrations that are slightly elevated relative to Tekran systems with a flow of 10 L m^{-1}, but this depends on the underlying particle size distribution, which is unknown at the present time. Particulate matter larger than the cutpoint is discarded.

The air then enters the denuder, which is annular glassware coated with potassium chloride. The GOM in the air stream adheres to the surface of the denuder and is removed from

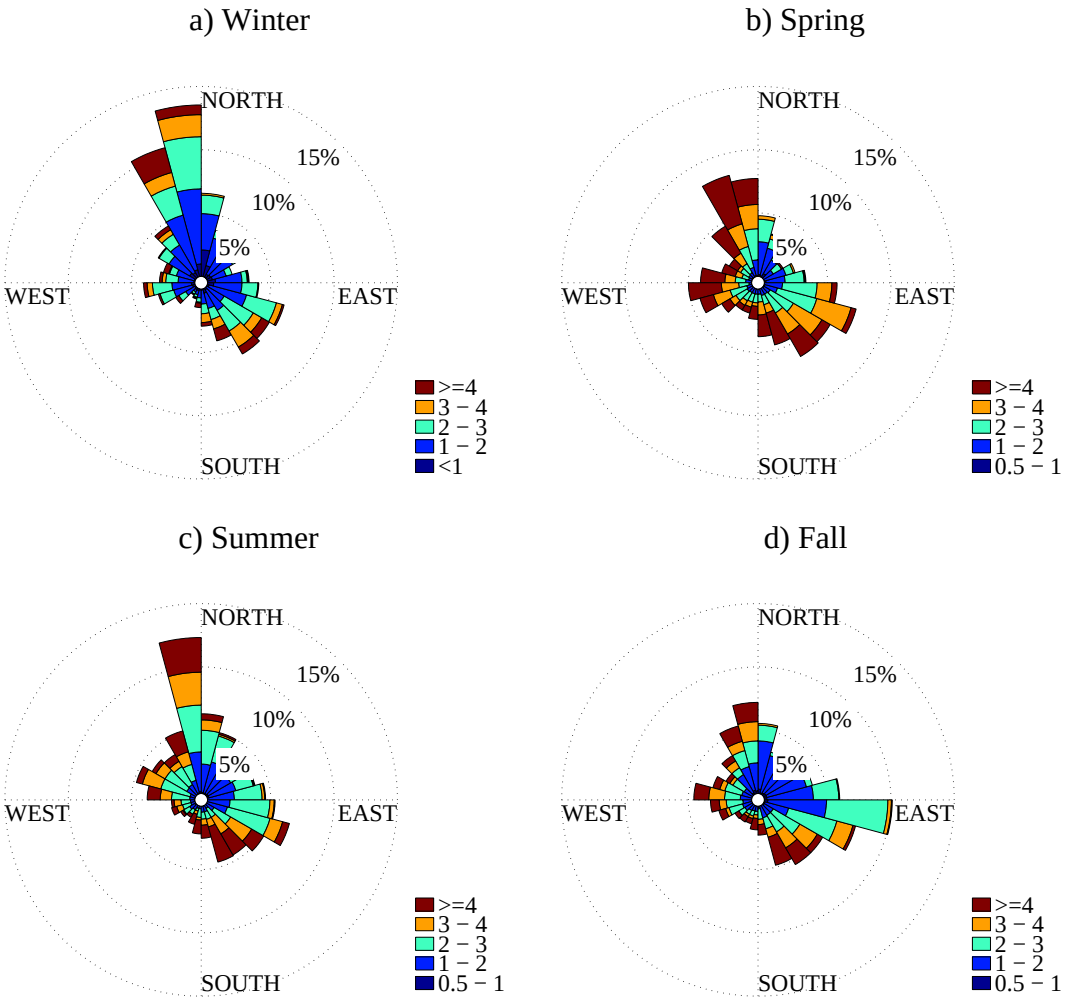

Figure 2.3: Seasonal wind roses (m s^{-1}) for the UT96 site as measured by a sonic anemometer from 1 July 2009 through 30 June 2011.

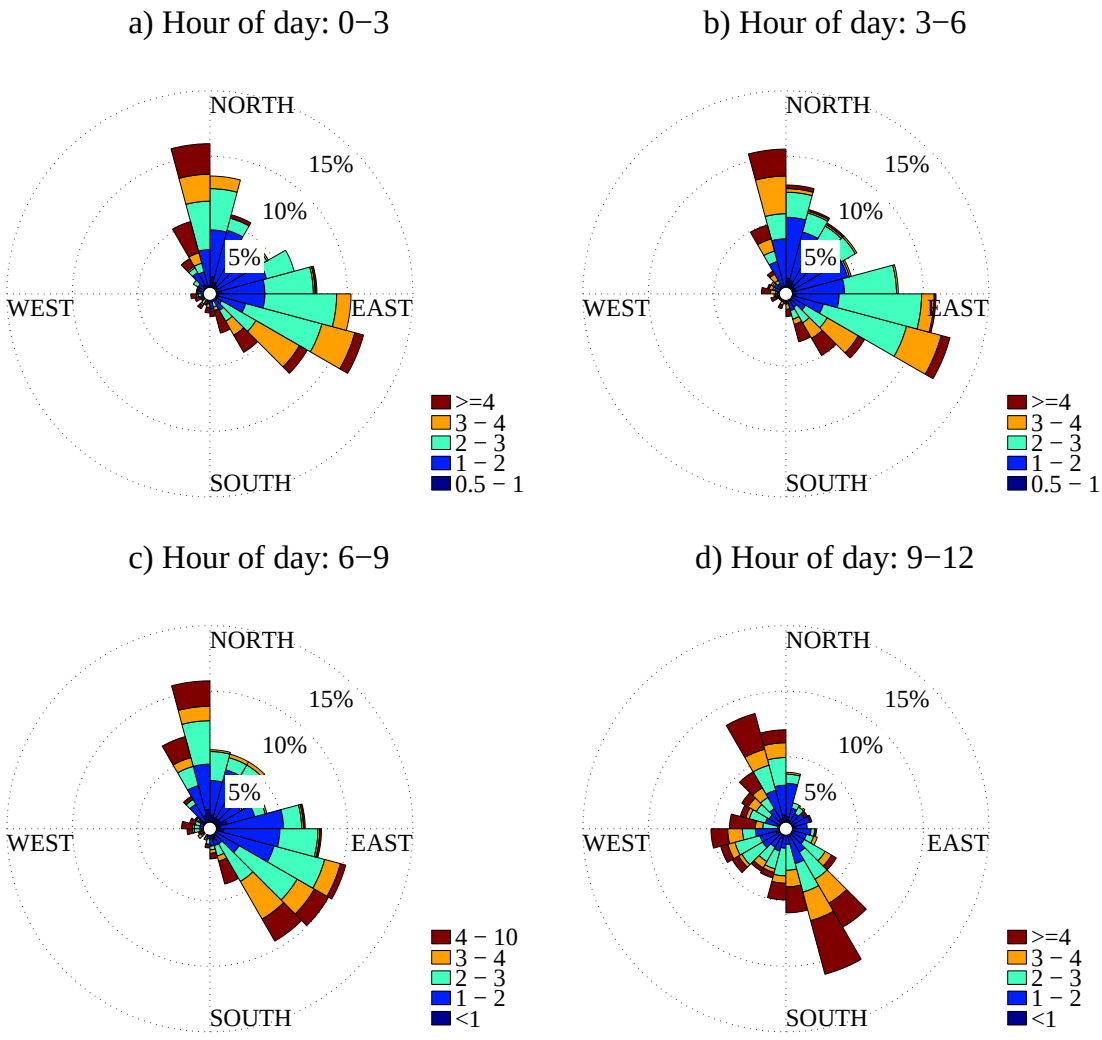

Figure 2.4: Diurnal wind roses (m s^{-1}) for the UT96 site as measured by a sonic anemometer from 1 July 2009 through 30 June 2011 from midnight to 0900.

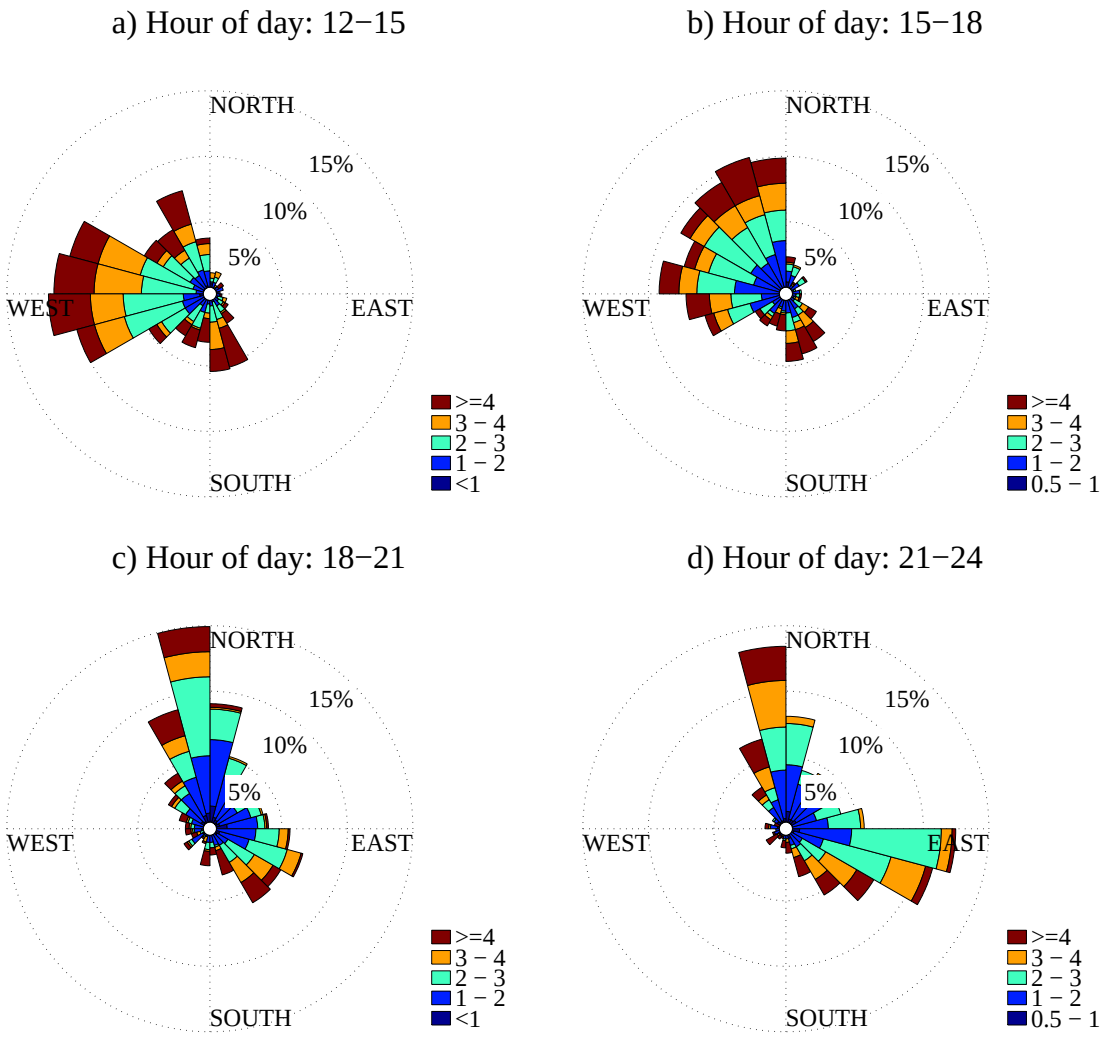

Figure 2.5: Diurnal wind roses (m s^{-1}) for the UT96 site as measured by a sonic anemometer from 1 July 2009 through 30 June 2011 from noon to 2100.

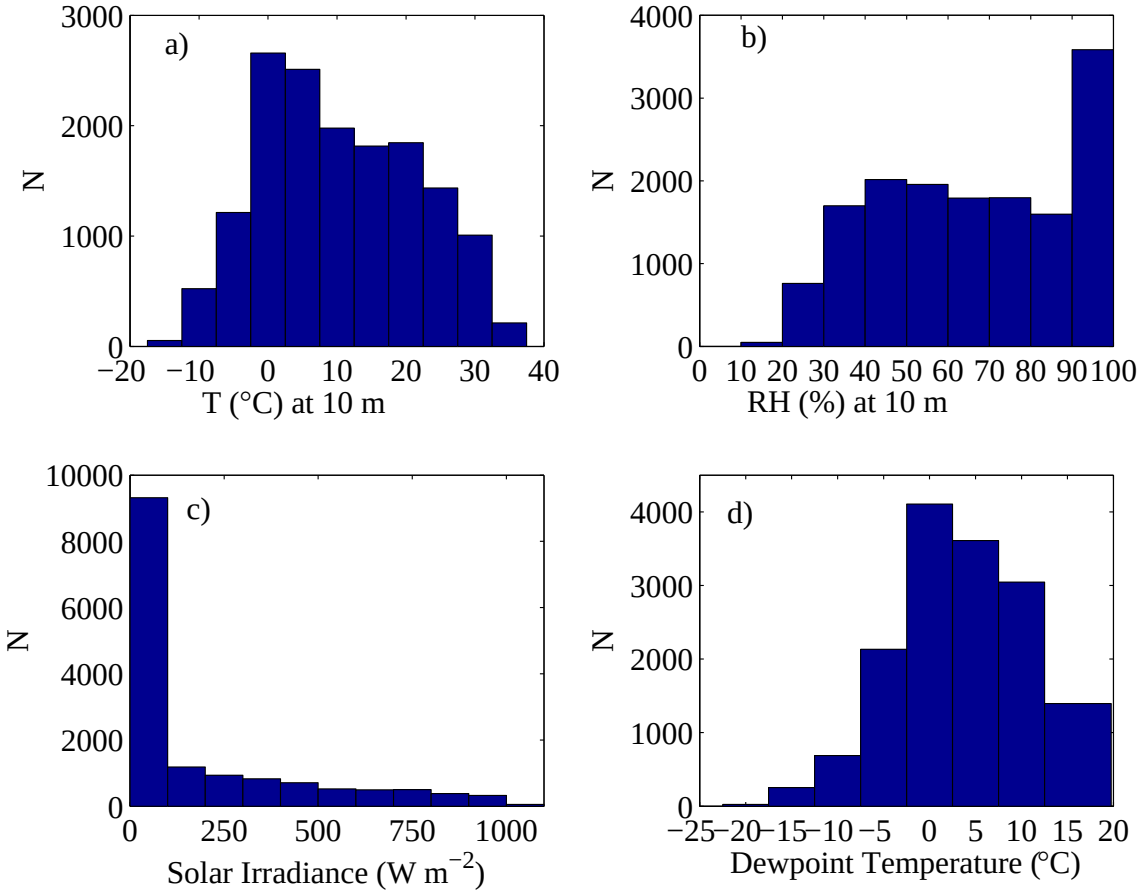

Figure 2.6: Histograms of the primary meteorological variables at UT96 from 1 July 2009 through 31 June, 2011. a) temperature, b) relative humidity, c) solar radiation, and d) dewpoint temperature.

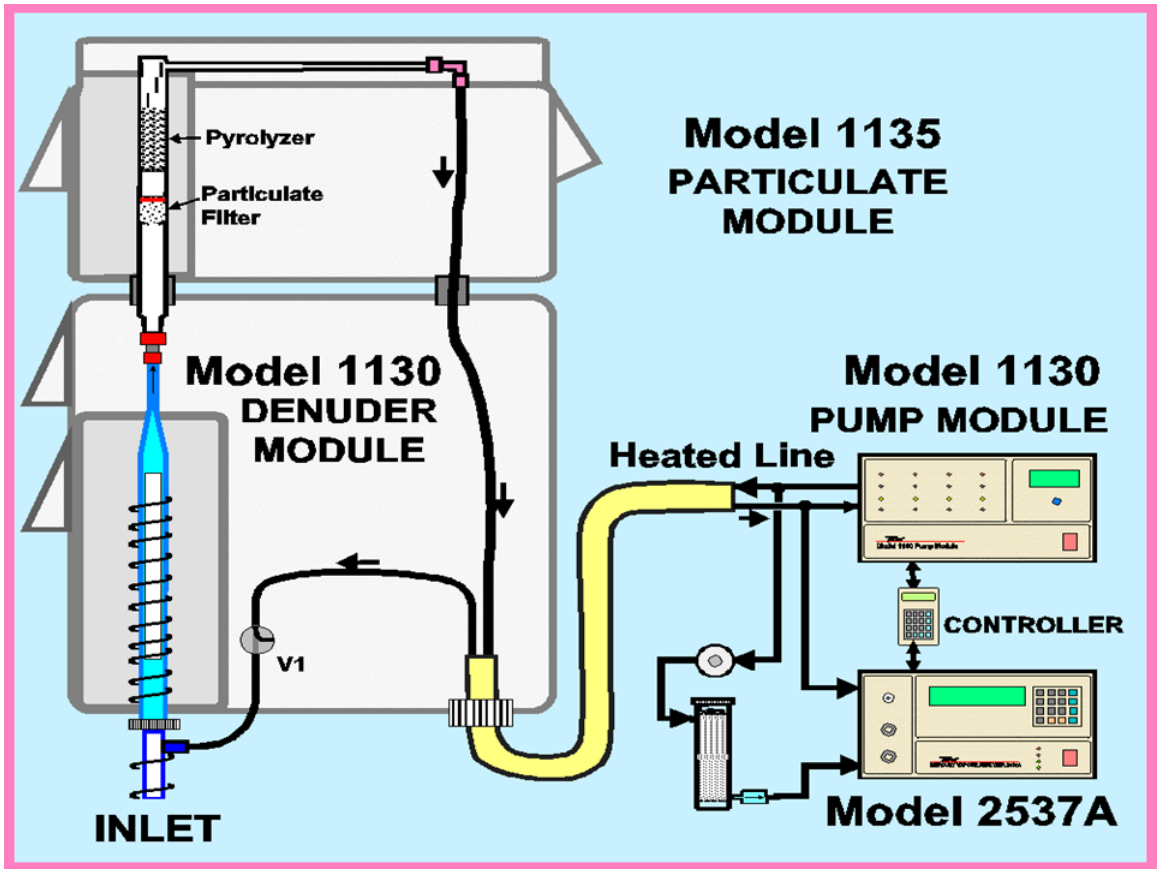

Figure 2.7: Schematic of Tekran ambient air mercury analyzer system (Courtesy of Tekran Instruments).

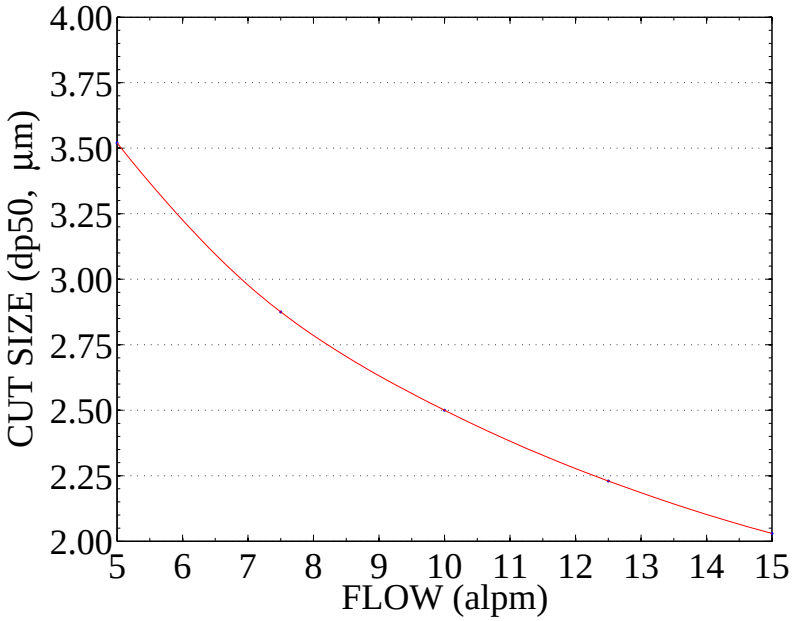

Figure 2.8: Flow versus PBM 50% particle-size cutpoint as a function of flow rate (Courtesy of Tekran Instruments). Note: Temperature effect other than volumetric flow is only important over ~100°C due to the increase in air viscosity.

the airstream. The airstream then leaves the denuder and enters the regenerable particulate filter (RPF) which contains a quartz filter. Particulate matter in the airstream (including PBM) are collected by the quartz filter. At this point, the only form of mercury remaining in the airstream is GEM. The airstream flows over one of two gold cartridges, named A and B. GEM forms a temporary amalgam with the gold. After 5 minutes of collecting GEM on one of the gold cartridges, A for example, a solenoid switches the air stream to flow over cartridge B for 5 minutes. Meanwhile, ultra high purity argon flows over cartridge A as it is heated. This process liberates the GEM and is referred to as desorption. A UV lamp emitting light at 253.7 nm shines onto the GEM causing the mercury to fluoresce. The fluoresced light then enters a photomultiplier tube where the signal is integrated. The integrated signal from the photomultiplier tube and the volume of ambient air that flowed over cartridge A are then used to calculate the concentration of GEM in the atmosphere. Cartridges A and B alternate collection and desorption/measurement at 5 minute intervals for 2 hours. At the end of the 2 hour period, collection of ambient air stops while the

PBM and GOM collected during the previous 2-hour period are measured. One at a time, the RPF and denuder are heated to 800°C and 500°C, respectively. The heating desorbs the mercury from the quartz filter and glassware and converts it to GEM. The converted GEM then flows down the tubing toward cartridge A or B to be measured in the same fashion described above. The desorption and measurement of PBM and GOM takes one hour. Consequently, during any 24-hour period, UT96 will at most collect 96 GEM data points, 8 PBM data points, and 8 GOM data points. The difference in the length of the collection periods of GEM versus PBM and GOM is due to the differences in atmospheric concentrations. GEM is measured in $\mathrm{ng\ m^{-3}}$ with a typical concentration of 1.58 $\mathrm{ng\ m^{-3}}$ while PBM and GOM are measured in $\mathrm{pg\ m^{-3}}$ with typical concentrations of 5.7 $\mathrm{pg\ m^{-3}}$ and 2.6 $\mathrm{pg\ m^{-3}}$, respectively.

The Tekran 2537B undergoes an automated calibration once every 72 hours during which a permeation tube emits a known quantity of mercury into the system to be measured. Results of this calibration are used in future conversions of the signal from the photomultiplier tube to an atmospheric mercury concentration. Once per month, a manual calibration is performed whereby a digital syringe is used to inject a known quantity of mercury from an external source (Tekran Model 2505) into the flow over the cartridges to verify the performance of the system.

The data collected from the Tekran 2537B undergoes four levels of quality assurance. The first level separates the output of the Tekran 2537B by mercury species. The second level marks individual data points as either valid or invalid based on both automated and manual quality assurance protocols (AMNet, 2011a). The third level has all of the invalid data removed from it. The fourth level applies a correction factor to data measured before 9 June 2011. (Part of the Tekran system was set up for 1-hour cycles while the Tekran was actually running 2-hour cycles.) Level four also consolidates the data into three Matlab matrices, one for each species. Only fourth-level, quality-assured data are used in this thesis.

Similar to Lynam and Keeler (2005), Poissant et al. (2005), and Liu et al. (2010), the method detection limit (MDL) for PBM and GOM was calculated as three times the standard deviation of the system blank, which gives an overall MDL of 1.5 pg m^{-3}. Where data is analyzed by season, the MDL is calculated and used by season (Fig. 2.9). The method detection limit for GEM is <0.1 $\mathrm{ng\ m}^{-3}$ (Tekran, 2007), and no UT96 GEM data is below this threshold.

2.3 Nonparametric Statistical Descriptors and Tests

The speciated atmospheric mercury measurements made at the UT96 AMNet site are distinctly non-Gaussian. As a result, typical statistical tests that assume a Gaussian distribution of the underlying data cannot be used to characterize the data. This finding is consistent with other studies of speciated atmospheric mercury. To overcome this problem, various researchers have used the Wilcoxon test (Lynam and Keeler, 2005; Gratz et al., 2009; Liu et al., 2010) and the Kruskal-Wallis test (Abbott et al., 2008; Gratz et al., 2009; Liu et al., 2010). These, and other, nonparametric statistical tools are described in this

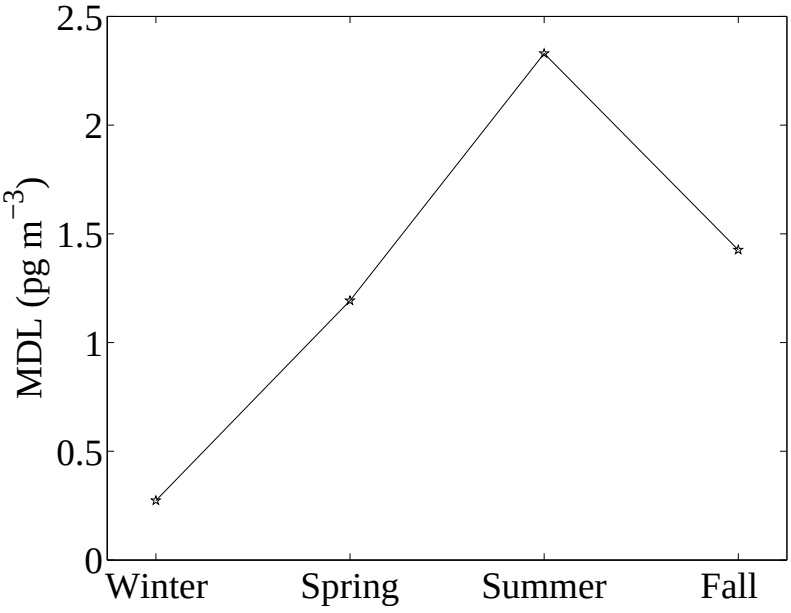

Figure 2.9: Method detection limit for PBM and GOM by season.

section.

2.3.1 Nonparametric Statistical Descriptors

The trimean is a weighted average of the median and the quartiles, and is defined as:

$$\text{trimean} = \frac{q_{0.25} + 2 * q_{0.5} + q_{0.75}}{4} \tag{2.1}$$

where $q_{0.5}$ is the median while $q_{0.25}$ and $q_{0.75}$ are the lower and upper quartiles, respectively. The trimean describes the "location" of the data and is less sensitive to outliers than the mean (Wilks, 2006).

The median absolute deviation (MAD) is analogous to the standard deviation, but is less sensitive to outliers. The MAD is defined as:

$$\text{MAD} = median\,|x_i - q_{0.5}| \tag{2.2}$$

where x_i represents each data point in the data set (Wilks, 2006).

The skewness coefficient (γ) is a dimensionless measure of the symmetry of a data set about the mean and is sensitive to outliers because of the cubes (Eq. 2.3).

$$\gamma = \frac{\frac{1}{n-1}\sum_{i=1}^{n}(x_i - \overline{x})^3}{s^3} \tag{2.3}$$

Data with long right tails (such as the mercury measurements) are positively skewed and will have a large value for γ. A dimensionless measure of skewness that is less sensitive to outliers is the Yule-Kendall (Y-K) index, which describes the skewness of the central 50% of data (Eq. 2.4 where IQR is the interquartile range).

$$\gamma_{YK} = \frac{q_{0.25} - 2q_{0.5} + q_{0.75}}{\mathrm{IQR}} \tag{2.4}$$

Right-skewed data will have a positive Yule-Kendall index (Wilks, 2006).

2.3.2 Wilcoxon Test

The Wilcoxon test, also known as the Mann-Whitney test, is a method used to describe whether two populations of data are statistically different from one another without the assumption that the underlying data is Gaussian (Wilks, 2006). The test assumes that the two data samples are random samples from their respective populations (serially independent) and that there is mutual independence between the two populations (unpaired data), and it tests for a possible difference in location (Conover, 1980; Wilks, 2006). The null hypothesis is that the two data samples have been drawn from the same distribution. The test can be done with either a one-sided or a two-sided alternative hypothesis (Wilks, 2006). Using this test on serially correlated data can lead to unwarranted rejection of the null hypothesis (Wilks, 2006). A method of addressing the problem of serial correlation is described below.

The total number of observations is given by N and is related to population 1 and population 2 by the following:

$$N = n_1 + n_2. \tag{2.5}$$

The two populations of data are combined into one pool and ranked. The smallest observation receives a rank 1 while the largest data point receives a rank N (Wilks, 2006). If two or more data points have the same value (a tie in rank), all of the tied data receives the average rank that those data points would have received had there not been a tie (Conover, 1980). The large pool of data with the given ranks is then separated again into the two populations, and the rank sum statistics (R_1 and R_2) are calculated (Wilks, 2006).

R_1 is the sum of the ranks held by members of population 1. Likewise, R_2 is the sum of the ranks held by members of population 2. R_1 and R_2 are related by:

$$R_1 + R_2 = 1 + 2 + ... + N = \frac{(N)(N+1)}{2}. \tag{2.6}$$

If the null hypothesis is true and $n_1 = n_2$, then $R_1 \approx R_2$ because under the null hypothesis, there is no reason for a given observation to be in one population instead of the other. If the sample sizes are different, then the relationship

$$\frac{R_1}{n_1} \approx \frac{R_2}{n_2} \tag{2.7}$$

suggests that the null hypothesis is true. Statistical significance can be tested using either of the Mann-Whitney U-statistics:

$$U_1 = R_1 - \frac{n_1}{2}(n_1 + 1) \tag{2.8}$$

and

$$U_2 = R_2 - \frac{n_2}{2}(n_2 + 1). \tag{2.9}$$

U_1 and U_2 are related by

$$(U_1 + U_2) = (n_1)(n_2) \tag{2.10}$$

(Wilks, 2006). If n_1 and n_2 are both larger than about 10, then the large sample approximation can be made, i.e. the Mann-Whitney U-statistic can be approximated as Gaussian with

$$\mu_U = \frac{n_1 n_2}{2} \tag{2.11}$$

and

$$\sigma_U = \left[\frac{n_1 n_2 (n_1 + n_2 + 1)}{12}\right]^{1/2} \tag{2.12}$$

(Conover, 1980; Wilks, 2006). Finally,

$$z = \frac{U_1 - \mu_U}{\sigma_U} \tag{2.13}$$

can be used to look up probabilities in Gaussian probability tables for the chosen level of significance (typically 5% in this thesis) (Wilks, 2006). The significance level indicates the probability with which the null hypothesis will be rejected when it is true (von Storch, 1995).

2.3.3 Kruskal-Wallis Test

The Kruskal-Wallis test (KW test) is an extension of the Wilcoxon test from 2 to k independent populations, and the populations can all be of different sizes (Conover, 1980). Using the Kruskal-Wallis test in a case with two populations is equivalent to using the two-sided Wilcoxon test (Hájek et al., 1999). There are four assumptions about the data that must be met in order for the Kruskal-Wallis test to be valid:

1. All populations are random samples from their respective populations.
2. In addition to independence within each population, there is mutual independence among the various populations.
3. The measurement scale is at least ordinal.
4. Either a) the *k* population distribution functions of all samples are identical, or b) some of the population distribution functions are weighted toward larger values than others (Conover, 1980).

The problem of serial correlation is addressed below. The null hypothesis is that all *k* populations are identical. The alternative hypothesis is that some of the populations tend to furnish greater observed values than other populations. If the null hypothesis is rejected, there is a procedure to determine which pairs of populations are different from each other (Conover, 1980).

Each population contains n_i observations ($i = 1, 2, ...k$), and N is the total total number of observations.

$$N = \sum_{i=1}^{k} n_i \tag{2.14}$$

As with the Wilcoxon test, all N observations are combined into one pool and ranked from 1 (smallest observation) to N (largest observation). Ties again receive the average rank. The pool of data is then separated back into the *k* populations with the corresponding ranks. The rank sum statistic R_i is then calculated for each population:

$$R_i = \sum_{j=1}^{n_i} rank(X_{ij}) \tag{2.15}$$

where X_{ij} refers to the jth observation within population i. After R_i has been calculated for each population, the test statistic T can then be calculated (Eq. 2.16) (Conover, 1980).

$$T = \frac{12}{N(N+1)} \sum_{i=1}^{k} \left(\frac{R_i^2}{n_i} \right) - 3(N+1) \tag{2.16}$$

To test the null hypothesis at the level of significance α ($\alpha = 0.05$ for 5%, i.e. 95% confidence), the chi-square distribution is used. The chi-square distribution value with $k - 1$ degrees of freedom at the $1 - \alpha$ quantile is called CS. If T is greater than CS, the null hypothesis is rejected (Conover, 1980).

If the null hypothesis has been rejected, the following procedure can be used to deter-

mine which pairs of populations tend to differ. If inequality 2.17 is satisfied, then populations g and h tend to be different (Conover, 1980).

$$\left|\frac{R_g}{n_g} - \frac{R_h}{n_h}\right| > t_{1-\frac{\alpha}{2}} \left(S^2 \frac{N-1-T}{N-k}\right)^{1/2} \left(\frac{1}{n_g} + \frac{1}{n_h}\right)^{1/2} \tag{2.17}$$

In inequality 2.17, $t_{1-\frac{\alpha}{2}}$ is the $1-\frac{\alpha}{2}$ quantile of the t distribution with $N-k$ degrees of freedom while:

$$S^2 = \frac{N(N+1)}{12} \tag{2.18}$$

(Conover, 1980).

Substantial portions of GOM and PBM data are below the MDL, so an additional requirement was added to the Kruskal-Wallis test. If the medians of both populations g and h are below the MDL, then those two populations are automatically statistically the same, and the procedure above is not used.

2.3.4 Serial Correlation

As mentioned above, both the Wilcoxon test and the Kruskal-Wallis test assume that the data being tested is not serially correlated, and using these tests on serially correlated data can lead to unwarranted rejection of the null hypothesis (Conover, 1980; Wilks, 2006). von Storch (1995) suggests "pruning the data" as a method of addressing the issue of serial correlation for both the Mann-Kendall test and Student's t-test. The Mann-Kendall test and Student's t-test are not used in this thesis. However, it seems reasonable to apply the solution to the Wilcoxon and Kruskal-Wallis tests for two reasons: 1) This solution is suggested for multiple statistical tests, implying a level of generality and 2) Student's t-test is the parametric analog of the Wilcoxon test.

"Pruning the data" simply means forming a subset of data in which each data point

is temporally well separated. Consecutive data points in the pruned subset will not be autocorrelated. The benefit of pruning the data is the following: given that the time interval between data points in the data subset is long enough, the test operates as specified by the user. The drawback of pruning the data is that a substantial portion of the data is not used in the analysis (von Storch, 1995). A pruning function was created that takes the first data point of each 3 hr time block (i.e., every data point in the pruned data is at least 3 hrs from the next one). It is noted where this function is used.

CHAPTER 3

ANNUAL, SEASONAL, AND DIURNAL PATTERNS

This chapter will focus on characterizing the temporal variability of atmospheric mercury at the UT96 site on time scales ranging from annual to a few hours. This analysis will not only provide a broad overview of the data, it will also help identify potentially interesting scientific processes and/or chemical transformations that may be studied in greater detail in the future.

3.1 Statistical Summary

This section will provide a statistical summary of the UT96 mercury data set from 1 July 2009 to 30 June 2011. The GEM concentration is generally well below 5 $\mathrm{ng\ m^{-3}}$ with only a few well-defined extreme events (Fig. 3.1a). These extremely high GEM events are most likely due to plumes from local or regional sources. Lynam and Keeler (2005) also observed fairly constant GEM concentrations that were interrupted by episodes with large increases in concentration due to the impact of a plume on their site in Detroit, Michigan. While the majority of the GEM data lies within the range of 1-2 $\mathrm{ng\ m^{-3}}$, there are some well defined mercury depletion events when the GEM concentration drops below 1.0 $\mathrm{ng\ m^{-3}}$ (Fig. 3.1b). Mercury depletion events are important because the mercury that is depleted from the atmosphere is likely being deposited to the ground and/or surface water where it can enter into the ecosystem and contribute to bio-accumulation of mercury. In addition, the physical and/or chemical processes responsible for these mercury depletion events are not well understood.

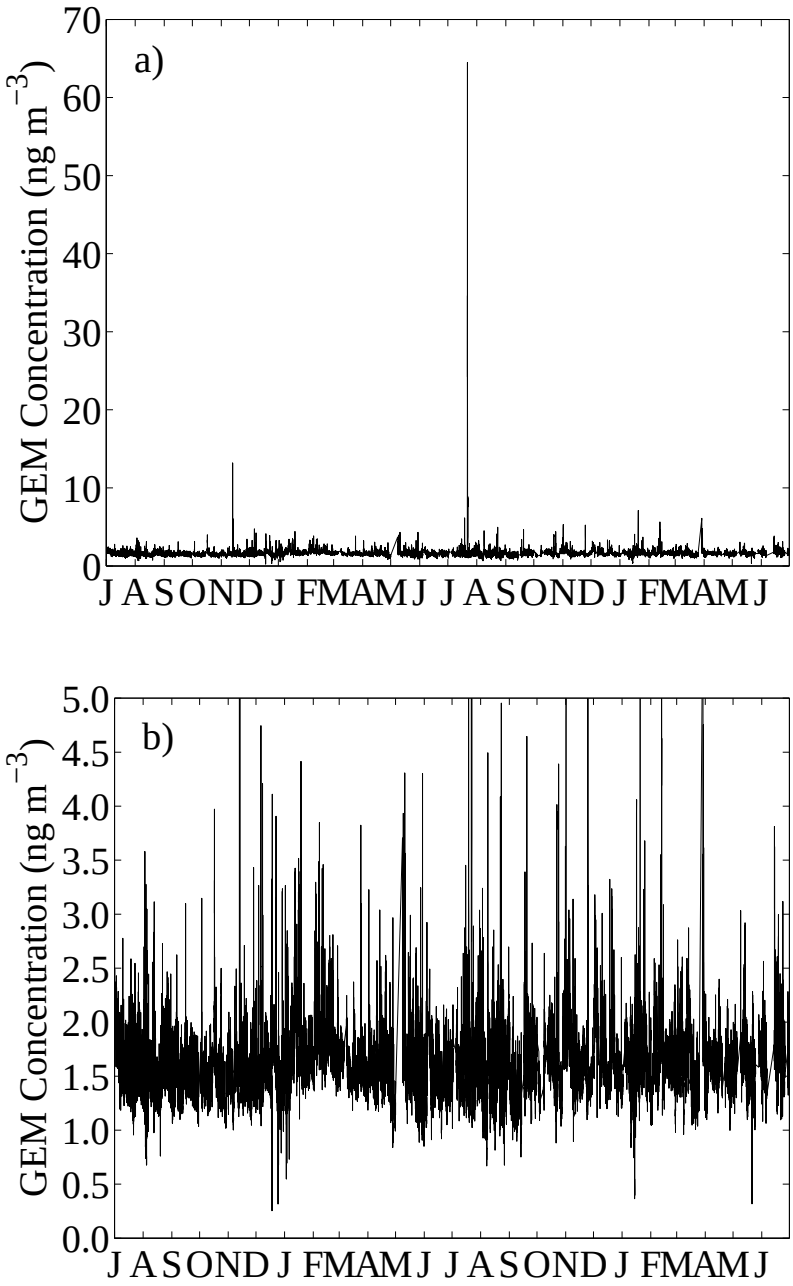

Figure 3.1: Time series of GEM measured at the UT96 site from July 2009 through June 2011. a) is the complete time series including outliers, while b) has truncated axes to show more detail for the majority of the data.

The PBM concentration is generally less than 60 $\mathrm{pg\ m^{-3}}$ with some sporadic extremely high events (Fig. 3.2). The extremely high PBM events are most likely due to plumes from local or regional sources. In general, the PBM concentrations are typically less than 0.4% of total atmospheric mercury concentrations, compared to 99.5% for GEM. This large disparity results from the vastly different atmospheric residence times for the two species.

The GOM concentration is generally less than 20 $\mathrm{pg\ m^{-3}}$ except for afternoons in the warmer months (Fig. 3.3a). The strong seasonality of GOM concentrations is apparent in Figure 3.3 with lower concentrations generally occurring during the winter months. Unlike GEM and PBM, the highest GOM concentration events do not occur in isolation, but rather as a seasonal phenomenon. This suggests that the highest GOM concentrations are most likely influenced by meteorological conditions rather than plumes from local or regional sources.

The MDL for a Tekran for GEM is <0.1 $\mathrm{ng\ m^{-3}}$ (Tekran, 2007). The MDL for PBM and GOM, which is calculated as 3 times the standard deviation of the zero-air cycle field blanks, is typically between 2.2 and 5.4 $\mathrm{pg\ m^{-3}}$ (e.g., Lynam and Keeler, 2005; Poissant et al., 2005; Abbott et al., 2008; Liu et al., 2010). However, for the UT96 data, the MDL for PBM and GOM is only 1.5 $\mathrm{pg\ m^{-3}}$. For PBM, 7% of the data set is below the MDL, while 37% of the GOM data is below the MDL.

As discussed earlier, none of the three species of atmospheric mercury exhibit a Gaussian distribution (Fig. 3.4). The distributions of all three species of mercury are skewed significantly to the right. The distinctly non-Gaussian distributions mean that many of the traditional metrics used for describing Gaussian data sets are not appropriate for this data set.

A statistical summary of two years of mercury measurements (1 July 2009 to 30 June 2011) is provided in Table 3.1. Using the medians, GEM comprised 99.47% of total atmospheric mercury measured at UT96, while PBM and GOM comprised 0.36% and 0.16%, respectively. These results are similar to that of Poissant et al. (2005), who found that

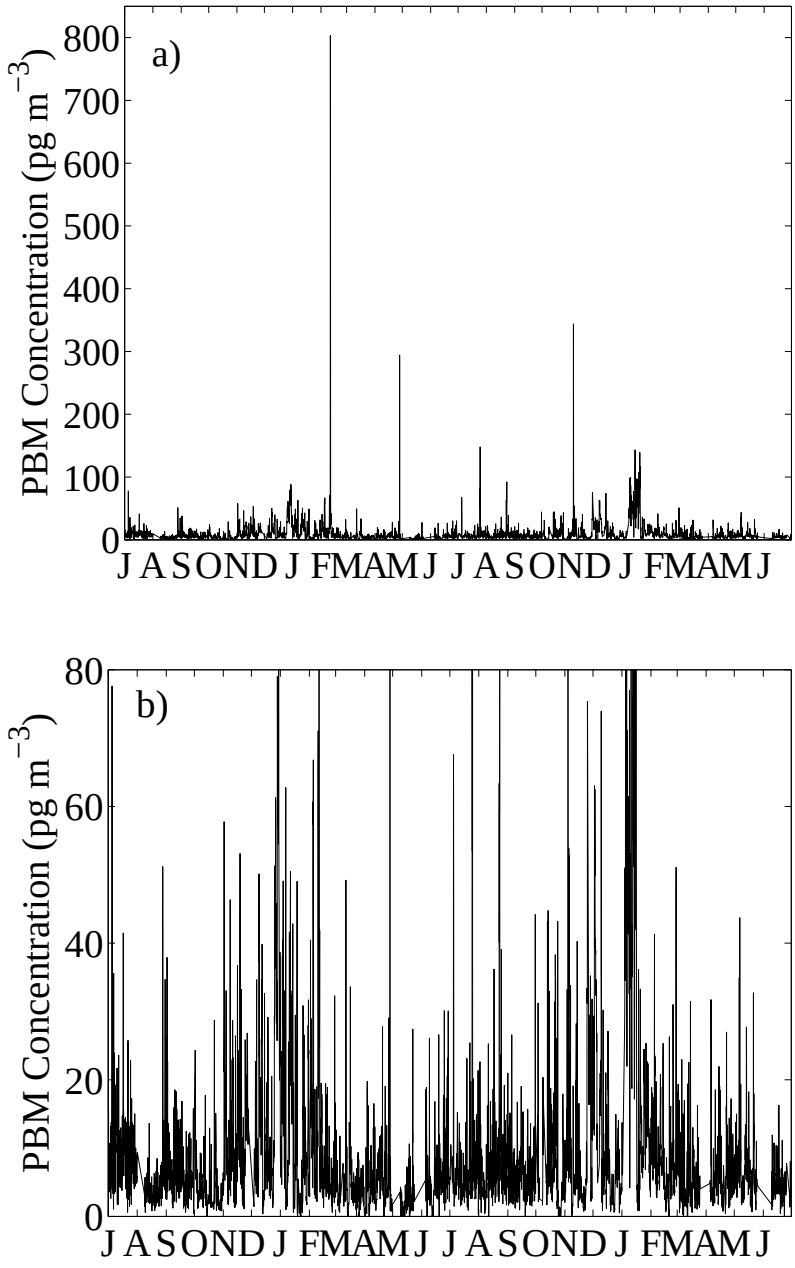

Figure 3.2: Time series of PBM measured at the UT96 site from July 2009 through June 2011. a) is the complete time series including outliers, while b) has truncated axes to show more detail for the majority of the data.

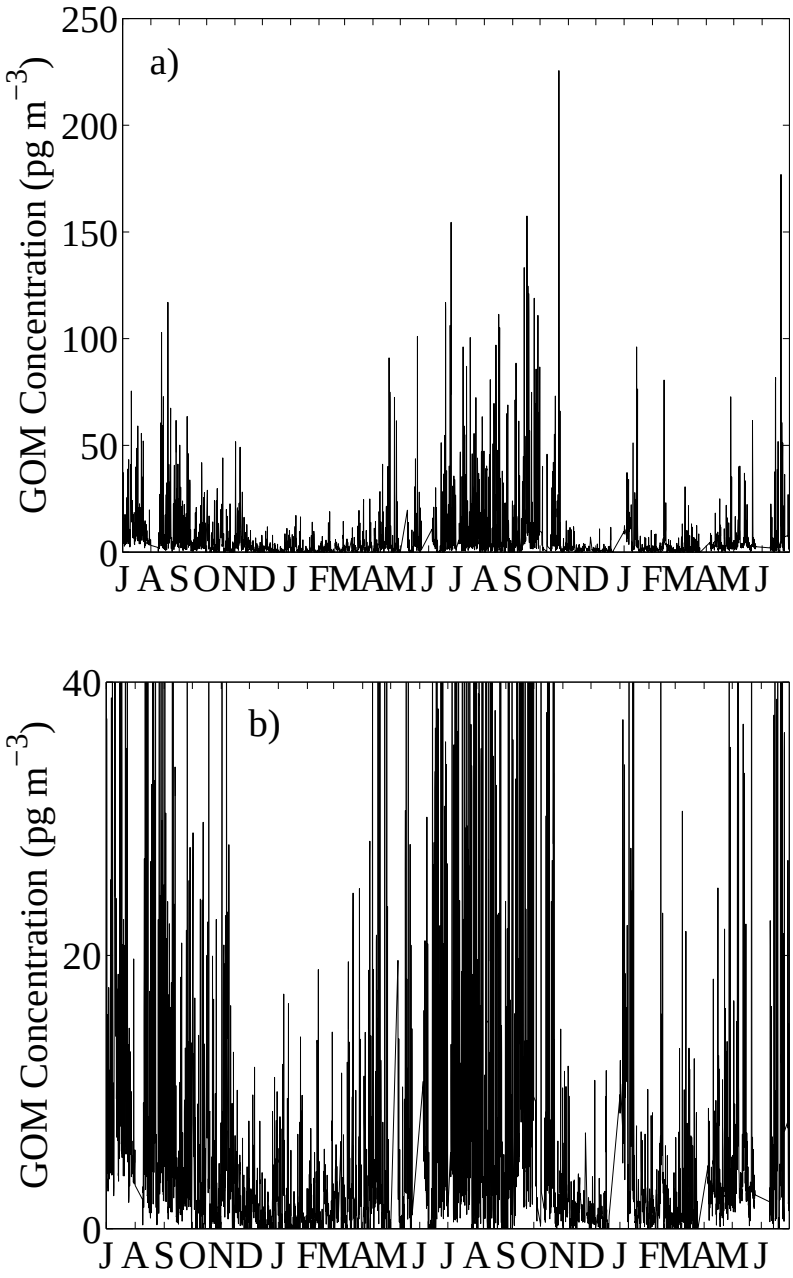

Figure 3.3: Time series of GOM measured at the UT96 site from July 2009 through June 2011. a) is the complete time series including outliers, while b) has truncated axes to show more detail for the majority of the data.

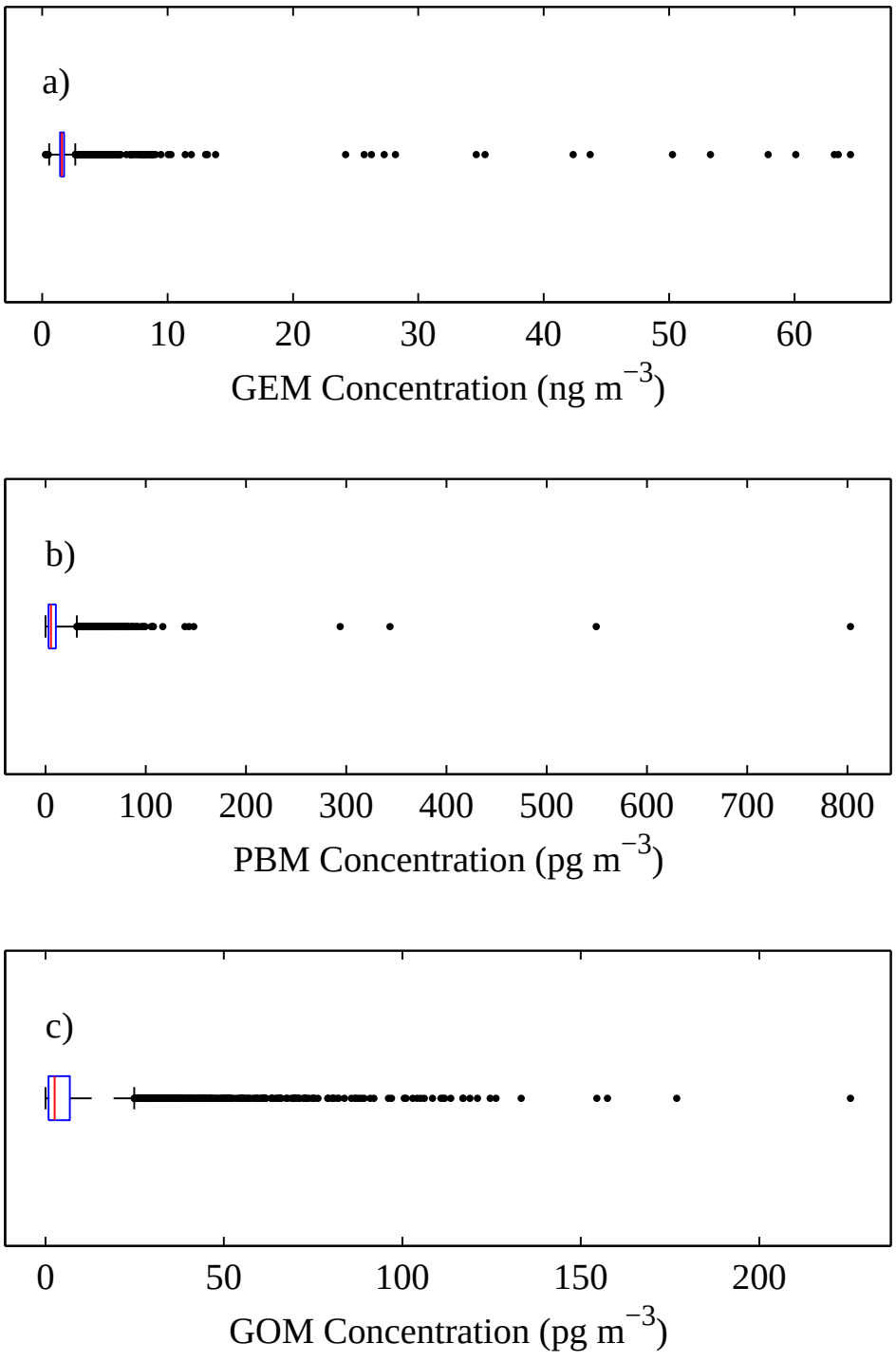

Figure 3.4: Box plots for a) GEM, b) PBM, and c) GOM measured at the UT96 site from July 2009 through June 2011. The blue box encompasses data between the quartiles, and the red line is the median. The whiskers have a maximum length of 3*IQR, and outliers beyond the whiskers are plotted individually.

Table 3.1: Statistical summary of the atmospheric mercury speciation data collected at the UT96 site from 1 July 2009 through 30 June 2011.

	GEM ($\mathrm{ng\ m^{-3}}$)	PBM ($\mathrm{pg\ m^{-3}}$)	GOM ($\mathrm{pg\ m^{-3}}$)
Number of Data Points*	111674§	4901	4894
Minimum	0.25	0.0	0.0
Maximum	64.47	803.2	225.6
Half Percentile ($q_{0.005}$)	1.01	0.0	0.0
Lowest Decile ($q_{0.10}$)	1.31	1.8	0.0
Lower Quartile ($q_{0.25}$)	1.44	3.3	0.9
Median ($q_{0.5}$)	1.58	5.7	2.6
Upper Quartile ($q_{0.75}$)	1.74	10.3	6.9
Upper-Most Decile ($q_{0.9}$)	1.92	19.7	18.1
99.5 Percentile ($q_{0.995}$)	2.92	82.0	96.1
Mean ($\overline{x}$)	1.62	9.9	7.2
Trimean	1.58	6.3	3.2
Spread (IQR)	0.3	7.0	6.0
Standard Deviation (s)	0.62	19.5	14.2
MAD	0.15	3.0	2.1
Skewness Coefficient (γ)*	61.6	20.8	5.0
Y-K Index*	0.05	0.3	0.4

*These are the only rows that do not have units of mercury concentration.
§There are more GEM data points because 24 GEM data points are typically measured in any 3-hour time period while only one PBM data point and one GOM data point are measured during that time.

GEM comprised 98.4% of atmospheric mercury using average concentrations on a year of data in Quebec, Canada. The median concentrations of GEM, PBM and GOM at UT96 were 1.58 $\mathrm{ng\ m^{-3}}$, 5.7 $\mathrm{pg\ m^{-3}}$ and 2.6 $\mathrm{pg\ m^{-3}}$, respectively. A year of speciated mercury concentration observations in Quebec, Canada yielded median concentrations of 1.61 $\mathrm{ng\ m^{-3}}$, 9 $\mathrm{pg\ m^{-3}}$ and 1 $\mathrm{pg\ m^{-3}}$, for GEM, PBM and GOM, while the maximum observed concentrations were 10.4 $\mathrm{ng\ m^{-3}}$, 1527 $\mathrm{pg\ m^{-3}}$ and 387 $\mathrm{pg\ m^{-3}}$, respectively (Poissant et al., 2005).

GEM has the overall greatest variability, as it has the largest MAD. Table 3.1 also demonstrates the non-Gaussian nature of the data for all three species via the skewness coefficients and Y-K indices, which would be zero under Gaussian conditions. In addition, the means and medians have the same value under Gaussian conditions, and this is not the

case in the mercury data. Of the three mercury species measured at UT96, GOM is most strongly skewed to the right, as shown by the Y-K indices.

Approximately 3% of all GEM data points are classified as enhancement events with concentrations > 2.2 $\mathrm{ng\ m^{-3}}$ (Abbott et al., 2008). Abbott et al. (2008) defined an enhancement event as "a measured concentration that exceeds trans-Pacific, coastal U.S. concentrations, suggesting possible local or regional source input." Mean concentrations of PBM and GOM observed at various rural locations in the U.S. are generally below 10 $\mathrm{pg\ m^{-3}}$ (e.g., Caldwell et al., 2006; Abbott et al., 2008; Liu et al., 2010). A comparison of UT96 data with both rural (Dexter) and urban (Detroit) sites in Michigan (Liu et al., 2010) is shown in Table 3.2. With regards to GEM, UT96 appears to be between rural and urban, although the maximum concentration measured at UT96 is more than double that seen in Detroit, Michigan. UT96 is also between rural and urban with regard to PBM. GOM concentrations at UT96 are closer to those observed in Dexter than Detroit. Overall, UT96 can be characterized as a moderately urban site.

Table 3.2: Comparison of UT96 data with similar rural (Dexter, MI) and urban (Detroit, MI) speciated mercury data measured by Liu et al. (2010).

	minimum*	median	maximum*	% Above NH pool
rural GEM ($\mathrm{ng\ m^{-3}}$)	0.26	1.47	14.82	(not given)
UT96 GEM ($\mathrm{ng\ m^{-3}}$)	0.25	1.58	64.47	29
urban GEM ($\mathrm{ng\ m^{-3}}$)	0.36	2.09	25.60	84
rural PBM ($\mathrm{pg\ m^{-3}}$)	1.2	4.8	90.6	(not given)
UT96 PBM ($\mathrm{pg\ m^{-3}}$)	0.0	5.7	803.2	56
urban PBM ($\mathrm{pg\ m^{-3}}$)	1.1	9.7	1345.2	75
rural GOM ($\mathrm{pg\ m^{-3}}$)	1.2	1.2	121.7	(not given)
UT96 GOM ($\mathrm{pg\ m^{-3}}$)	0.0	2.6	225.6	32
urban GOM ($\mathrm{pg\ m^{-3}}$)	1.1	6.8	2472.9	62

*For PBM and GOM, Liu et al. (2010) replaced below-detection values with one half of the MDLs, which were 2.2 $\mathrm{pg\ m^{-3}}$ and 2.4 $\mathrm{pg\ m^{-3}}$ for urban and rural sites, respectively. This was not done for the UT96 data.

3.2 Seasonal Patterns

Although the vast majority of total atmospheric mercury is in the form of GEM during every season (Table 3.3), each species of mercury undergoes statistically significant seasonal variations (Figs. 3.5-3.8). GEM concentrations are highest in the winter and decrease in each subsequent season to reach a minimum during the fall (Fig. 3.5a). The KW test shows GEM in every season is statistically different from every other season (Fig. 3.5b) at the 95% confidence level. To reduce serial correlation problems for the KW test, the GEM data were pruned to 3 hours (see Section 2.3.4).

The GEM concentrations are ~7% lower in fall than they are during winter. The high winter GEM coincides with stagnant air conditions caused by persistent surface temperature inversions. Relatively high winter GEM concentrations have also been observed in Shenandoah National Park, Virginia (Converse et al., 2010) and Reno, Nevada (Stamenkovic et al., 2007). GEM concentrations were also higher during winter than spring in Dexter, Michigan (Lynam and Keeler, 2005). This seasonality contrasts with that observed in Michigan and Idaho where GEM concentrations were observed to be slightly higher during summer than other seasons (Abbott et al., 2008; Liu et al., 2010).

PBM concentrations are highest during winter and lowest during the spring with moderate concentrations in the summer and fall (Fig. 3.6a). All of the PBM seasonal comparison pairs are statistically different using the KW test at the 95% confidence level with the exception of fall versus summer (Fig. 3.6b). The wintertime PBM median concentration is about twice that of spring. The relatively low springtime PBM concentrations most likely result from the scavenging of particles by precipitation (Fig. 3.7). Elevated winter

Table 3.3: Percent of total Hg comprised by each species separated by season.

	GEM (%)	PBM (%)	GOM (%)
Winter (DJF)	99.4	0.5	0.1
Spring (MAM)	99.6	0.3	0.2
Summer (JJA)	99.3	0.3	0.4
Fall (SON)	99.4	0.4	0.2

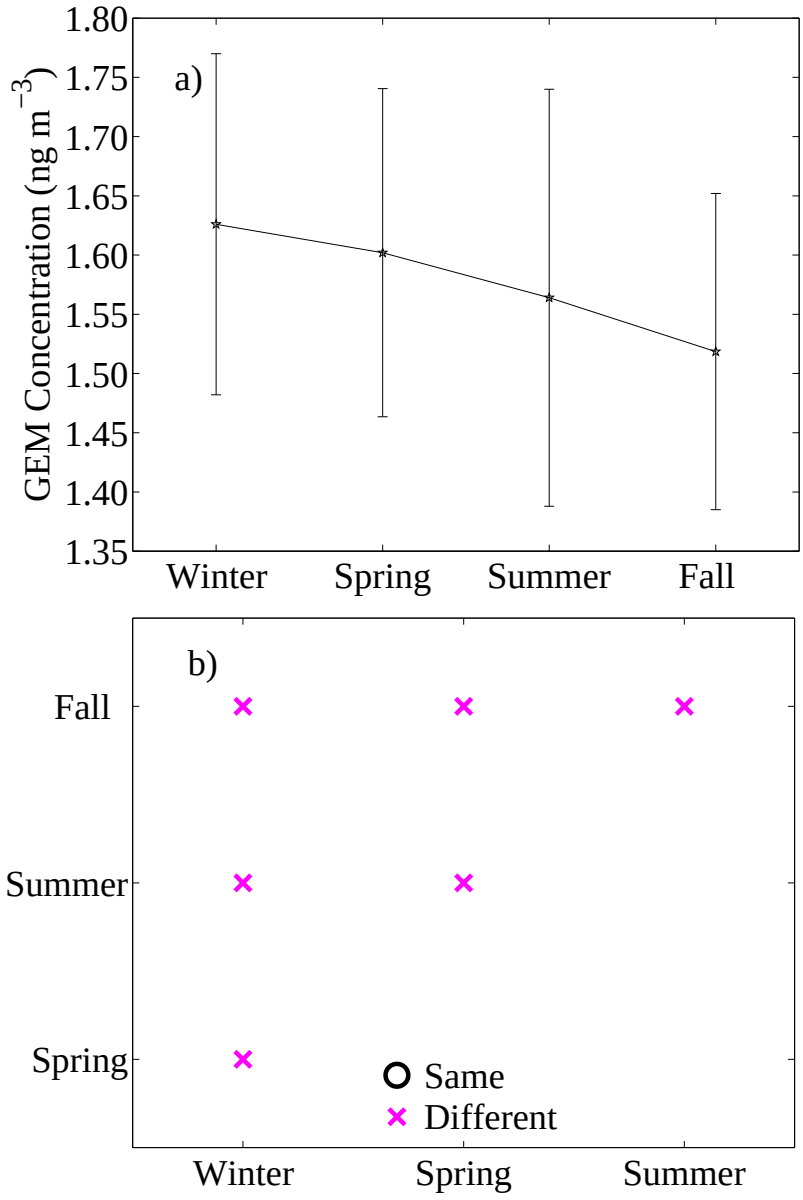

Figure 3.5: Seasonal GEM concentrations for 1 July 2009 through 30 June 2011. a) medians with MAD error bars, and b) results of the KW test.

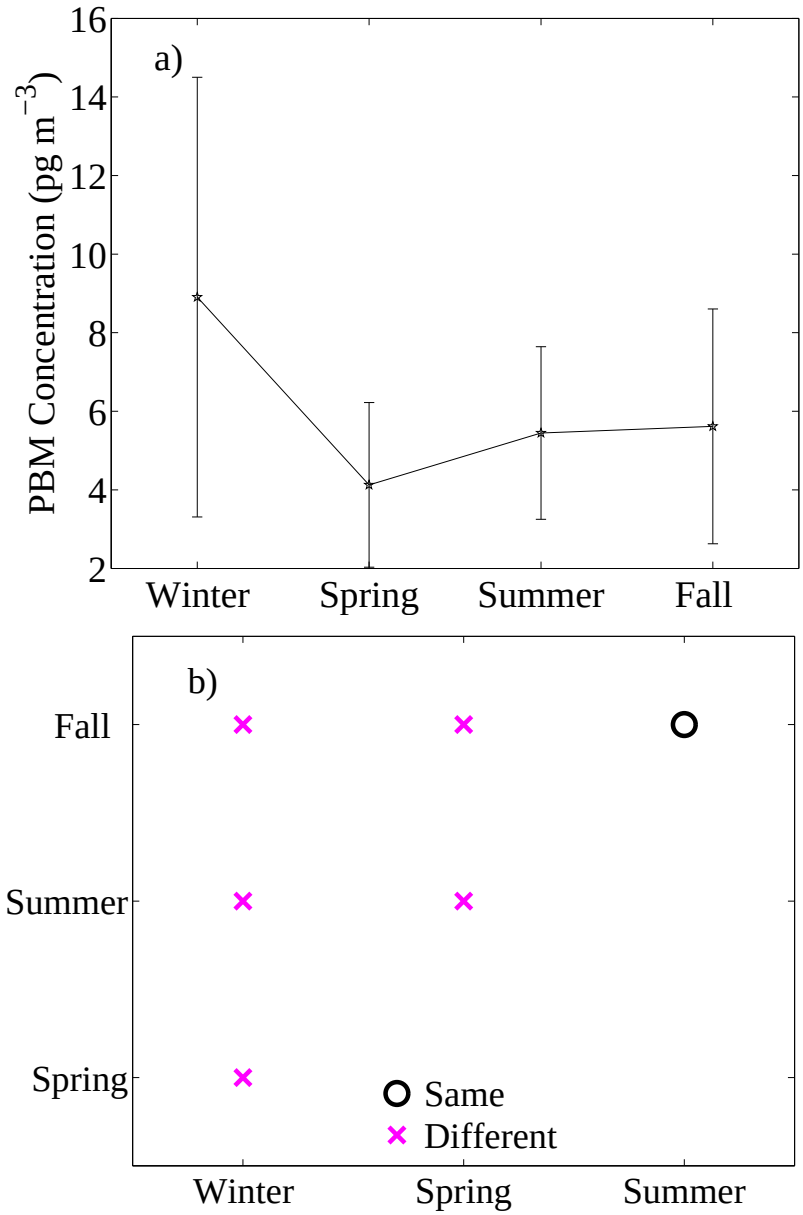

Figure 3.6: Seasonal PBM concentrations for 1 July 2009 through 30 June 2011. a) medians with MAD error bars, and b) results of the KW test.

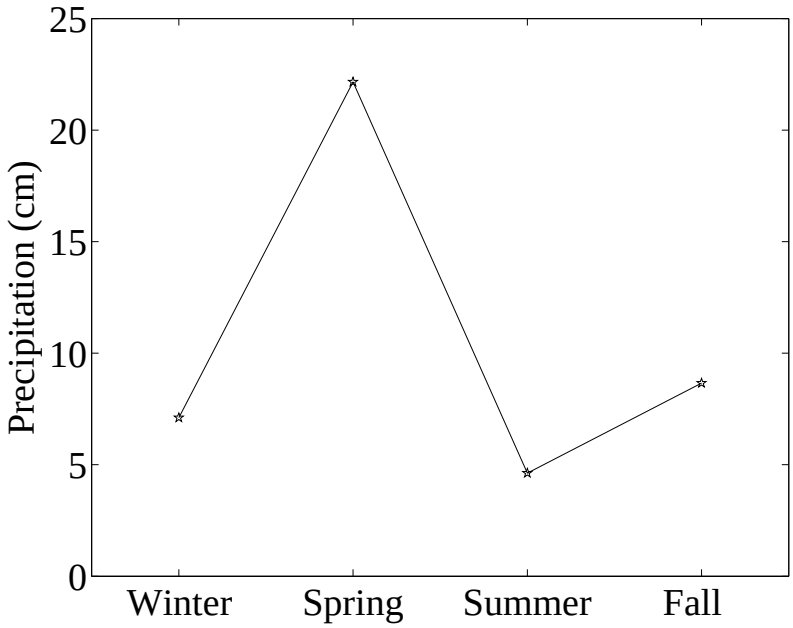

Figure 3.7: Seasonal precipitation observed at the KHIF weather station on Hill Air Force Base 1 July 2009 to 30 June 2011.

PBM has also been observed in Japan (Sakata and Asakura, 2007), Michigan (Liu et al., 2010), and near the Chesapeake Bay (Mason et al., 1997). This is thought to be due to temperature-dependent adsorption or condensation of GOM and GEM onto atmospheric particles (Sakata and Asakura, 2007). The elevated winter concentrations may also be due to "increased production of electricity from coal and heating activities" (Liu et al., 2010). Poissant et al. (2005) also suggested that some high winter concentrations could be related to house heating or other combustion facilities. In contrast, southern Florida, which does not have strong seasonal temperature variations, did not exhibit strong seasonal variability for PBM (Guentzel et al., 2001).

GOM has a very distinctive summer maximum and winter minimum (Fig. 3.8a). All of the GOM seasonal comparison pairs are statistically different at the 95% confidence level using the KW test (Fig. 3.8b). The summertime GOM median concentration is ~6 times greater than that of winter. Elevated summer GOM has also been observed in southern Florida (Guentzel et al., 2001), Michigan (Liu et al., 2010), and Idaho (Abbott et al.,

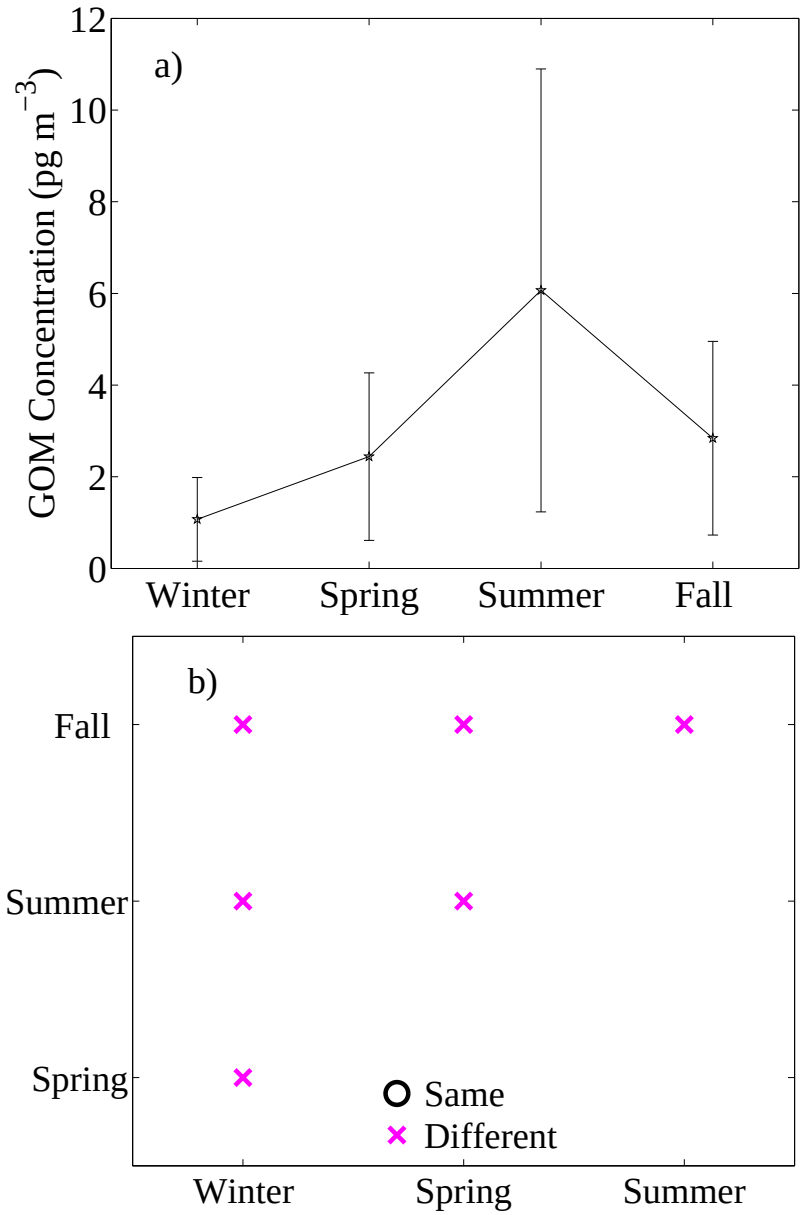

Figure 3.8: Seasonal GOM concentrations for 1 July 2009 through 30 June 2011. a) medians with MAD error bars, and b) results of the KW test.

2008). Poissant et al. (2005) observed high concentrations during winter in southern Quebec, Canada and suggested that they could be related to house heating or other combustion facilities. The high summertime GOM concentrations most likely result from the chemical transformation of GEM to GOM (Liu et al., 2010). Abbott et al. (2008) also suggest that photochemistry is involved in the production of GOM. Elevated summer GOM concentrations could also result from entrainment of free tropospheric air, which has higher GOM concentrations, into the boundary layer (Swartzendruber et al., 2006; Weiss-Penzias et al., 2009).

3.3 Diurnal Patterns

All three mercury species have statistically significant diurnal patterns (Figs. 3.9-3.11). GEM has relatively constant concentrations from about 2200 to 0700 MST and then dips by ~9% during the afternoon with the minimum occurring around 1600 MST (Fig. 3.9a). For GEM, 71% of the comparison pairs are statistically different from one another at the 95% confidence level using the KW test after pruning the data (Fig. 3.9b). If 0% of the comparison pairs were statistically different, there would be no diurnal variation, and if 100% of the comparison pairs were statistically different, that would indicate that every 3-hour time block of the day is statistically different from every other 3-hour time block. The afternoon dip in GEM concentration could result from the conversion of GEM to GOM and/or PBM or from the enhancement of dry deposition during the more turbulent afternoon period. It is also possible that ambient air over the lake has lower concentrations of GEM, and this is transported to UT96 by the lake breeze during the afternoon. Caldwell et al. (2006) observed no discernible diurnal pattern for GEM in south central New Mexico.

The PBM diurnal variation is similar to that of GEM with relatively constant concentrations from about 2200 to 1000 MST (Fig. 3.10a) and a minimum occurring at 1600 MST. For PBM, only 46% of the comparison pairs were statistically different from one another (Fig. 3.10b). The afternoon decrease in PBM is ~25%, which is larger than that

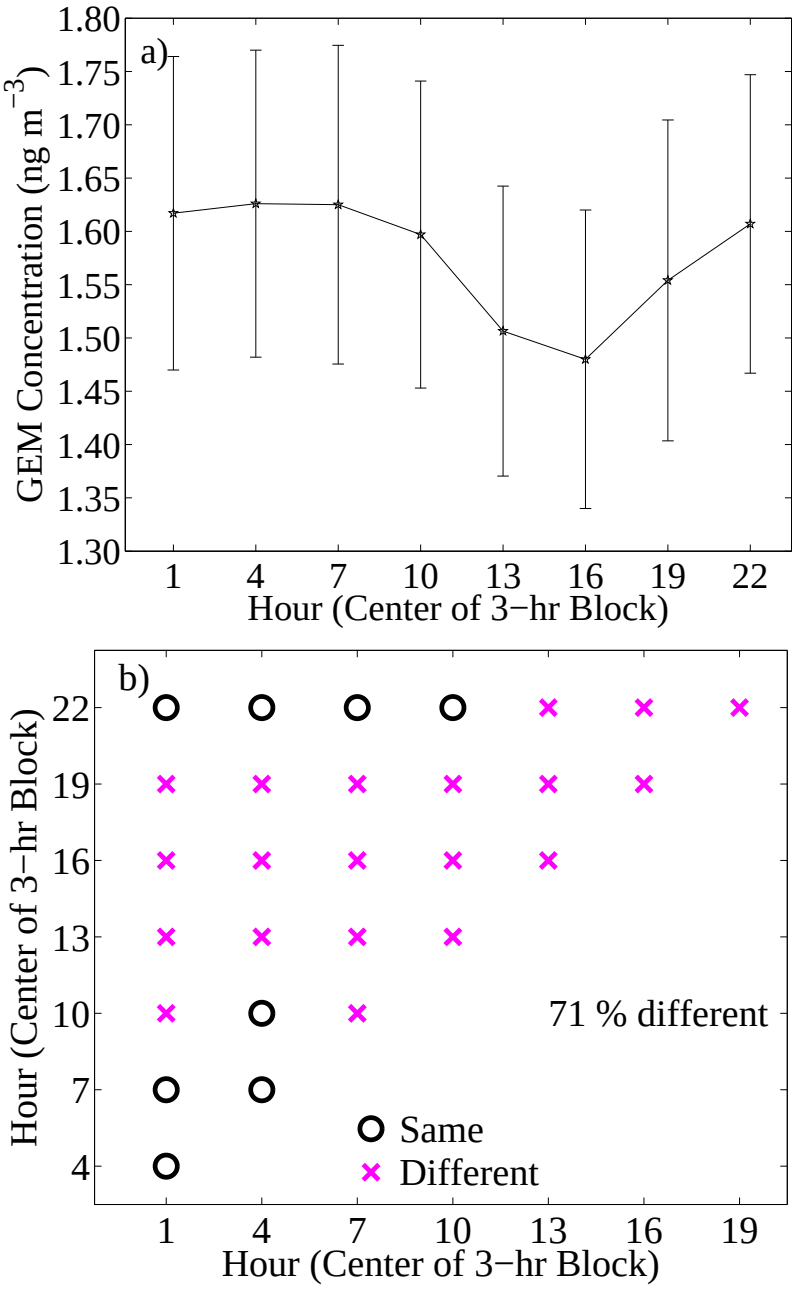

Figure 3.9: Diurnal GEM concentrations for 1 July 2009 through 30 June 2011. a) medians with MAD error bars, and b) results of the KW test. The time stamp on a given datum denotes the end of the adsorption period.

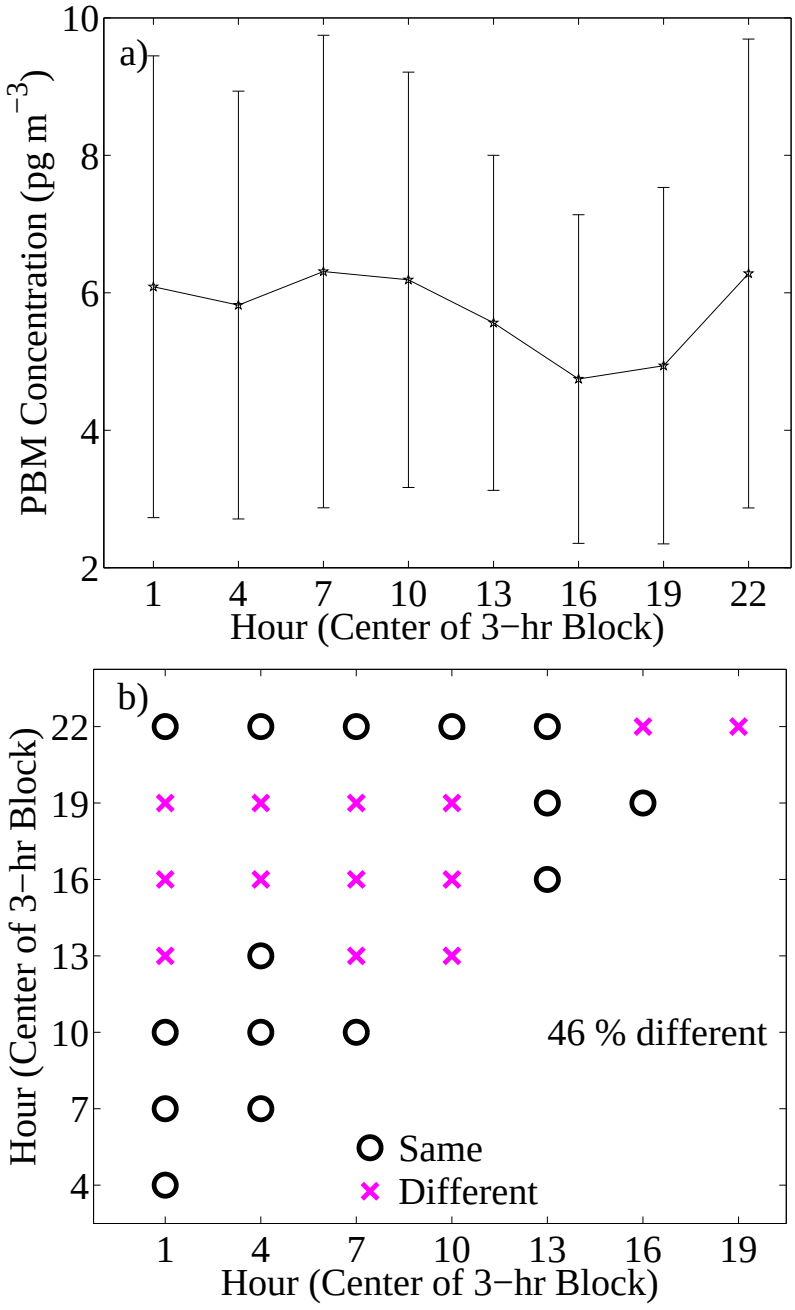

Figure 3.10: Diurnal PBM concentrations for 1 July 2009 through 30 June 2011. a) medians with MAD error bars, and b) results of the KW test. The time stamp on a given datum denotes the end of the adsorption period. Three-hour medians (based on the time stamp) were used for the diurnal analysis to match the data collection schedule of the Tekran detector. There is some overlap among the bins. For example, data points with an adsorption period from 03:00-5:00 will be in the 04:00 time bin, while data with an adsorption period from 04:00-6:00 will be in the 07:00 time bin.

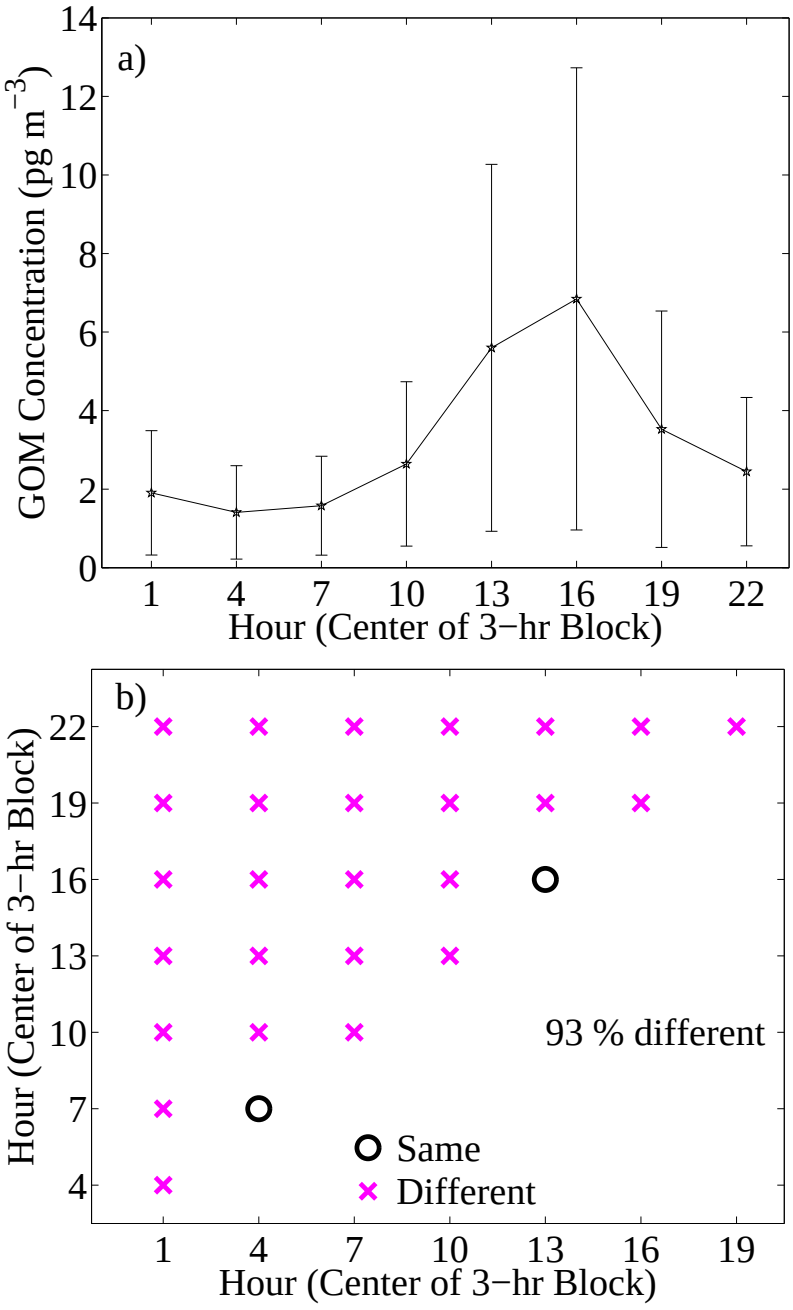

Figure 3.11: Diurnal GOM concentrations for July 1, 2009 through June 30, 2011. a) medians with MAD error bars, and b) results of the KW test. The time stamp on a given datum denotes the end of the adsorption period. Three-hour medians (based on the time stamp) were used for the diurnal analysis to match the data collection schedule of the Tekran detector. There is some overlap among the bins. For example, data points with an adsorption period from 03:00-5:00 will be in the 04:00 time bin while data with an adsorption period from 04:00-6:00 will be in the 07:00 time bin.

of GEM. Conversion of PBM to GOM could contribute to the dip in PBM. However, no known studies have investigated this potential conversion. Afternoon conversion of PBM to GEM seems unlikely given that GEM also exhibits an afternoon dip. This would be quite difficult to observe given that the change in PBM concentration (~0.002 $\mathrm{ng\ m^{-3}}$) is so small relative to GEM concentrations. The afternoon dip in PBM concentrations could be from enhancement of dry deposition during the more turbulent afternoon period. If air over the lake has less PBM than air over the land, then the lake breeze could be contributing to the afternoon dip in PBM as well. This result contrasts with the diurnal pattern observed in Quebec, Canada, which had an afternoon peak in concentration which correlated with solar radiation and wind speed (Poissant et al., 2005). Caldwell et al. (2006) observed no discernible diurnal pattern for PBM in south central New Mexico.

GOM has a very different diurnal pattern (Fig. 3.11a) from GEM and PBM with the daily maximum at 1600 MST and a minimum in the early morning hours (i.e., 0400-0700 MST). The 1600 MST peak median GOM concentration is nearly 5 times larger than the 0400 MST median concentration. For GOM, 93% of the comparison pairs were statistically different from one another (Fig. 3.11b), indicating that the diurnal pattern in GOM is stronger than it is for either GEM or PBM. This diurnal pattern is consistent with observations in Michigan (Lynam and Keeler, 2005; Liu et al., 2010), Quebec, Canada (Poissant et al., 2005), and Storm Peak Laboratory, Colorado (Fain et al., 2009). Abbott et al. (2008) observed daytime high concentrations of GOM and nighttime lows during summer in Idaho. Caldwell et al. (2006) observed the lowest GOM concentrations at night in south central New Mexico, which they suggested could be due to either local photochemistry in the boundary layer or entrainment of free tropospheric air during daytime growth of the boundary layer. Liu et al. (2010) attributed the pattern primarily to photochemical oxidation of GEM. Near the shore of the Dead Sea, Israel, daytime high GOM concentrations were observed concurrently with high BrO concentrations, GEM depletion events, and low ozone concentrations. Obrist et al. (2010) concluded that the BrO was likely causing the

GEM to convert to GOM, and attributed the lack of mass balance between the declines in GEM and increases in GOM to rapid deposition of GOM. The proximity of the UT96 site to the GSL and the persistent afternoon lake breeze creates a possibility that halogen species, such as Br, enhance the GEM transformation to GOM.

3.4 Diurnal Patterns by Season

Since GEM, PBM, and GOM all exhibit both seasonal and diurnal variations, it is reasonable to expect that the diurnal patterns may vary by season as well. Figure 3.12 shows the median speciated mercury concentrations by hour of day and month. This figure is only intended for visualization purposes, while results from the KW statistical tests are shown in Figures 3.13-3.15. Figures 3.13-3.15 are analogous to Figures 3.9-3.11, except that the data has been broken down by season and instead of showing the result of the KW test for each comparison pair (all of the 3-hour time blocks), only the percent of the comparison pairs that were statistically different from one another are presented.

GEM tends to have a relative minimum during the afternoon for spring through fall (Fig. 3.12a). The contours in Figure 3.12a represent the lower decile, the quartiles, and the median. This pattern has the largest amplitude in the summer (Fig. 3.13b). GEM does not exhibit a diurnal pattern during winter. GEM was pruned for the seasonal diurnal statistics tests, and Figure 3.13a-b shows pruned data. During spring and summer, 71% of comparison pairs are statistically different, while 39% of comparison pairs were statistically different during fall (Fig. 3.13b). No comparison pairs are statistically different during winter. Figure 3.12a suggests that February was a particularly high month for GEM. Figure 3.12a was not pruned because it was not used for statistical tests. GEM exhibits the most coherent diurnal pattern during spring and summer when there is an overnight plateau followed by an afternoon dip (Fig. 3.13a). A similar pattern exists during fall, but with a smaller amplitude. The seasonality of the afternoon dip is consistent with the hypotheses that GEM photochemically converts to GOM and that increased dry deposition occurs

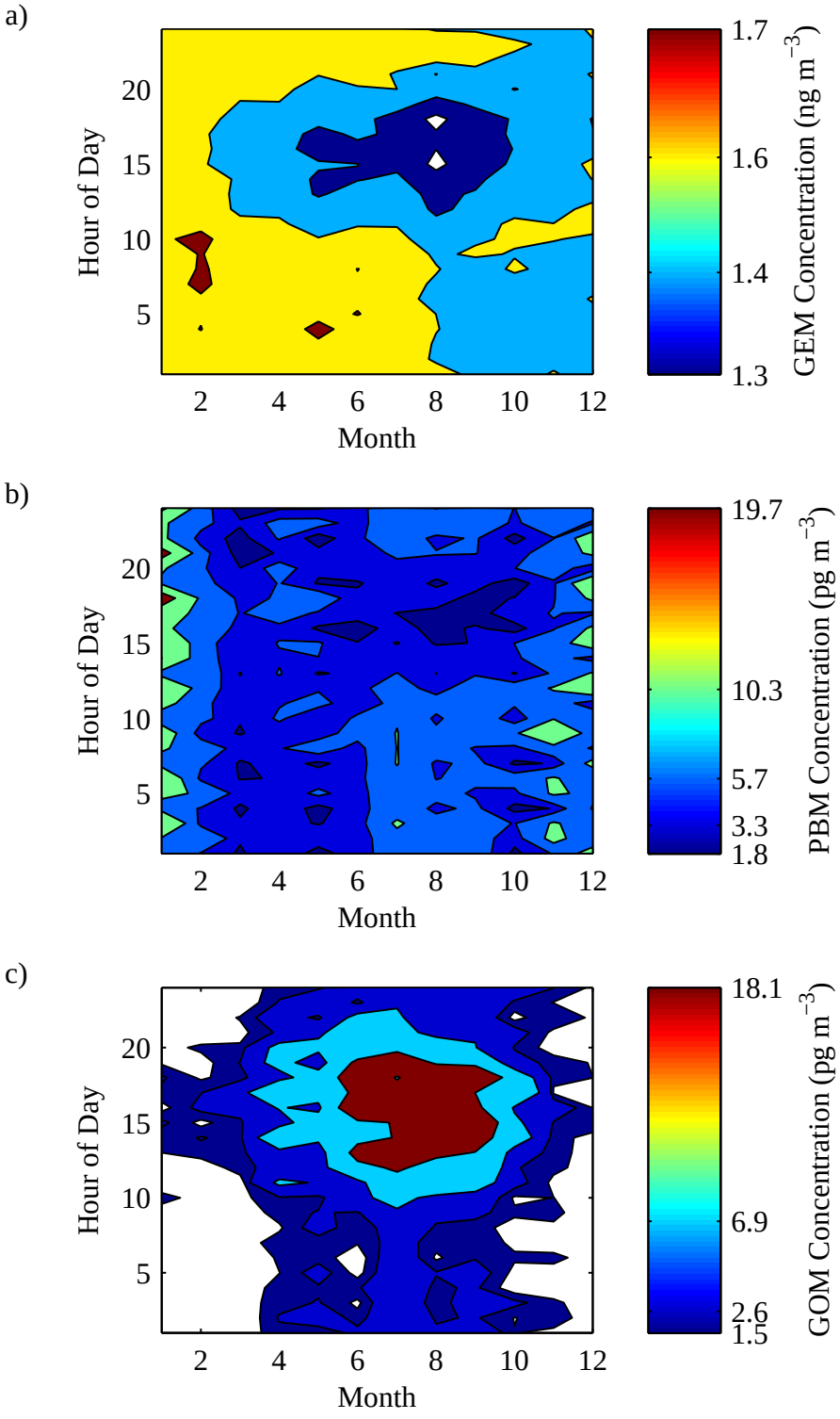

Figure 3.12: Monthly diurnal pattern in 1-hour time blocks for a) median GEM, b) median PBM, and c) median GOM concentrations.

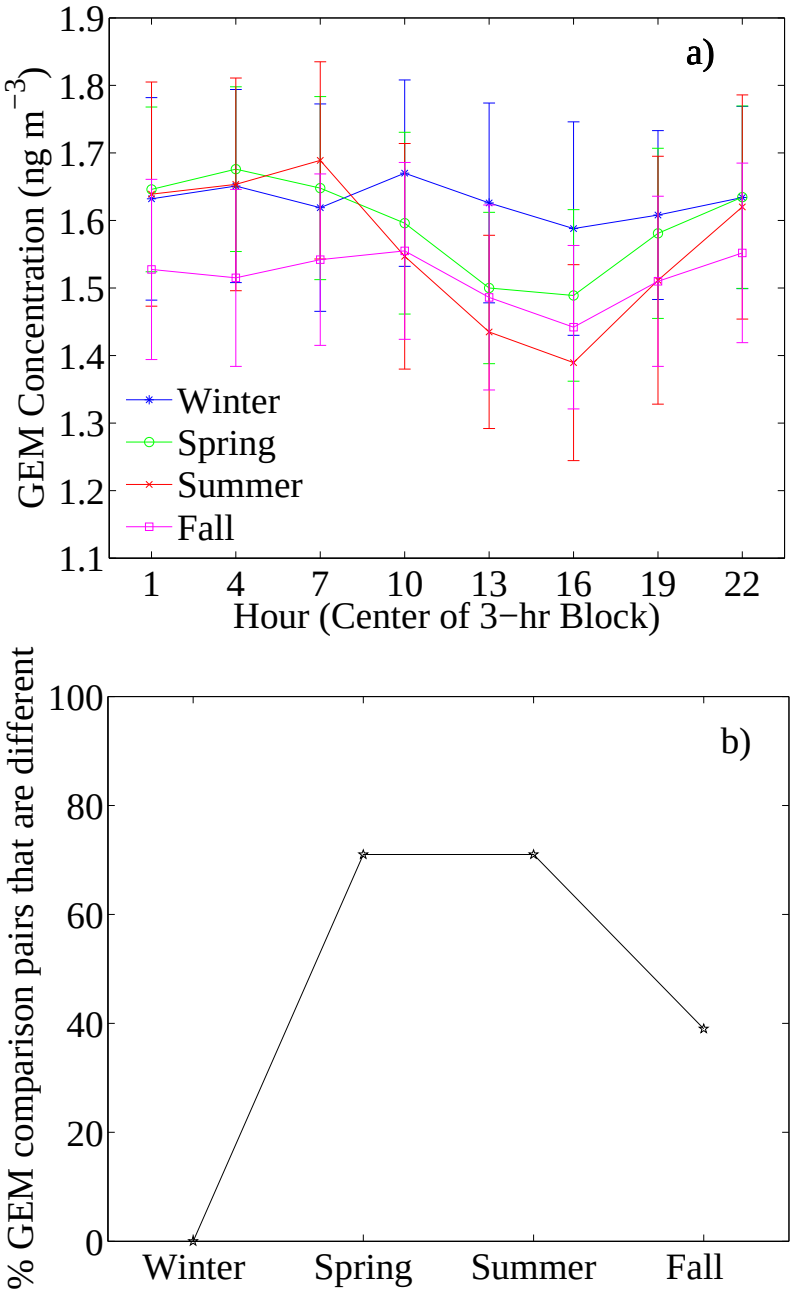

Figure 3.13: Seasonal diurnal pattern of (pruned) GEM concentrations for 1 July 2009 through 30 June 2011. a) medians with MAD error bars (3-hour blocks), and b) shorthand results of the KW test.

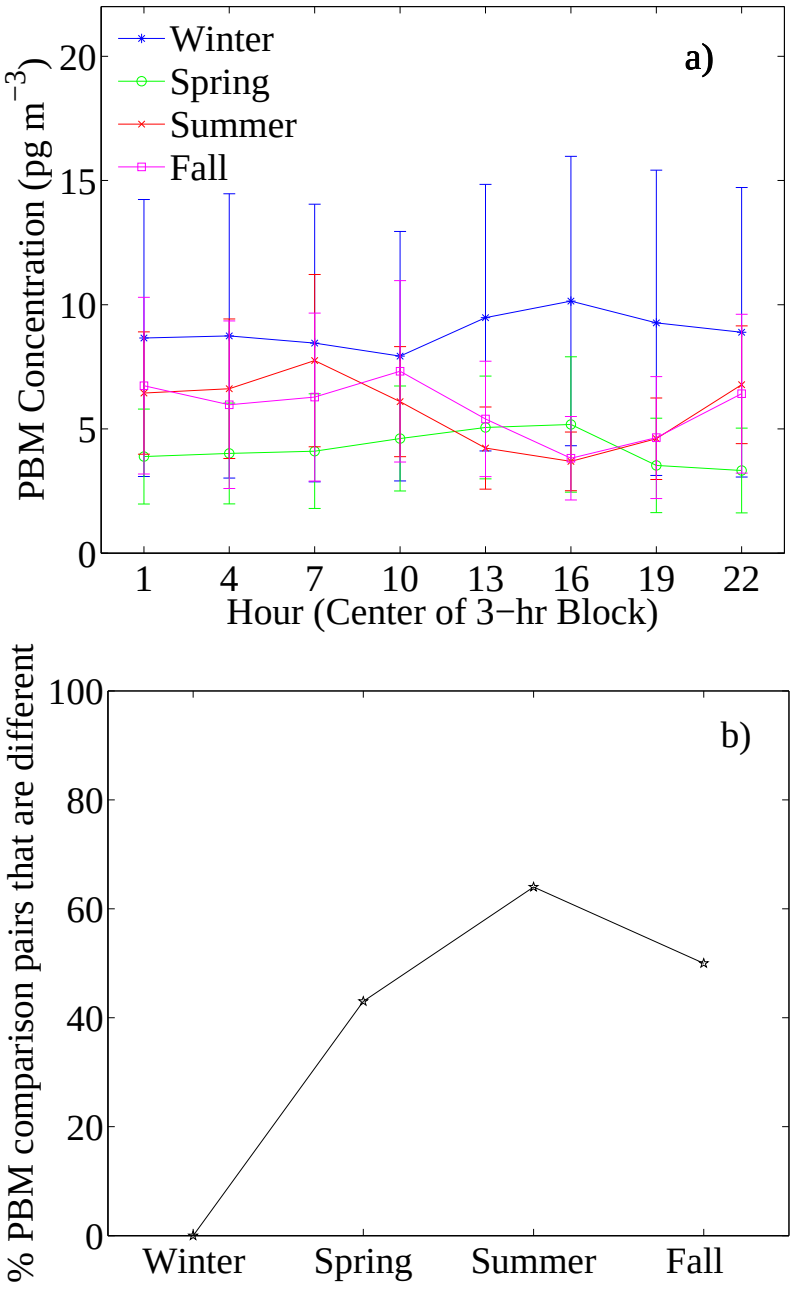

Figure 3.14: Seasonal diurnal pattern of PBM concentrations for 1 July 2009 through 30 June 2011. a) median with MAD error bars (3-hour blocks), and b) shorthand results of the KW test.

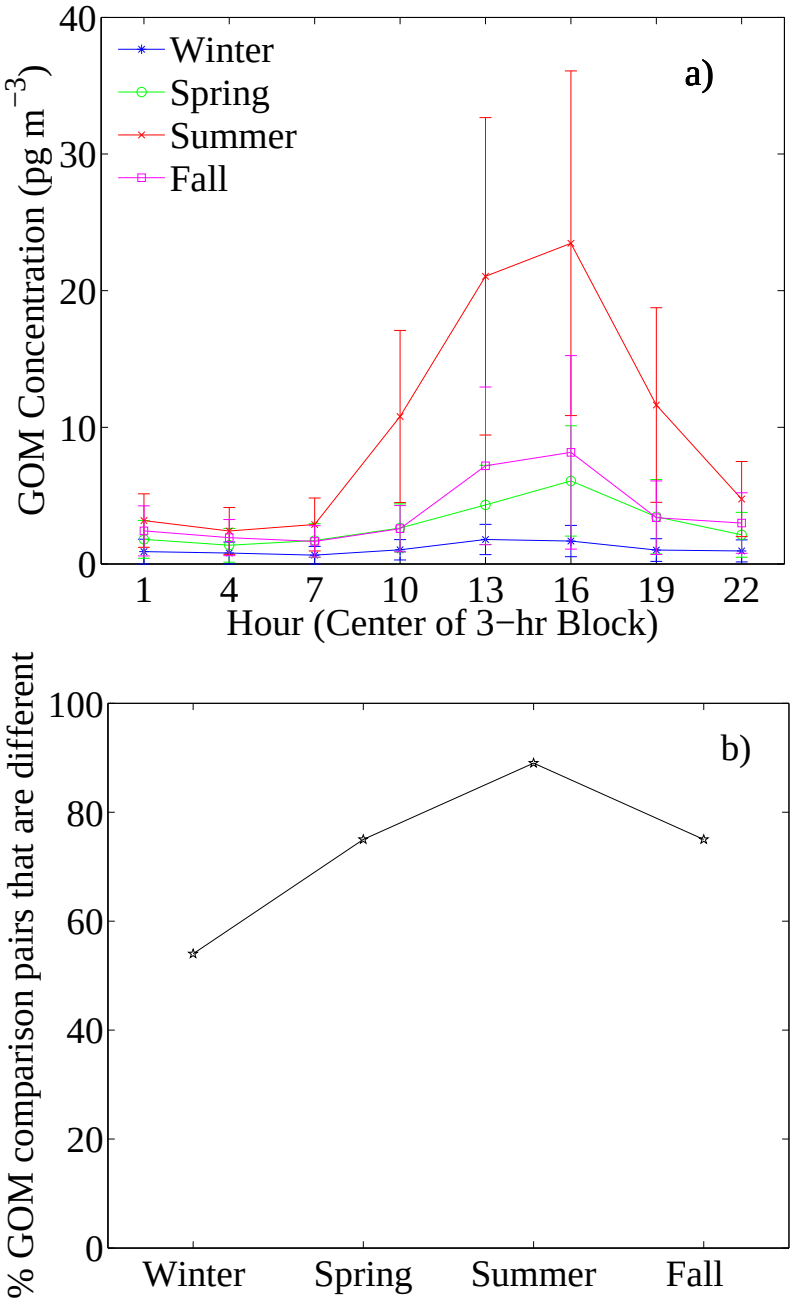

Figure 3.15: Seasonal diurnal pattern of GOM concentrations for 1 July 2009 through 30 June 2011. a) median with MAD error bars (3-hour blocks), and b) shorthand results of the KW test.

during the afternoon due to increased turbulence.

Relative to GEM and GOM, PBM has weak diurnal patterns by month (Fig. 3.12b). The contours in Figure 3.12b represent the upper and lower deciles, the quartiles, and the median. PBM exhibits the most coherent and strongest diurnal pattern during summer, resembling a sinusoidal curve (3.14a) with a peak around 0700 MST and a minimum around 1600 MST. The summer PBM diurnal pattern is statistically significant with 64% of the comparison pairs being statistically different in the KW test (Fig. 3.14b). Spring and fall PBM exhibited a weaker diurnal pattern with 43% and 50% of the comparison pairs being statistically different, respectively. Winter exhibited no diurnal pattern with all of the comparison pairs being statistically the same. This pattern is most consistent with the hypothesis that PBM is more effectively removed from the atmosphere by dry deposition during the turbulent afternoons of the warmest months.

GOM exhibits a distinct diurnal and monthly pattern (Fig. 3.12c). The contours in Figure 3.12c represent the MDL, median, upper quartile, and upper decile. GOM shows strong seasonal variations in the diurnal pattern throughout the year (Fig. 3.15a). The results of the KW test for the various seasons range between 54% (winter) and 89% (summer) of the comparison pairs being statistically different from one another (Fig. 3.15b). Median GOM is 5 $\mathrm{pg\ m^{-3}}$ or lower from about 2200 to 0700 MST throughout the year. GOM then increases after 0700 MST to peak around 1600 MST. The amplitude of this midday increase in GOM depends strongly on season. During fall through spring, the median diurnal peak is < 10 $\mathrm{pg\ m^{-3}}$. Summer GOM is quite remarkable with a median diurnal peak > 20 $\mathrm{pg\ m^{-3}}$. The seasonality of the diurnal pattern is consistent with the hypotheses that GEM photochemically converts to GOM or that entrainment of higher concentration GOM from above the boundary layer (e.g., Swartzendruber et al., 2006; Weiss-Penzias et al., 2009).

3.5 Extreme Events

A cursory examination of extreme events (both high and low) may provide insight into processes that either increase or decrease speciated mercury concentrations. This is not intended as a rigorous statistical analysis, but rather as a guide to topics that may be of interest for future research. An "extreme event" is arbitrarily defined as the collection of mercury concentration data points on any given day that are at or above the 99.5 percentile for high events or at or below the 0.5 percentile or the MDL for low events.

3.5.1 Extreme GEM Events

The 99.5 percentile corresponds to a GEM concentration of 2.92 $\mathrm{ng\ m^{-3}}$. At least one high GEM event has occurred during every month from July 2009 through June 2011, except during July 2009 and April 2011 (Tables 3.4-3.5). The longest event occurred on 22 July 2010 and lasted 11 hours. Abbott et al. (2008) observed most of their enhancement events (above 2.2 $\mathrm{ng\ m^{-3}}$) in Idaho during spring and summer. The median length of enhancement events in Idaho was 5 hours, while several lasted 14-21 hours during stable air flow. The 0.5 percentile corresponds to a GEM concentration of 1.01 $\mathrm{ng\ m^{-3}}$. Low GEM events have occurred during every season (Tables 3.6- 3.7). The longest low GEM events occurred during 3-5 August 2009 and 13 January, 2011 each lasting for more than 8 hours. There are seven calendar days in the GEM data set during which both high and low GEM events occurred: 3-4 and 12 August 2009, 18 December 2009, 28 April 2010, 30 May 2010, and 22 August 2010. Also, several high and low GEM events have occurred on consecutive days. The close temporal proximity of high and low GEM events may be of interest for future research to investigate whether the high and low events are related to one another and what physical mechanisms would drive such large swings in GEM concentrations.

High GEM events have occurred throughout the day, but high events are least common during the late afternoon (Fig. 3.16a). Low GEM events, in contrast, exhibit a quasi-

Table 3.4: High GEM events 1-40 (99.5%, i.e. above 2.92 $\mathrm{ng\ m^{-3}}$) for the first two years of data at the UT96 site.

Event #	Year	Month	Day	Duration	# Data Points	Peak Hg $(\mathrm{ng\ m^{-3}})$
1	2009	August	2	19:05 - 19:05	1	3.58
2			3	22:15 - 22:15	1	3.28
3			4	22:35 - 22:35	1	3.05
4			12	22:25 - 23:20	2	3.11
5		September	15	21:05 - 21:05	1	3.10
6		October	3	07:55 - 08:00	2	3.15
7			17	01:15 - 03:00	22	3.97
8		November	13	02:10 - 12:00	17	13.18
9			28	11:00 - 11:00	1	3.43
10		December	3	20:55 - 20:55	1	3.27
11			6	08:15 - 08:35	5	4.75
12			8	03:25 - 09:35	4	4.21
13			18	10:05 - 16:15	9	4.11
14			22	16:15 - 20:40	16	3.91
15			29	13:00 - 13:55	3	3.24
16	2010	January	1	18:30 - 18:30	1	3.26
17			11	18:15 - 22:25	24	3.16
18			12	07:20 - 13:30	25	3.43
19			15	20:05 - 23:55	26	3.21
20			16	00:00 - 03:00	23	3.52
21			17	21:15 - 23:35	15	3.40
22			18	17:35 - 18:35	13	4.42
23		February	3	15:05 - 21:00	5	3.30
24			6	18:15 - 22:10	20	3.48
25			7	16:55 - 17:00	2	3.85
26			10	17:05 - 17:15	3	3.42
27			11	04:45 - 17:30	30	3.46
28		March	24	09:15 - 09:30	4	3.82
29		April	2	00:35 - 00:35	1	3.23
30			13	23:05 - 23:05	1	3.04
31			28	01:35 - 01:35	1	2.97
32		May	8	12:15 - 12:30	4	3.71
33			9	06:15 - 07:15	12	3.93
34			10	21:15 - 21:25	3	4.31
35			11	02:00 - 02:00	1	3.27
36			16	23:05 - 23:05	1	2.99
37			28	03:20 - 03:25	2	3.24
38			30	03:20 - 04:35	16	4.30
39		June	3	22:55 - 22:55	1	2.92
40		July	15	19:40 - 19:40	1	3.45

Table 3.5: High GEM events 41-77 (99.5%, i.e. above 2.92 $\mathrm{ng\ m^{-3}}$) for the first two years of data at the UT96 site.

Event #	Year	Month	Day	Duration	# Data Points	Peak Hg $(\mathrm{ng\ m^{-3}})$
41	2010	July	18	23:35 - 23:55	5	6.14
42			19	00:00 - 01:25	4	5.05
43			21	23:15 - 23:55	8	64.47
44			22	00:05 - 11:55	72	50.27
45			30	20:50 - 20:50	1	3.04
46		August	2	22:40 - 22:45	2	3.24
47			8	19:50 - 19:55	2	4.49
48			22	07:30 - 08:25	5	4.09
49			23	07:15 - 09:00	9	4.96
50		September	17	21:15 - 21:20	2	3.39
51			19	22:45 - 23:00	4	4.65
52		October	22	09:15 - 09:55	9	4.01
53			24	06:30 - 06:45	4	4.39
54			31	17:45 - 17:45	1	3.63
55		November	1	08:25 - 09:15	10	5.30
56			4	09:25 - 09:25	1	3.04
57			5	09:25 - 09:25	1	2.96
58			8	22:35 - 22:35	1	3.14
59			25	00:15 - 01:15	13	5.22
60		December	2	13:20 - 13:50	4	3.18
61			3	02:40 - 12:00	4	2.99
62			10	11:00 - 11:00	1	3.01
63			18	14:45 - 14:55	3	3.32
64			20	17:45 - 18:20	4	3.23
65	2011	January	16	14:55 - 15:15	5	4.06
66			20	12:30 - 13:15	7	7.12
67			24	09:55 - 09:55	1	3.23
68			25	12:00 - 12:05	2	3.68
69		February	11	17:50 - 18:55	11	3.55
70			12	18:25 - 18:55	7	5.62
71			14	18:25 - 18:25	1	3.09
72		March	29	10:15 - 23:15	14	6.10
73			30	04:35 - 05:00	6	3.62
74		May	9	05:15 - 05:15	1	3.03
75		June	14	19:45 - 23:15	9	3.81
76			19	00:50 - 00:55	2	3.00
77			23	20:45 - 20:45	1	3.12

Table 3.6: Low GEM events 1-40 (0.5%, i.e. below 1.01 $\mathrm{ng\ m^{-3}}$) for the first two years of data at the UT96 site.

Event #	Year	Month	Day	Duration	# Data Points	Minimum Hg $(\mathrm{ng\ m^{-3}})$
1	2009	July	21	15:10 - 15:10	1	0.96
2		August	3	11:05 - 19:45	86	0.74
3			4	10:20 - 20:45	96	0.68
4			5	06:05 - 15:30	6	0.94
5			6	13:10 - 18:40	2	0.99
6			12	13:55 - 16:55	6	0.98
7			19	12:53 - 13:03	3	0.76
8		November	6	11:15 - 11:15	1	1.00
9		December	17	18:15 - 18:15	1	0.97
10			18	03:35 - 09:35	9	0.25
11			24	20:25 - 21:15	11	0.32
12			25	09:00 - 09:15	4	0.68
13			26	22:55 - 22:55	1	1.00
14			28	07:15 - 07:35	5	0.79
15			30	16:15 - 16:15	1	0.99
16	2010	January	2	20:15 - 20:40	6	0.55
17			3	09:10 - 09:20	3	0.70
18			5	22:15 - 22:25	3	0.73
19		April	27	21:15 - 22:55	4	0.84
20			28	00:15 - 00:15	1	0.99
21			30	16:55 - 16:55	1	0.99
22		May	26	12:40 - 17:00	6	0.89
23			29	17:00 - 20:20	9	0.91
24			30	13:20 - 18:45	25	0.91
25			31	12:20 - 18:40	32	0.85
26		June	8	19:20 - 19:20	1	0.91
27			19	11:25 - 17:55	13	0.92
28		August	3	13:20 - 16:45	7	0.93
29			5	15:35 - 19:55	5	0.93
30			6	13:15 - 19:55	9	0.91
31			7	11:00 - 17:35	24	0.67
32			11	10:20 - 10:20	1	0.98
33			15	18:20 - 18:25	2	1.00
34			16	15:20 - 16:00	7	0.81
35			21	17:30 - 17:35	2	0.95
36			22	11:30 - 11:30	1	1.00
37			25	15:05 - 18:50	15	0.88
38			26	14:40 - 16:00	7	0.68
39		September	4	14:50 - 15:50	5	0.91
40			6	15:25 - 21:30	3	0.99

Table 3.7: Low GEM events 41-54 (0.5%, i.e. below 1.01 $\mathrm{ng\ m^{-3}}$) for the first two years of data at the UT96 site.

Event #	Year	Month	Day	Duration	# Data Points	Minimum Hg $(\mathrm{ng\ m^{-3}})$
41	2010	September	8	18:40 - 19:50	5	0.93
42			9	00:20 - 03:40	3	0.90
43			13	12:30 - 17:00	37	0.75
44		October	21	14:30 - 15:20	11	0.88
45		November	9	07:35 - 07:35	1	0.90
46	2011	January	10	15:15 - 19:45	20	0.84
47			13	11:15 - 19:40	20	0.75
48			14	13:15 - 15:00	21	0.37
49			15	14:20 - 14:35	3	0.93
50		February	27	17:05 - 17:40	4	0.98
51		March	8	11:40 - 11:40	1	0.96
52		April	27	15:25 - 15:25	1	1.00
53		May	21	12:25 - 12:45	5	0.32
54			24	16:55 - 16:55	1	1.00

Gaussian distribution centered on the late afternoon (Fig. 3.16b). Both the high and low event distributions are consistent with the diurnal pattern observed in Section 3.3.

The weather conditions during which high GEM events occurred are shown in Figures 3.17-3.18. The winds during high GEM events (Fig. 3.17) are consistent with the general winds observed at UT96 (Fig. 2.3). There does not appear to be a relationship between temperature and the likelihood of high GEM events, except that relatively few high GEM data points were measured while the temperature was in the 10-20$^{\circ}\mathrm{C}$ range (Figs. 2.6a and 3.18a). The histogram for RH during high GEM events (Fig. 3.18b) is similar to the histogram of two years of RH data at UT96 (Fig. 2.6a) except that there appears to be a deficit of high GEM events between roughly 60-80% RH. The histogram for solar radiation during high GEM events (Fig. 3.18c) is similar to the histogram of two years of solar radiation data at UT96 (Fig. 2.6c). There appears to be no relationship between high GEM events and dewpoint temperature (Figs. 2.6d and 3.18d). One possible explanation for the high GEM events is local anthropogenic sources. Abbott et al. (2008) observed that GEM enhancement events in Idaho were not associated with any particular type of weather, and concluded that the GEM enhancement events were likely coming

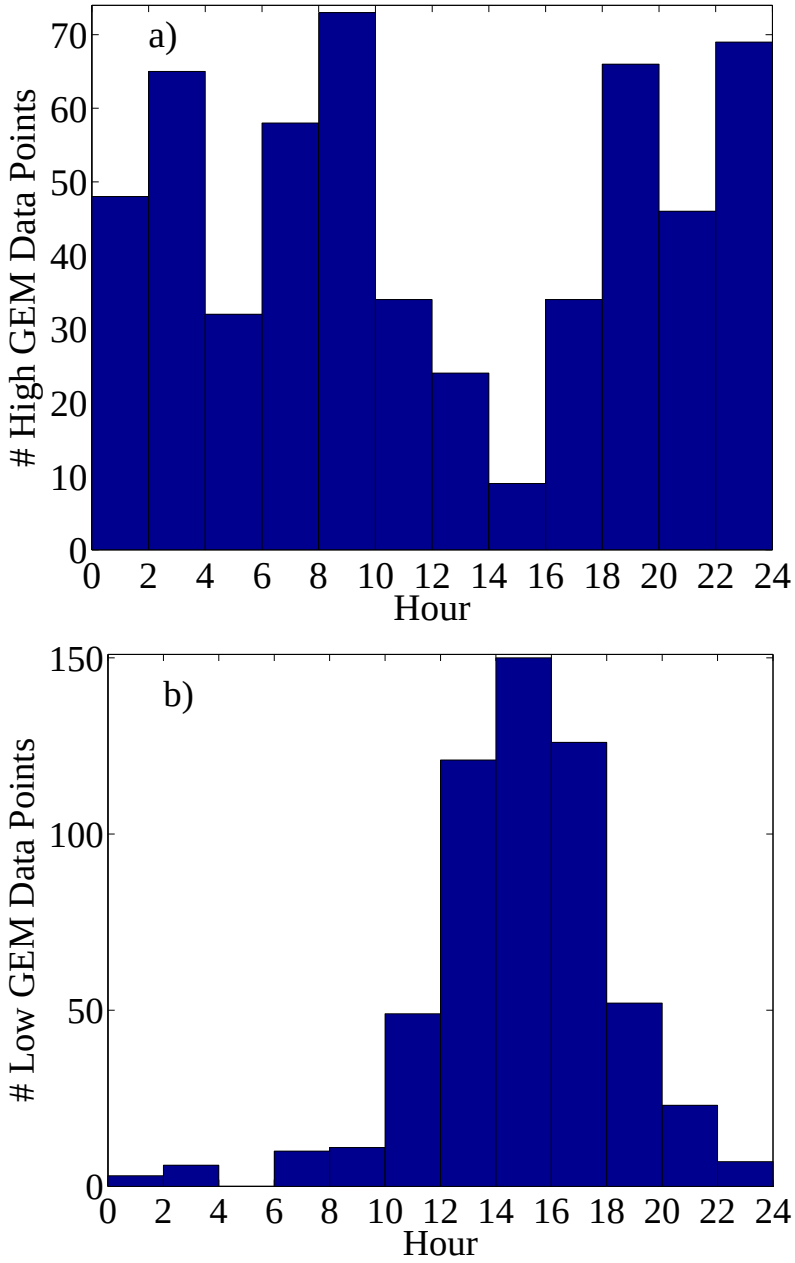

Figure 3.16: Histograms of the times of day for extreme GEM events with 2-hour time resolution: a) high GEM events, and b) low GEM events. Note: The timestamps represent the end of the adsorption period (i.e., the GEM was collected during the five minutes preceding the time stamp).

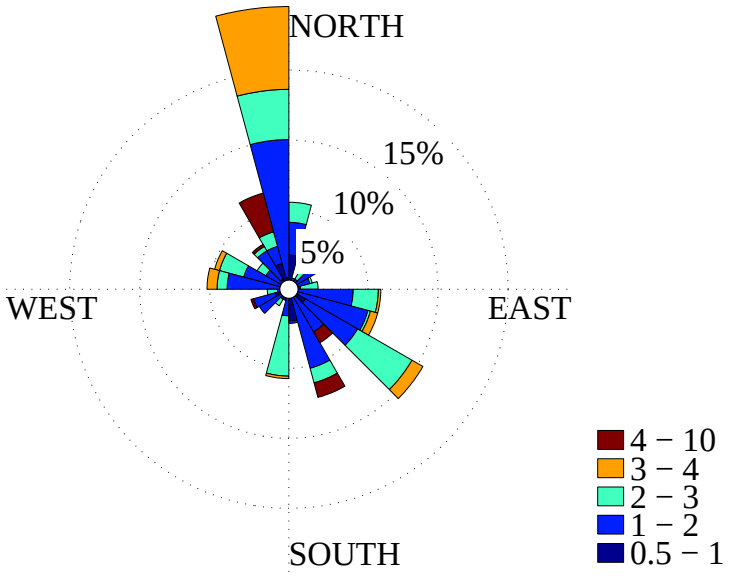

Figure 3.17: Wind rose (m s^{-1}) at the UT96 site for high GEM conditions.

from known anthropogenic and natural sources in the region, and possibly additional undocumented sources. The predominant source contributions in Idaho were from western Utah and northern Nevada (Abbott et al., 2008).

The weather conditions during which low GEM events occurred are shown in Figures 3.19-3.20. There is a deficit of low GEM events when the wind is coming from the east and south-east directions. This is not surprising because the closest urban areas are in that sector. The temperatures measured during low GEM events have a bimodal distribution (Fig. 3.20a), which is inconsistent with the overall temperature distribution at UT96 (Fig. 2.6a). There is only one low GEM data point measured while the temperature was between 2.5 °C and 13 °C. This suggests that multiple temperature-dependent processes promote low GEM, one of which could be photochemical conversion of GEM to GOM at high temperatures. Another could be adsorption onto atmospheric particles at low temperatures (conversion to PBM). The RH distribution measured during low GEM events (Fig. 3.20b) exhibits bimodality corresponding to the temperature distribution (Fig. 3.20a). There is no obvious relationship between solar radiation and low GEM events (Fig. 3.20c), except that

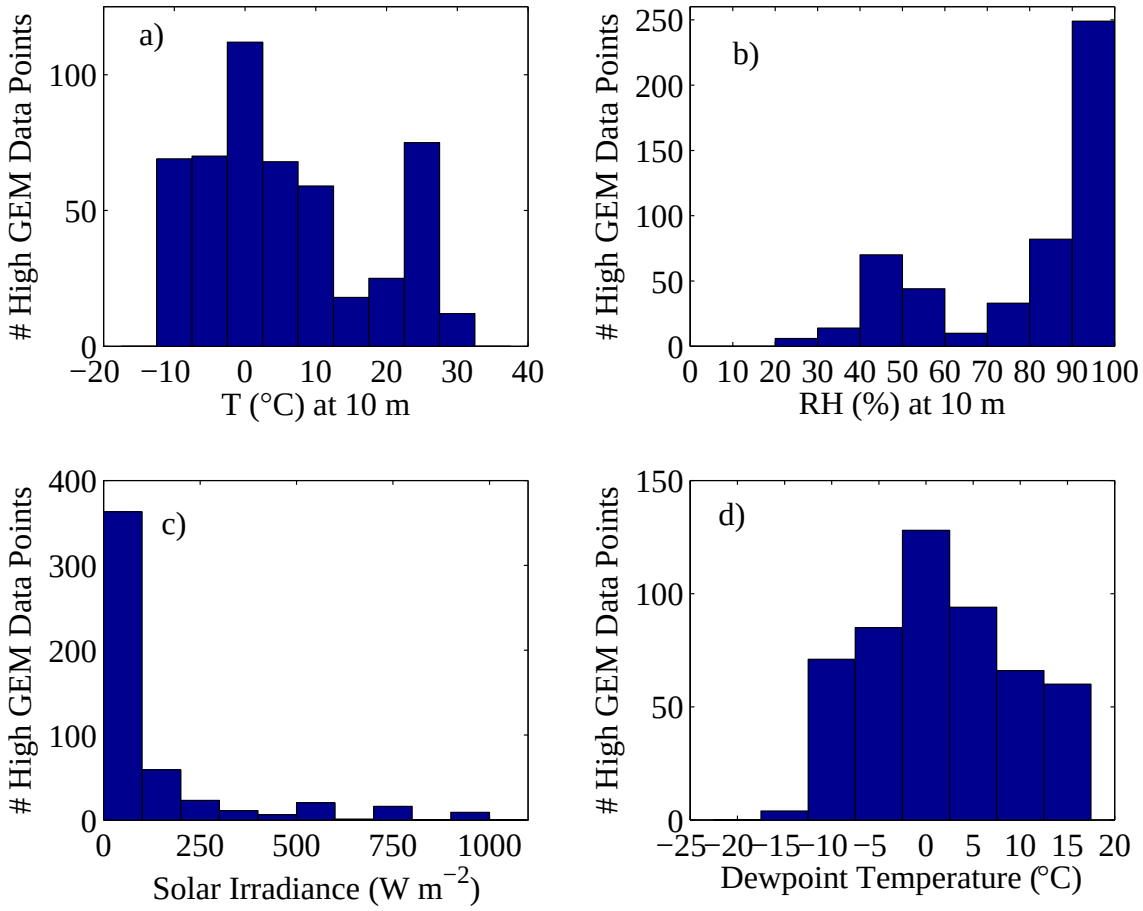

Figure 3.18: Histograms of the weather during high GEM data: a) temperature, b) relative humidity, c) solar radiation, and d) dewpoint temperature.

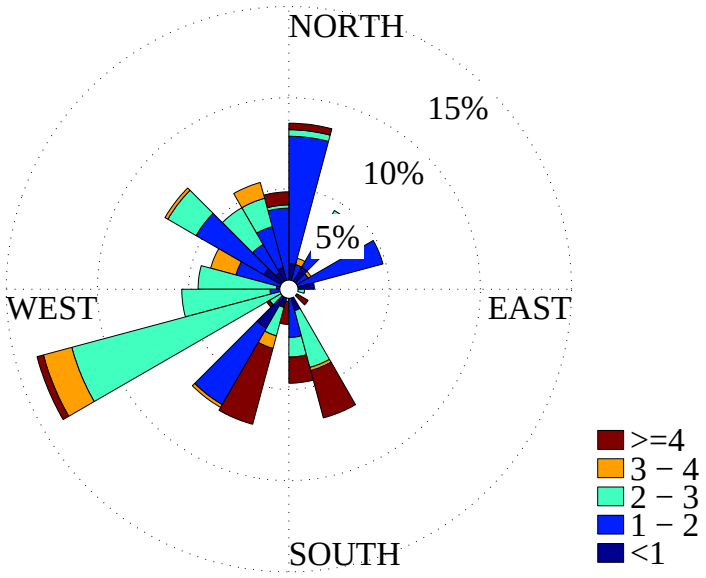

Figure 3.19: Wind rose (m s^{-1}) at the UT96 site for low GEM conditions.

there are not as many data points in the lowest bin as one might expect based on Figure 2.6c. The dewpoint temperature distribution observed during low GEM events (Fig. 3.20d) is generally consistent with the overall dewpoint temperature distribution (Fig. 2.6d), except that there are not as many data points near $0°C$ as one might expect. The results of this section are consistent with what might be expected if there were summertime conversion of GEM to GOM and wintertime conversion of GEM to PBM. The summertime GEM to GOM conversion is suggested by several variables: 1) the predominance of low GEM events during the afternoon, which is the time of day at which all high GOM events occur (see below), and 2) some low GEM events favor high temperature and low RH. The wintertime conversion of GEM to PBM is suggested by: 1) subfreezing mercury depletion events, and 2) high wintertime PBM.

3.5.2 Extreme PBM Events

The 99.5 percentile corresponds to a PBM concentration of 82.0 pg m^{-3}. The longest events occurred during January 2011 (Table 3.8). In addition, 8 of the 14 high PBM events

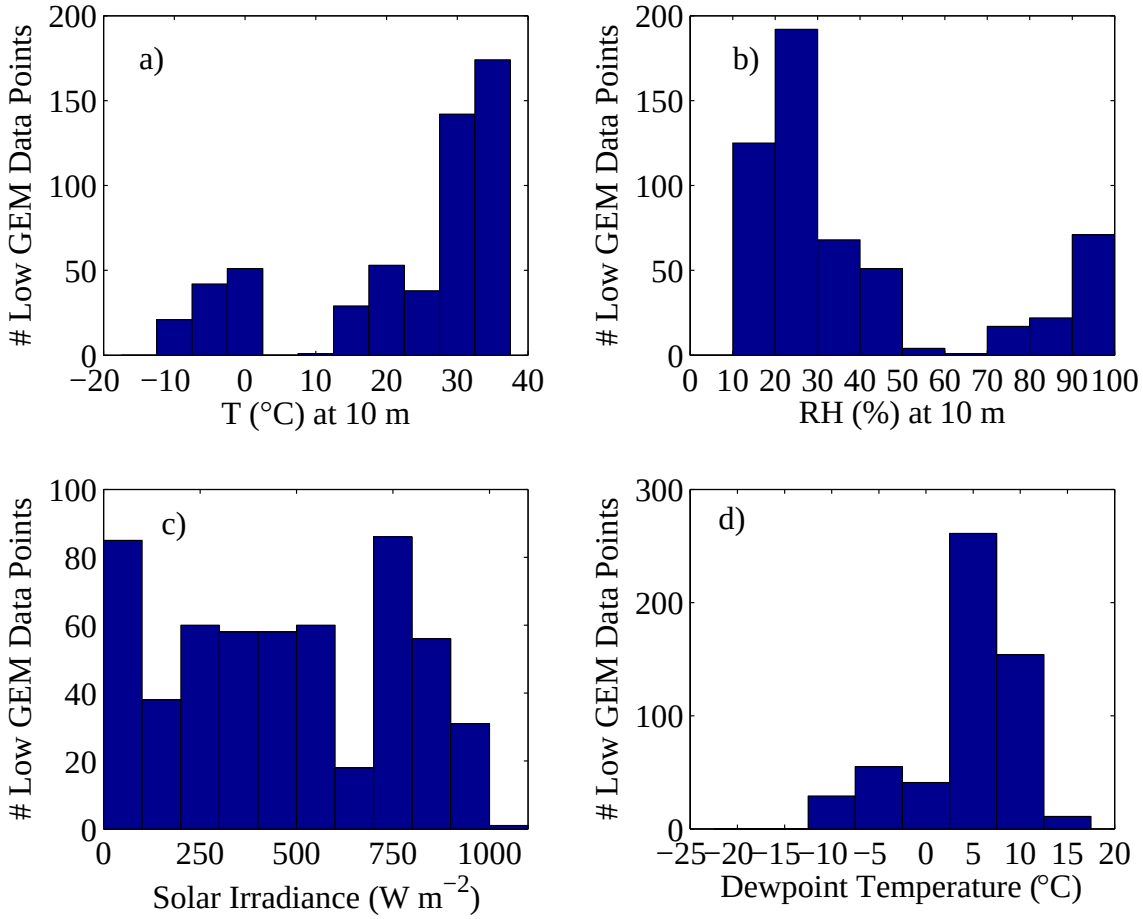

Figure 3.20: Histograms of the weather during low GEM data: a) temperature, b) relative humidity, c) solar radiation, and d) dewpoint temperature.

Table 3.8: High PBM events (99.5%, i.e. above 82.0 $\mathrm{pg\ m^{-3}}$) for the first two years of data at the UT96 site.

Event #	Year	Month	Day	Duration	# Data Points	Peak Hg $(\mathrm{pg\ m^{-3}})$
1	2009	December	30	03:00 - 03:00	1	88.3
2	2010	February	11	06:00 - 09:00	2	803.2
3		April	28	02:00 - 02:00	1	294.0
4		July	25	05:00 - 05:00	1	147.9
5		August	23	09:00 - 09:00	1	92.3
6		November	4	08:00 - 11:00	2	343.9
7	2011	January	4	20:55 - 23:55	2	98.3
8			5	02:55 - 23:55	3	99.5
9			10	17:00 - 20:00	2	143.3
10			12	14:00 - 14:00	1	97.2
11			13	09:00 - 15:00	3	95.5
12			14	21:00 - 21:00	1	86.8
13			15	03:00 - 22:00	3	139.1
14			16	01:00 - 04:00	2	117.1

observed during the two years of operation at UT96 occurred during January 2011. The 25 July 2010 event occurred the morning after a major fireworks holiday in Utah (Pioneer Day). It is worth noting that elevated PBM concentrations were observed overnight following each of the major fireworks holidays (Independence Day and Pioneer Day) during both 2009 and 2010. Comparing Tables 3.4-3.5 with Table 3.8 reveals that 5 of the 14 high PBM events occurred on the same calendar day as high GEM events (four of which were concurrent). Meanwhile, comparing Tables 3.6-3.7 and 3.8 shows that 6 of the 14 high PBM events occurred on the same calendar day as low GEM events (four of which were concurrent). Approximately 7% of all PBM data is below the MDL (1.5 $\mathrm{pg\ m^{-3}}$), so all of this data is considered to be low events. Low PBM data is included in this section, but a table is not included for brevity.

Neither the high nor low PBM events appear to favor any part of the day (Fig. 3.21). The weather conditions during which high PBM events occurred are shown in Figures 3.22-3.23. The winds during high PBM events (Fig. 3.22) are calm and do not appear to have a preferential direction. High PBM events appear to favor lower temperatures (Figs.

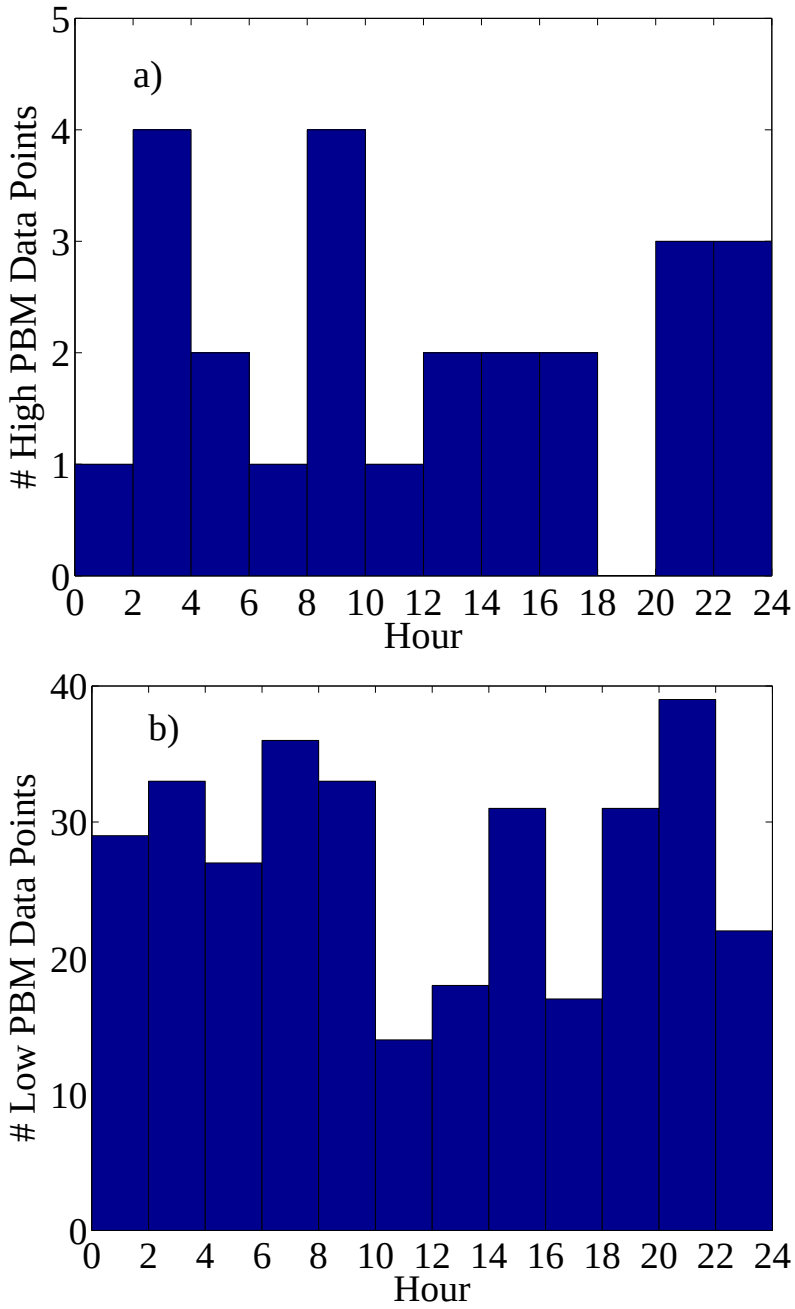

Figure 3.21: Histograms of the times of day for extreme PBM events with 2-hour time resolution: a) high PBM events and, b) low PBM events. It should be noted that (b) includes 7% of the entire PBM data set. The timestamps represent the end of the adsorption period (i.e., the PBM was collected during the two hours preceding the time stamp).

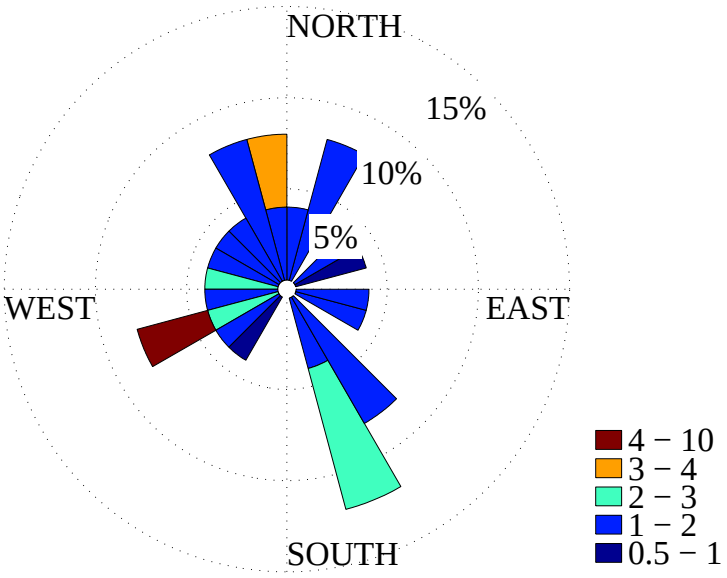

Figure 3.22: Wind rose (m s^{-1}) at the UT96 site for high PBM conditions.

2.6a and 3.23a), but high PBM events have occurred at a broad range of temperatures. In the histogram of two years of RH data at UT96 (Fig. 2.6b), the highest bin (RH close to 100%) is about twice the height of the other bins. In the histogram including only RH data during high PBM events (Fig. 3.23b), the highest bin is much more than twice the height of the other bins. In addition, no high PBM events have occurred while the RH was below 49%. Therefore, high PBM events tend to favor high RH. The histogram for solar radiation during high PBM events (Fig. 3.23c) is similar to the histogram of two years of solar radiation data at UT96 (Fig. 2.6c), except that no high PBM events have occurred while solar radiation was > 600 W m^{-2}. High PBM events slightly favor low dewpoint temperatures (Figs. 2.6d and 3.23d). Figure 3.23 is consistent with what might be expected if the sources of the high PBM events were predominantly local anthropogenic sources but may be influenced by RH. Perhaps high RH promotes adsorption of GEM and GOM onto aerosols to form PBM.

Low PBM events (below the MDL) represent approximately 7% of the entire PBM data set. The wind rose corresponding to the times of low PBM events (Fig. 3.24) is consistent

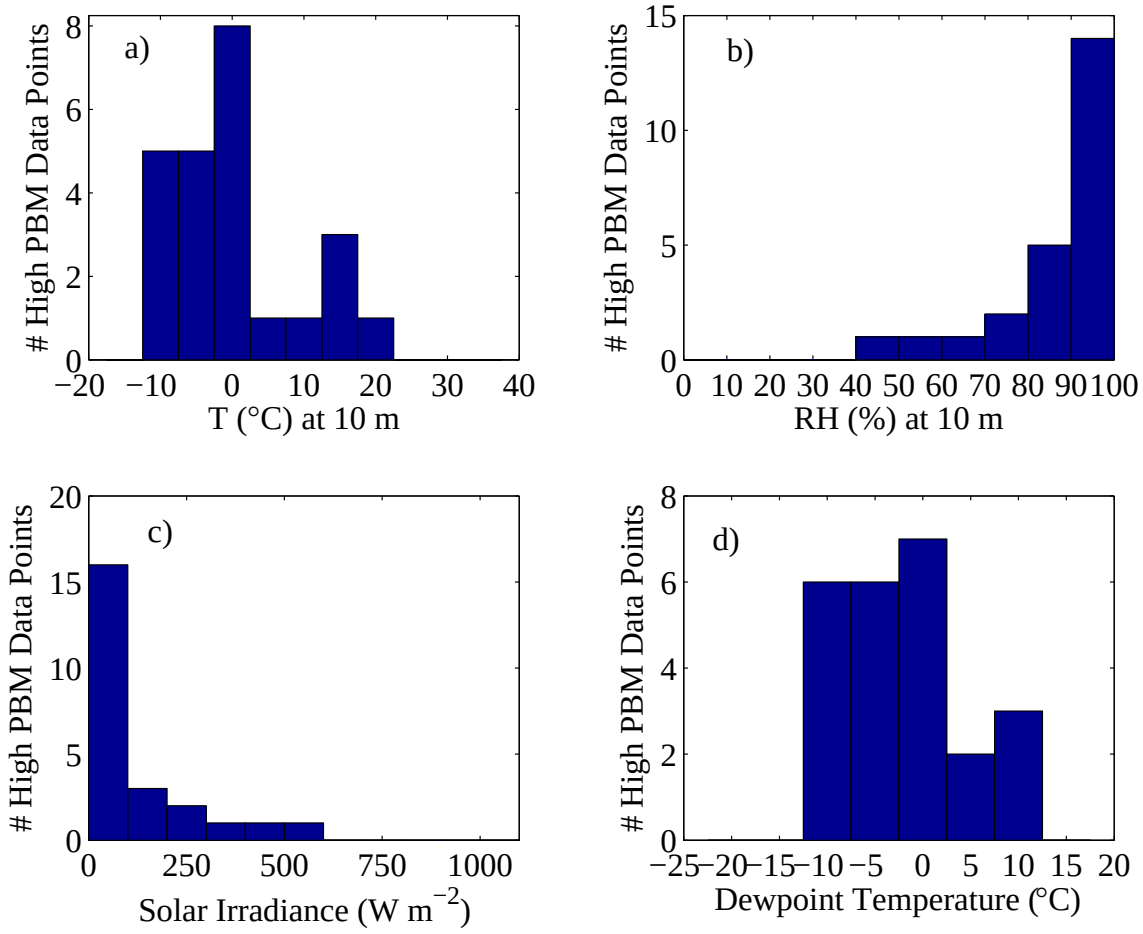

Figure 3.23: Histograms of the weather during high PBM data: a) temperature, b) relative humidity, c) solar radiation, and d) dewpoint temperature.

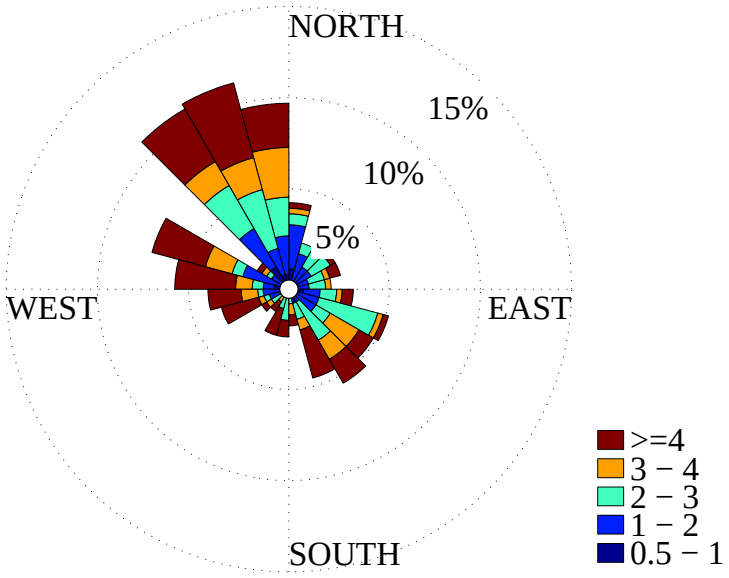

Figure 3.24: Wind rose (m s^{-1}) at the UT96 site for low PBM conditions.

with the overall wind rose (Fig. 2.3). Low PBM events have occurred during a broad range of temperatures (Fig. 3.25a). The RH distribution measured during low PBM events (Fig. 3.25b) is similar in shape to the overall RH distribution (Fig. 2.6b), but with relatively fewer data points below 70% RH. The solar radiation distribution measured during low PBM events (Fig. 3.25c) is very similar in shape to the overall solar radiation distribution (Fig. 2.6c). The dewpoint temperature distribution observed during low GEM events (Fig. 3.25d) and the overall dewpoint temperature distribution (Fig. 2.6d) both peak around 0°C and cover the range from roughly -20°C to 20°C. There is no striking relationship between the weather variables presented here and the occurrence of PBM concentrations below the MDL.

3.5.3 Extreme GOM Events

The 99.5 percentile corresponds to a GOM concentration of 96.1 pg m^{-3}. High GOM events have only occurred during the May-October months (Table 3.9). The highest concentration of GOM observed at UT96 is 225.6 pg m^{-3}, while the highest concentration

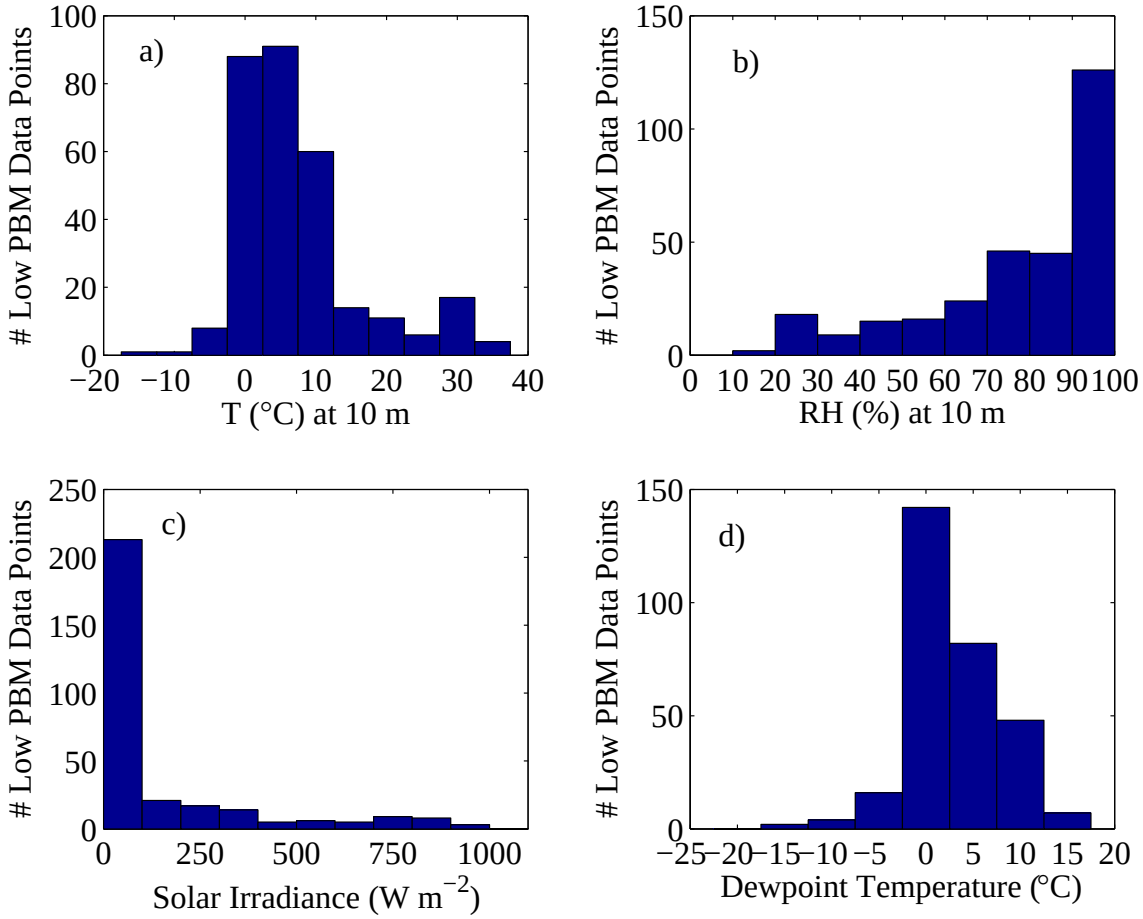

Figure 3.25: Histograms of the weather during low PBM data: a) temperature, b) relative humidity, c) solar radiation, and d) dewpoint temperature.

Table 3.9: High GOM events (99.5%, i.e. above 96.1 $\mathrm{pg\ m^{-3}}$) for the first two years of data at the UT96 site.

Event #	Year	Month	Day	Duration	# Data Points	Peak Hg $(\mathrm{pg\ m^{-3}})$
1	2009	August	12	15:05 - 15:05	1	103.0
2			19	14:28 - 14:28	1	117.0
3	2010	May	19	19:00 - 19:00	1	101.1
4		June	19	12:00 - 15:00	2	117.0
5			24	14:00 - 14:00	1	106.2
6			25	15:00 - 15:00	1	154.5
7		July	8	18:00 - 18:00	1	96.1
8			16	14:00 - 14:00	1	100.5
9		August	13	18:00 - 18:00	1	97.0
10			16	16:00 - 16:00	1	111.4
11			17	17:00 - 17:00	1	105.1
12		September	13	14:00 - 14:00	1	133.3
13			16	16:00 - 19:00	2	157.5
14			17	16:00 - 19:00	2	124.6
15			18	13:00 - 16:00	2	121.1
16			24	15:00 - 15:00	1	118.9
17			28	16:00 - 16:00	1	110.9
18		October	21	16:00 - 16:00	1	225.6
19	2011	June	21	14:00 - 17:00	2	176.9

observed in Detroit, Michigan during a short-term study was 270 $\mathrm{pg\ m^{-3}}$ (Lynam and Keeler, 2005). Two of the 19 high GOM events were followed within hours by high GEM events (Tables 3.4-3.5 and 3.9). Meanwhile, 6 of the 19 high GOM events occurred concurrently with low GEM events (Tables 3.6-3.7 and 3.9). No high PBM events occurred in close temporal proximity to a high GOM event. Approximately 37% of all GOM data is below the MDL (1.5 $\mathrm{pg\ m^{-3}}$), so all of this data is considered to be low events as the data may provide insight into processes that scavenge GOM. Low GOM data are included in this section, but a table is not included for brevity.

All High GOM events in the UT96 data set have occurred between noon and 2000 MST (adsorption from 1000 to 2000 MST), predominantly between 1400 and 1800 MST (Fig. 3.26a). Figure 3.26 shows histograms of the times of day at which high GOM events and low GOM events (below the MDL) occurred. GOM data below the MDL, in contrast,

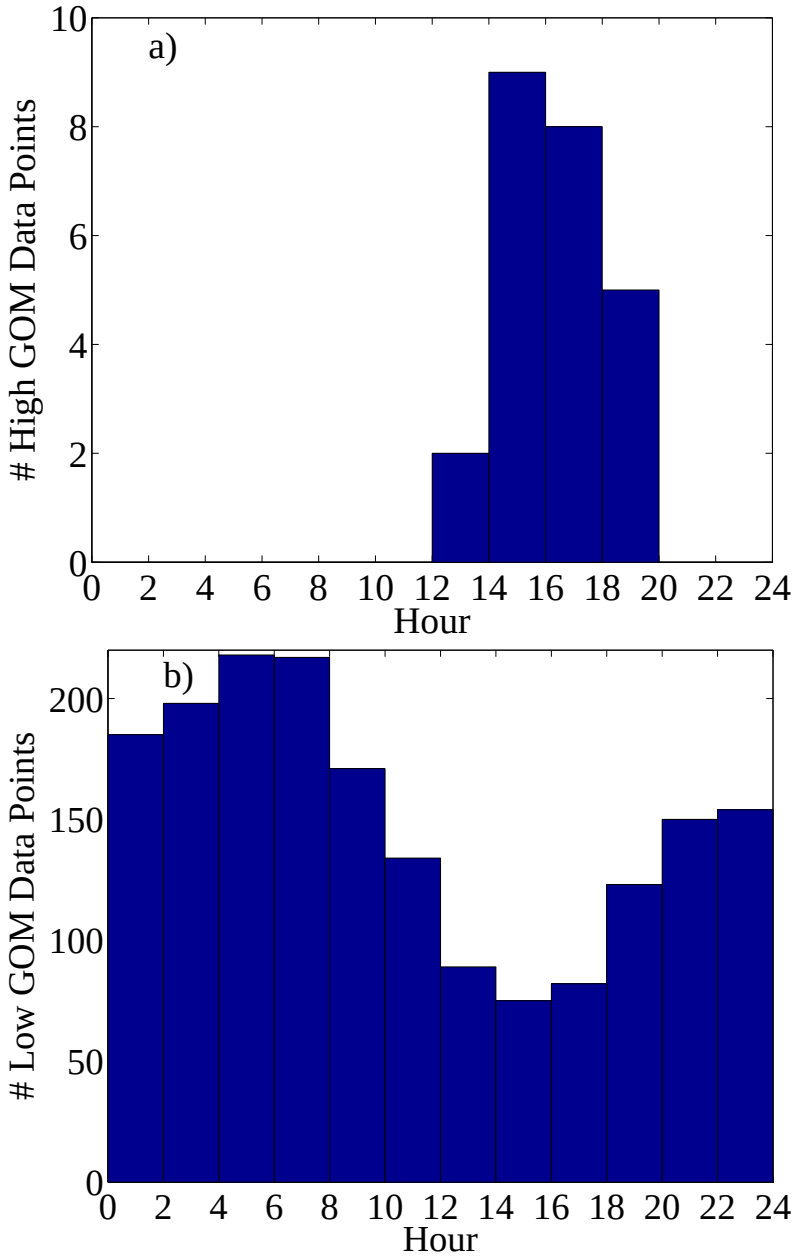

Figure 3.26: Histograms of the times of day for extreme GOM events with 2-hour time resolution: a) high GOM events, and b) low GOM events. It should be noted that (b) includes 37% of the entire GOM data set. The timestamps represent the end of the adsorption period (i.e., the GOM was collected during the two hours preceding the time stamp).

appear to follow a quasi-sinusoidal distribution with the peak during the early morning and minimum during the afternoon (Fig. 3.26b). The diurnal patterns exhibited in Figure 3.26 suggest that GOM concentrations are likely influenced by meteorological variables such as solar radiation, temperature, etc. and are not dominated by local anthropogenic sources. Both the high and low event distributions are consistent with the diurnal pattern observed in Section 3.3.

The weather conditions during which high GOM events occurred are shown in Figures 3.27-3.28. The winds are most likely to be from the northwest quadrant during high GOM events (Fig. 3.27), consistent with the typical afternoon wind patterns at UT96 (Fig. 2.4). All high GOM events have been observed while the temperature was between 17°C and 35°C, with the temperature predominantly above 23°C (Fig. 3.28a). No high GOM events have occurred while the RH was greater than 44%, and most high GOM events have occurred while the RH was below 30% (Fig. 3.28d). Fain et al. (2009) found that RH was the dominant factor affecting GOM concentrations, more dominant than either water vapor or temperature, and that high GOM concentrations were essentially always present whenever the RH was below ~40% at Storm Peak Laboratory during 28 April to 1 July, 2008. There is no obvious relationship between high GOM concentrations and solar radiation (Fig. 3.28e). This suggests that high GOM concentrations can occur on both sunny and cloudy days because, from Figure 3.26a, we know that all high GOM events have occurred during the afternoon/early evening. All high GOM events occurred while the dewpoint temperature was between 3°C and 12°C (Fig. 3.28d). Figure 3.28 is consistent with what might be expected if the sources of the high GOM events were strongly influenced by meteorological variables. High GOM events appear to be most likely to occur under conditions of high temperature and low RH. Sorting out the causal relationships among the various meteorological parameters with high GOM may be a topic of interest for future research.

Low GOM events (below the MDL) represent approximately 37% of the entire GOM data set. The wind rose corresponding to the times of low GOM events (Fig. 3.29) is

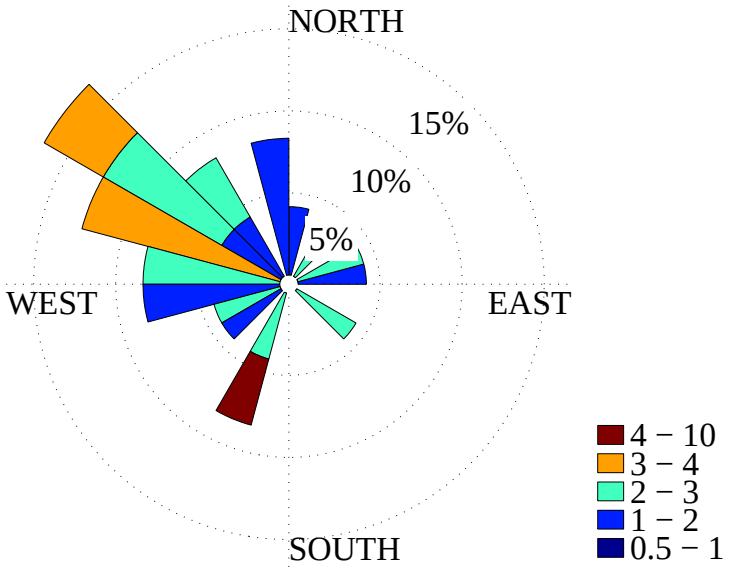

Figure 3.27: Wind rose (m s^{-1}) at the UT96 site for high GOM conditions.

consistent with the overall wind rose (Fig. 2.3). The temperature distribution observed during low GOM events (Fig. 3.30a) and the overall temperature distribution (Fig. 2.6a) both peak around 0°C and cover the range from roughly -15°C to 30°C. The RH distribution measured during low GOM events (Fig. 3.30b) is similar in shape to the overall RH distribution (Fig. 2.6b), but with relatively fewer data points around 40% RH. The solar radiation distribution measured during low GOM events (Fig. 3.30c) is very similar in shape to the overall solar radiation distribution (Fig. 2.6c). The dewpoint temperature distribution observed during low GEM events (Fig. 3.25d) and the overall dewpoint temperature distribution (Fig. 2.6d) both peak around 0°C and cover the range from roughly -20°C to 20°C. There is no striking relationship between the weather variables presented here and the occurrence of GOM concentrations below the MDL.

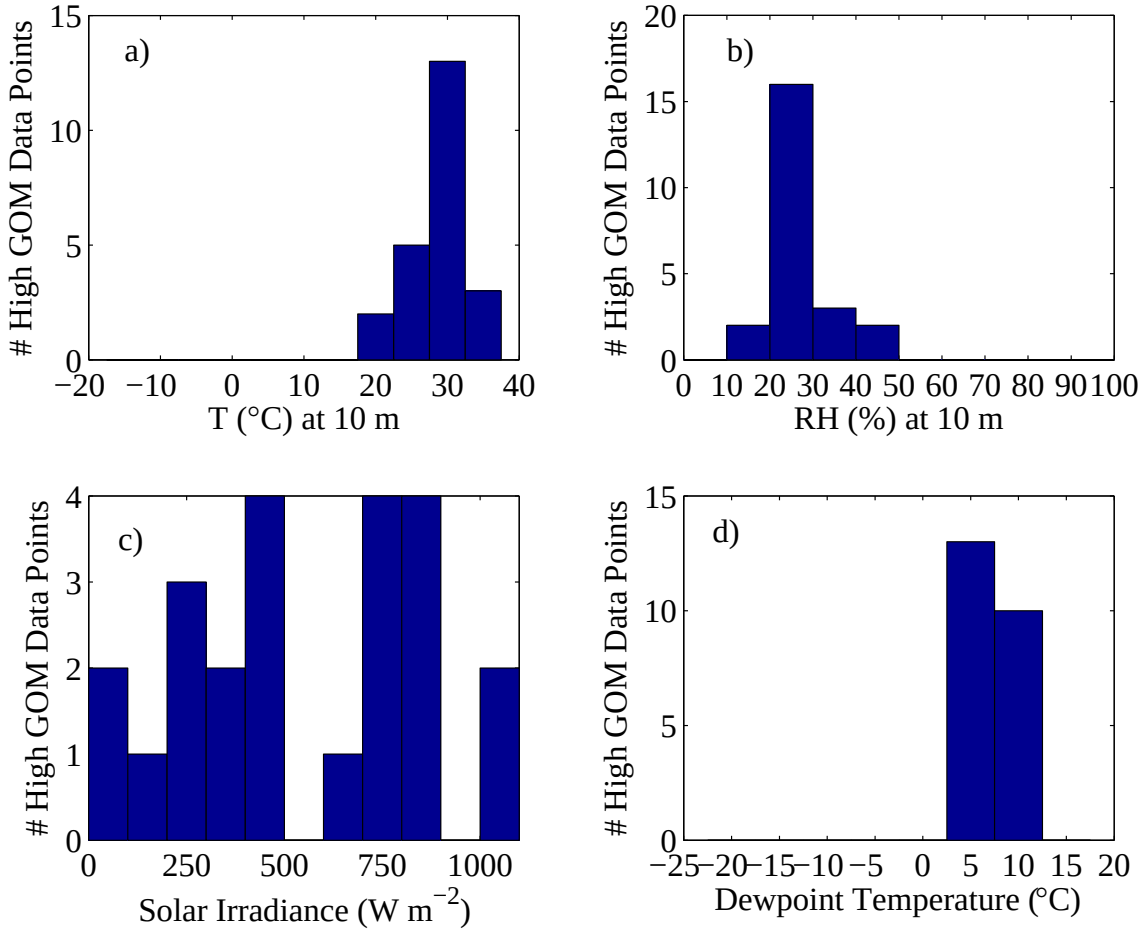

Figure 3.28: Histograms of the weather during high GOM data: a) temperature, b) relative humidity, c) solar radiation, and d) dewpoint temperature.

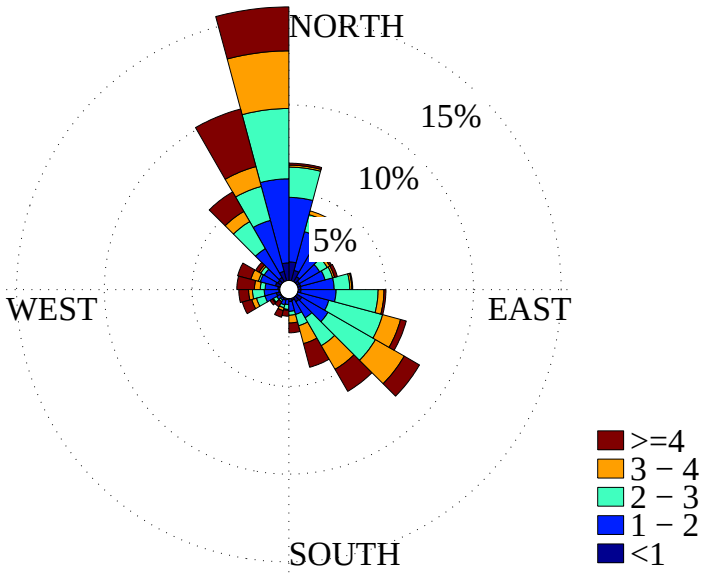

Figure 3.29: Wind rose (m s^{-1}) at the UT96 site for low GOM conditions.

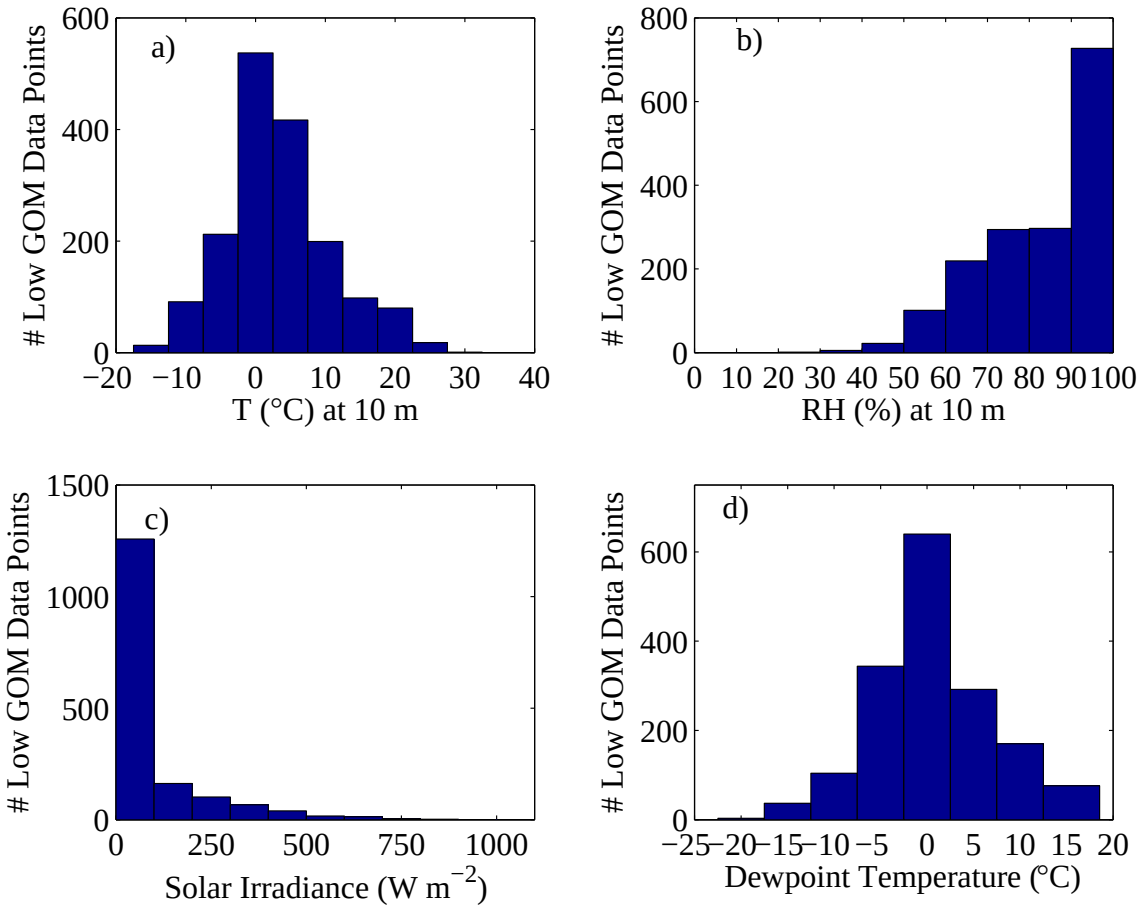

Figure 3.30: Histograms of the weather during low GOM data: a) temperature, b) relative humidity, c) solar radiation, and d) dewpoint temperature.

CHAPTER 4

INFLUENCES OF PRECIPITATION

This chapter will investigate three hypotheses relating to the wet scavenging of speciated atmospheric mercury. The first hypothesis is that precipitation will scavenge GOM and PBM, but not GEM. The second hypothesis is that heavy precipitation will scavenge GOM and PBM more efficiently than light precipitation. The final hypothesis is that different types of precipitation (snow, rain, or mixed) affect atmospheric mercury concentrations with varying efficiencies (i.e., mixed precipitation will scavenge GOM and PBM more efficiently than either rain or snow). These three hypotheses will be tested using the UT96 mercury data in conjunction with data from the KHIF weather station at Hill Air Force Base (Fig. 4.1), located 13.0 km northeast of UT96.

Throughout this chapter, mercury concentrations that were observed under dry atmospheric conditions are compared with mercury concentrations observed during or following a precipitation event. A concise method of comparing the two populations of data is to define a scavenging efficiency s as:

$$s = 1 - \frac{median(wet)}{median(dry)} \tag{4.1}$$

where wet refers to the population of mercury concentrations observed during or after precipitation and dry refers to the population of mercury concentrations observed during dry atmospheric conditions. If the wet and dry data are statistically the same, the scavenging efficiency is defined as 0.0. The scavenging efficiency suggests, on the timescale in question, what fraction of mercury is removed by precipitation. A positive result indicates

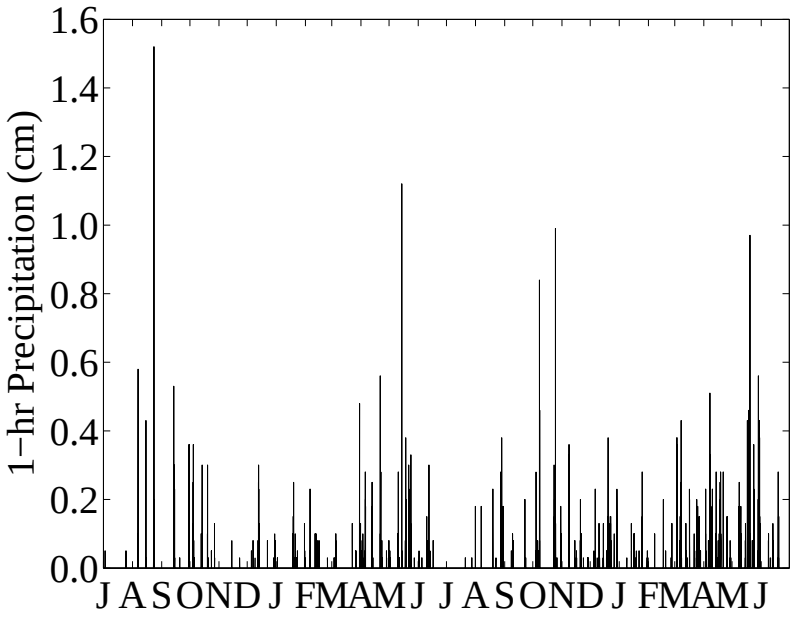

Figure 4.1: Precipitation measurements at KHIF from 1 July 2009 to 30 June 2011.

scavenging. For example, if $s = 0.2$, that would suggest that 20% of the mercury is typically removed by precipitation compared to the reference of observations made under dry atmospheric conditions. A negative scavenging efficiency would indicate that the presence of precipitation somehow promotes higher concentrations of mercury. The median was used in Equation 4.1 instead of the mean to limit the influence of outliers. This form of s compares the populations of wet and dry data and not necessarily individual precipitation events. Calculating s for individual precipitation events, at least for the 2-hour timescale analyses, would not be informative because of the strong diurnal patterns that exist for each of the mercury species.

4.1 Hypothesis #1: Precipitation Scavenging

Two sets of timescales were used to analyze dry versus wet data: 2-hour and 24-hour. In the 2-hour tests, a mercury datum was designated as "wet" if precipitation occurred during the 2 hours preceding the datum time stamp (adsorption period for GOM and PBM). The 24-hour tests (pre-post analysis) compared the mercury concentrations during the 24

hours of dry weather preceding precipitation with the mercury concentrations during the 24 hours after the initiation of precipitation. Two different timescales (2-hour and 24-hour) were used in the analysis for a couple of reasons. First, it was unclear what the appropriate timescale might be (i.e., how long the influence of precipitation might persist). Second, a direct before-and-after comparison cannot be done on the 2-hour timescale because the influence of precipitation would be overlaid on the diurnal patterns of mercury concentrations. The 2-hour timescale was chosen because that is the length of the adsorption period for GOM and PBM, meaning that precipitation occurred while the GOM and PBM were being collected. The 24-hour timescale addressed the diurnal cycle problem by encompassing an entire diurnal cycle in both the before and after data. It is anticipated that the influence of precipitation will be stronger on the 2-hour timescale than on the 24-hour timescale, and that the scavenging efficiencies in the 2-hour analyses will have larger absolute magnitudes than the corresponding 24-hour scavenging efficiencies.

4.1.1 Precipitation Scavenging Methodology (2-hour timescale)

The mercury data were designated as either “dry” or “wet” based on 1-hour precipitation measurements at KHIF (Horel et al., 2002). If nonzero precipitation was measured at KHIF within two hours preceding the time stamp for a mercury data point, then that data point was designated as “wet” because there was measurable precipitation at some point during the 2-hour adsorption cycle. Two hours was also used for GEM (5-min adsorption cycle) to ease the comparison between mercury species. If there was no measurable precipitation during the 48 hours preceding the time stamp of a given data point, it was designated as “dry.” Also, there are some gaps in the KHIF data set, and the corresponding mercury data is not included in the precipitation analysis. The 48-hour requirement for dry data and the gaps in the KHIF data result in ~33% of the data for each species of mercury eliminated from the precipitation analysis. This was worthwhile because it reduces contamination of the dry data with data points that may have been affected by recent precipitation.

For any 3-hour time period, 24 GEM data points are measured while only one PBM data point and one GOM data point are measured at the UT96 site. Consequently, serial correlation is likely to be a greater problem for GEM than for PBM and GOM. To address this issue, the GEM data set was pruned to have the same frequency of measurements as PBM and GOM using the methodology described in Section 2.3.4. All figures and tables in this chapter use pruned GEM data, except where the pruned and unpruned data subsets are briefly compared.

If precipitation did not affect atmospheric mercury concentrations, then subdividing the mercury data set into "wet" and "dry" subcategories would be essentially arbitrary. These subsets should have essentially the same (non-Gaussian) distributions as the mercury data set as a whole. Two tests were conducted to investigate whether the wet and dry subsets had the same distributions: the Wilcoxon test (described in Section 2.3.2) and the decile/MDL test. In the decile test, the lowest decile for the mercury data set as a whole was determined. Next, the percent of the subdivided data points that are smaller than the overall decile was calculated. If precipitation has no effect on the mercury concentrations, then the percent of subset data below the overall decile should be ~10%. If this percent is substantially different from 10%, that would be an indication that precipitation does affect mercury concentrations. A result for the dry subset below 10% and a result for the wet subset above 10% would suggest scavenging. This test was modified slightly for PBM and GOM because a substantial portion of the PBM and GOM data is below the MDL. For those species, the percent of the overall data set at or below the MDL was used instead of 10%.

For each mercury species, a comparison of the dry and wet data subsets for the full 2 years of data will be presented. The comparisons will then be broken down by season. Finally, the 24-hour analysis will be presented for each mercury species.

4.1.2 Precipitation Scavenging Methodology (24-hour timescale)

First, the beginning of a precipitation event was identified (i.e., there had been no precipitation for at least 48 hours before a wet data point). Second, the "before-wet" data were identified, which are all of the mercury data points measured during the 24 hours preceding the event datum. Third, the "after-wet" data were identified as the event datum and the data collected during the 24-hour period after precipitation began. This analysis did not consider whether precipitation continued after the initial wet datum. This procedure was repeated for the entire mercury data set. There was also a requirement that all events be at least 72 hours apart to avoid using the same data for multiple events and reduce serial correlation. There were 55 GOM events, 56 PBM events, and 82 GEM events that met these criteria. The before-wet and after-wet GEM data were pruned to address the problem of serial correlation using the methodology described in Section 2.3.4. The two-sided Wilcoxon test was conducted on the collection of before-wet and after-wet data to test whether these data populations were significantly different.

The purpose of using 24 hours of data before and after the onset of precipitation was to encompass an entire diurnal cycle. Simply comparing the one datum before and after the onset of precipitation would not have been informative because the change in mercury concentration due to precipitation would have been superimposed on the diurnal mercury fluctuations (Figs. 3.11-3.9). It is unclear how long the effects of precipitation last, but a reduction in mercury concentrations due to precipitation for part of the day should shift the after-wet data distribution relative to the before-wet data.

4.1.3 Precipitation Scavenging Results for GOM

Wet GOM is statistically lower than dry GOM at the 95% confidence level (two-sided Wilcoxon test) on a 2-hour timescale. Figure 4.2 shows the wet and dry GOM time series as well as the medians and MADs. This figure clearly shows that the wet GOM is significantly lower than dry GOM. Table 4.1 shows basic statistics for dry and wet GOM. The GOM

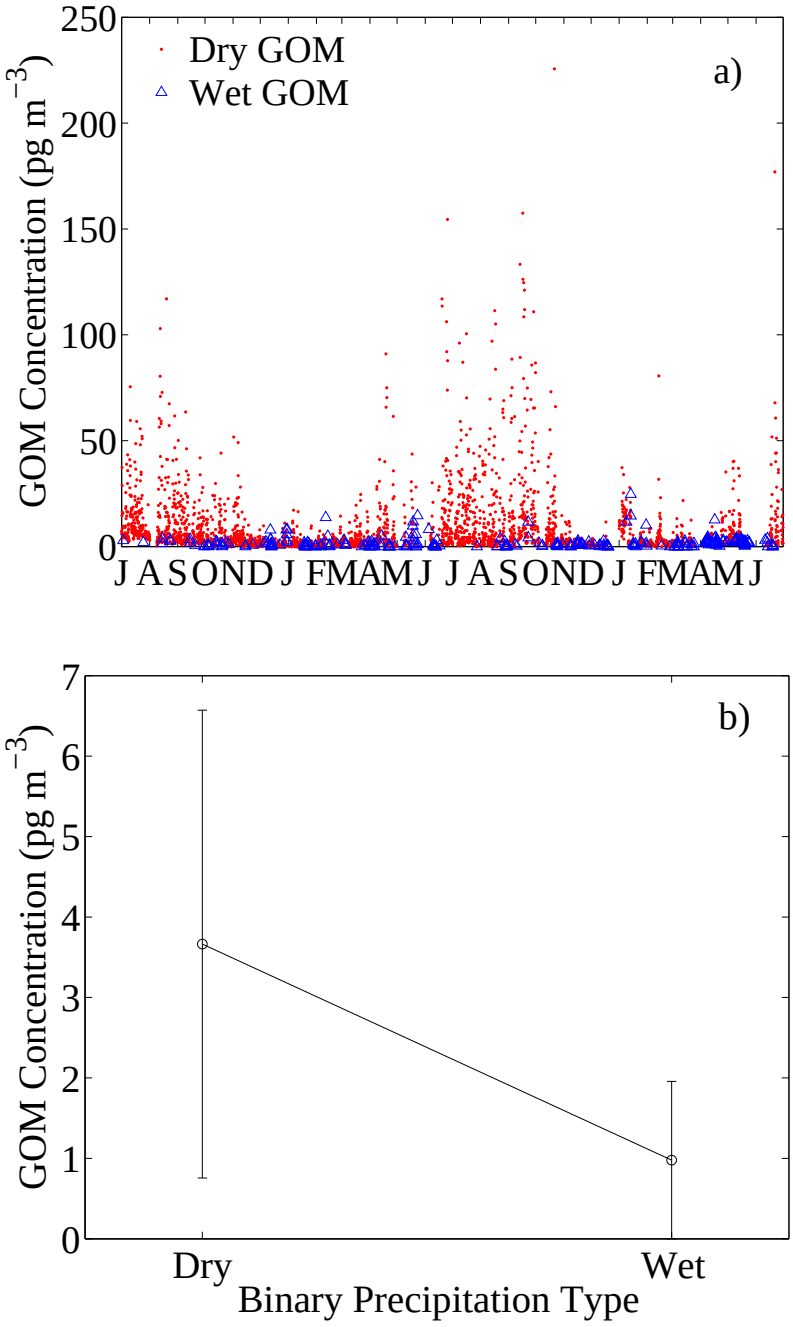

Figure 4.2: Dry and wet GOM (2-hour timescale) from 1 July 2009 to 30 June 2011: a) time series, and b) medians with MAD error bars.

Table 4.1: Statistical summary of dry and wet GOM on a 2-hour timescale ($\mathrm{pg\ m^{-3}}$, except # data points).

GOM	Dry	Wet
# Data Points	2960	310
Minimum	0.0	0.0
Maximum	225.6	24.7
Lower Quartile	1.3	0.2
Median	3.7	1.0
Upper Quartile	10.1	2.3
MAD	2.9	1.0

scavenging efficiency for precipitation on a 2-hour timescale is 0.7.

Approximately 37% of the entire GOM data set is below the MDL (1.5 $\mathrm{pg\ m^{-3}}$). If precipitation had no effect on GOM concentrations, then ~37% of both the dry and wet GOM data subsets should be below the MDL. Only 28% of the dry data set is below the MDL, while 59% of the wet GOM is below the MDL. Both this result and the Wilcoxon test support the hypothesis that GOM is efficiently scavenged by precipitation.

The 2-hour timescale Wilcoxon test results were extended to seasonal timescales to determine the robustness of the results (Fig. 4.3). This analysis revealed that wet GOM is statistically lower than dry GOM during all seasons and the scavenging efficiencies vary between 0.4 (spring) and 0.9 (summer). It is unclear why the scavenging efficiencies should have a seasonal dependence. It is possible that the scavenging efficiency depends on precipitation intensity or type, which are seasonally dependent. This possibility will be explored later in this chapter.

The before-wet and after-wet data are statistically different (Fig. 4.4) suggesting that precipitation scavenges GOM on a 24-hour timescale as well (two-sided Wilcoxon test, 95%). The scavenging efficiency, defined in Equation 4.1, is 0.6. These results suggest not only that precipitation scavenges a substantial fraction of GOM, but also that the scavenging of GOM by precipitation is persistent enough to be measurable on a 24-hour timescale. However, it is possible that the cloudy/cold weather associated with precipitation could suppress the typical (assumed) GEM to GOM photochemical conversion which would have

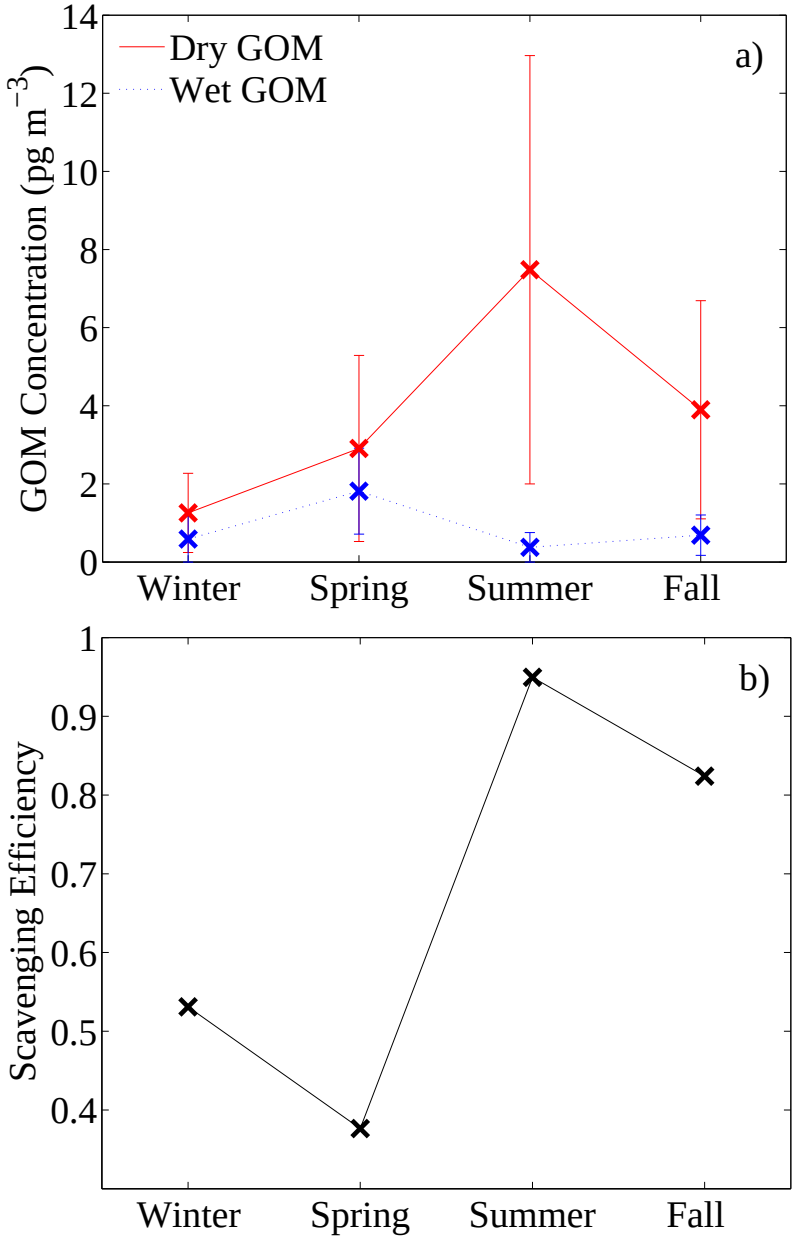

Figure 4.3: Dry and wet GOM a) medians by season, and b) seasonal scavenging efficiencies for GOM (2-hour timescale). Seasons were marked with an X when the dry and wet GOM were statistically different and with an O when they were statistically the same. (Wilcoxon test). Error bars are MADs.

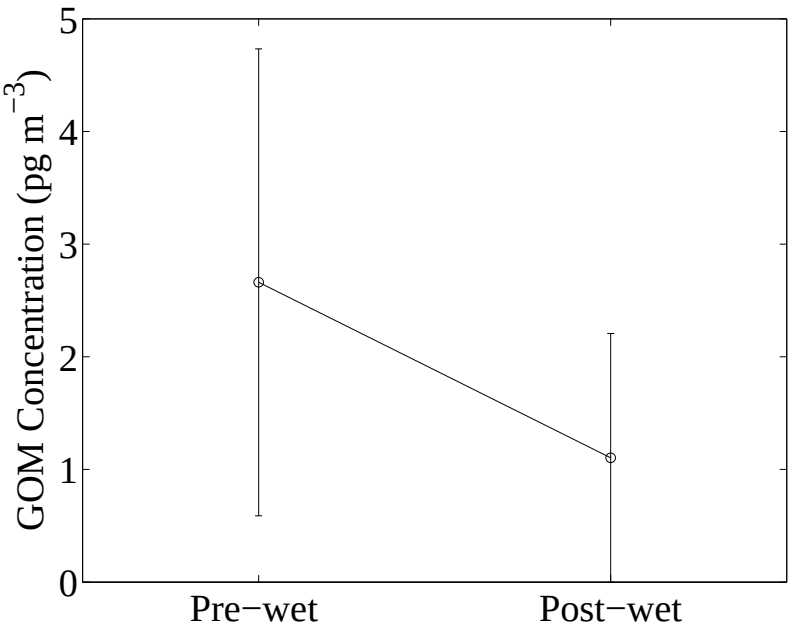

Figure 4.4: GOM precipitation scavenging for 55 separate precipitation events (24-hour timescale). Before-wet represents the median of the population of data points collected during the 24 hours preceding all of the qualifying precipitation events (420 data points). (See Section 4.1.2.) After-wet represents the median of the population of data points collected during and for 24 hours after the onset of all qualifying precipitation events (417 data points). Error bars are MADs.

the same effect on the data.

4.1.4 Precipitation Scavenging Results for PBM

Wet PBM is statistically lower than the dry PBM at the 95% confidence level (two-sided Wilcoxon test) on a 2-hour timescale. Figure 4.5 shows the wet and dry PBM time series with both full and truncated axes. The full axes plot acknowledges the outliers while the truncated axes plot allows the majority of the data to be seen. Figure 4.5 shows that there are both dry and wet PBM outliers, and there is clearly not a total suppression of PBM due to precipitation. Figure 4.6 shows that the wet PBM median is less than half of the dry PBM median. Table 4.2 shows basic statistics for dry and wet PBM. The PBM scavenging efficiency for precipitation on a 2-hour timescale is 0.6.

The extremely high concentration of 803.2 $\mathrm{pg\ m^{-3}}$ in the wet category (Table 4.2) was

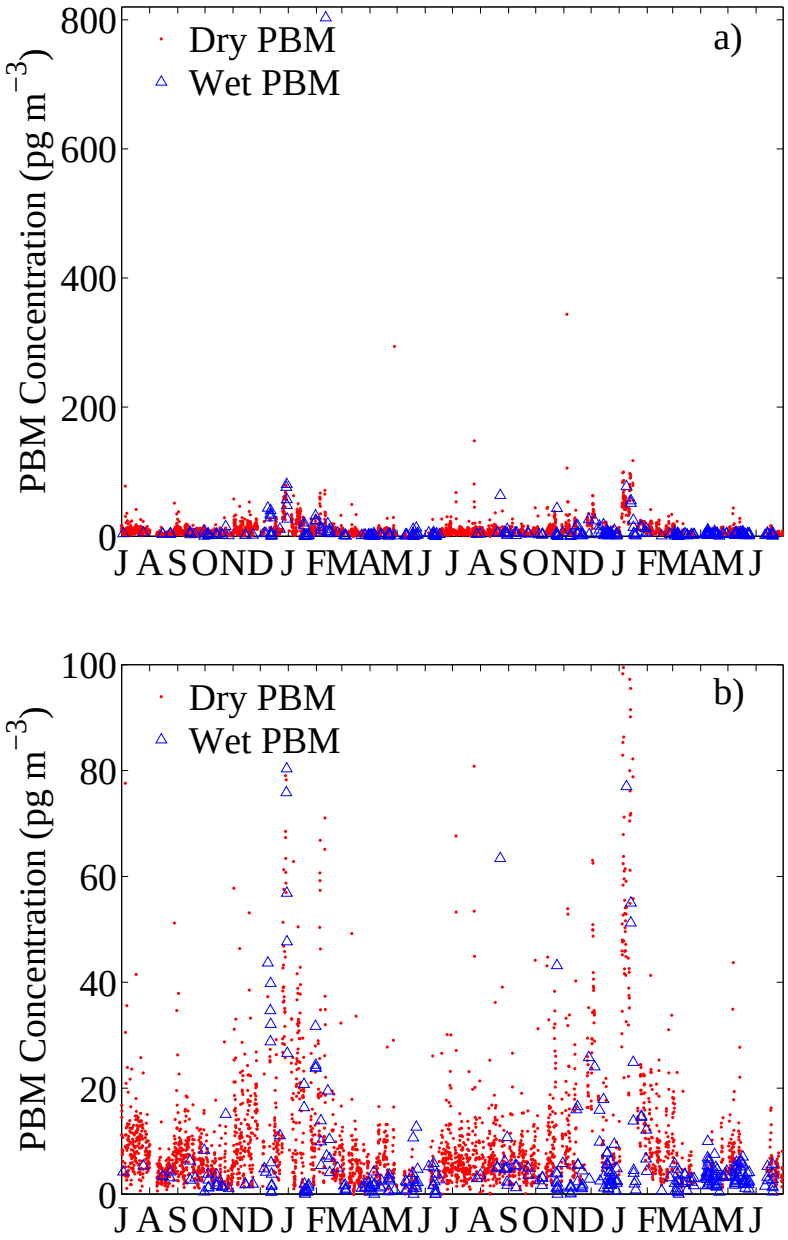

Figure 4.5: Dry and wet PBM from 1 July 2009 to 30 June 2011: a) time series, and b) time series with truncated axes (2-hour timescale).

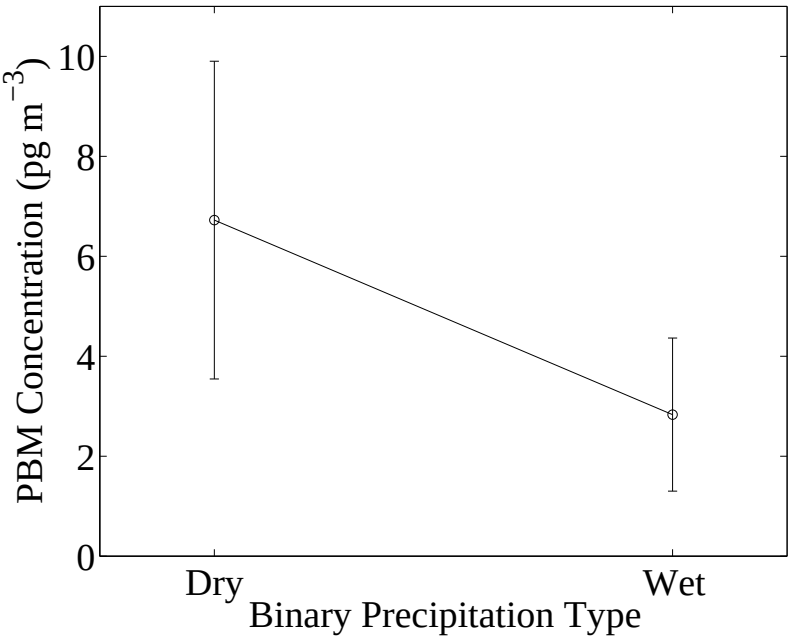

Figure 4.6: Dry and wet PBM from 1 July 2009 to 30 June 2011 medians with MAD error bars (2-hour timescale).

Table 4.2: Statistical summary of dry and wet PBM on a 2-hour timescale ($\mathrm{pg\ m^{-3}}$, except # data points).

PBM	Dry	Wet
# Data Points	2906	328
Minimum	0.0	0.0
Maximum	343.9	803.2
Lower Quartile	4.1	1.6
Median	6.7	2.8
Upper Quartile	11.5	5.1
MAD	3.2	1.5

measured on 11 February 2010 at 06:00 (the mercury was collected 04:00-06:00). This was part of a high PBM event, and was followed by a concentration of 549.6 $\mathrm{pg\ m^{-3}}$. This high PBM event was concurrent with a high GEM event. The highest GEM concentration observed during the corresponding adsorption period was 3.24 $\mathrm{ng\ m^{-3}}$. KHIF reported light snow and fog during that time. These high concentrations are thought to be due to a high concentration plume from a local industrial or urban source. The second-largest wet PBM event is 80.3 $\mathrm{pg\ m^{-3}}$.

Approximately 7% of the entire PBM data set is below the MDL (1.5 $\mathrm{pg\ m^{-3}}$). If precipitation had no effect on PBM concentrations, then ~7% of both the dry and wet PBM data subsets should be below the MDL. Only 3% of the dry data set is below the MDL, while 23% of the wet PBM is below the MDL. Both this result and the Wilcoxon test support the hypothesis that PBM is scavenged by precipitation.

The 2-hour timescale Wilcoxon test results for PBM were extended to seasonal time periods to determine the robustness of the results (Fig. 4.7). This analysis revealed that wet PBM is statistically lower than dry PBM for all seasons. The seasonal scavenging efficiencies vary between 0.4 and 0.7. It is unclear why the scavenging efficiency should vary be season. Once again, this might be due to seasonal variations in precipitation type and intensity.

The before-wet and after-wet data are statistically different (Fig. 4.8), suggesting that precipitation scavenges PBM on a 24-hour timescale as well (two-sided Wilcoxon test, 95%). The scavenging efficiency, defined in Equation 4.1, is 0.3, suggesting that precipitation scavenges some PBM on a 24-hour timescale.

4.1.5 Precipitation Scavenging Results for GEM

GEM has a low solubility, so it is not effectively scavenged by precipitation (Sakata and Asakura, 2007). For any 3-hour time period, 24 GEM data points are measured at the UT96 site. Consequently, GEM data were pruned (see Section 2.3.4) to one data point per

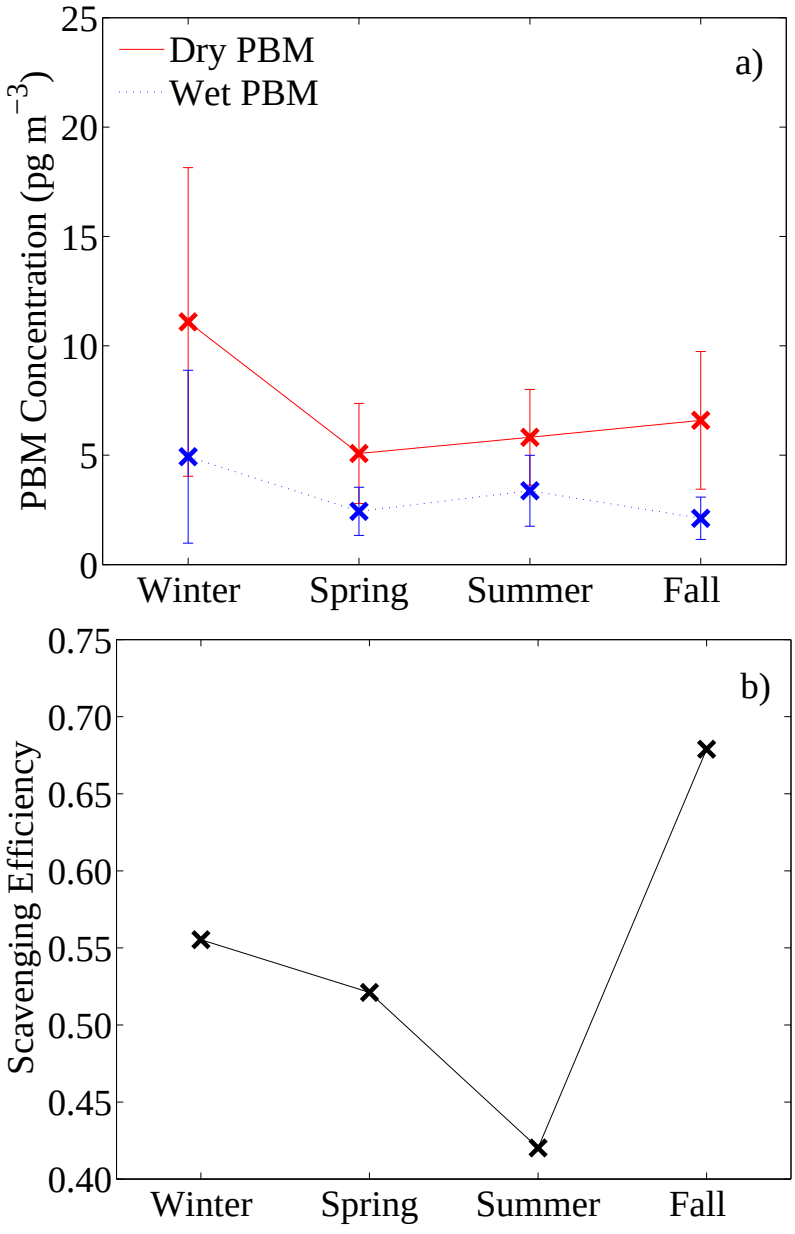

Figure 4.7: Dry and wet PBM a) medians by season and b) seasonal scavenging efficiencies for PBM (2-hour timescale). Seasons were marked with an X when the dry and wet PBM were statistically different and with an O when they were statistically the same (Wilcoxon test). Error bars are MADs.

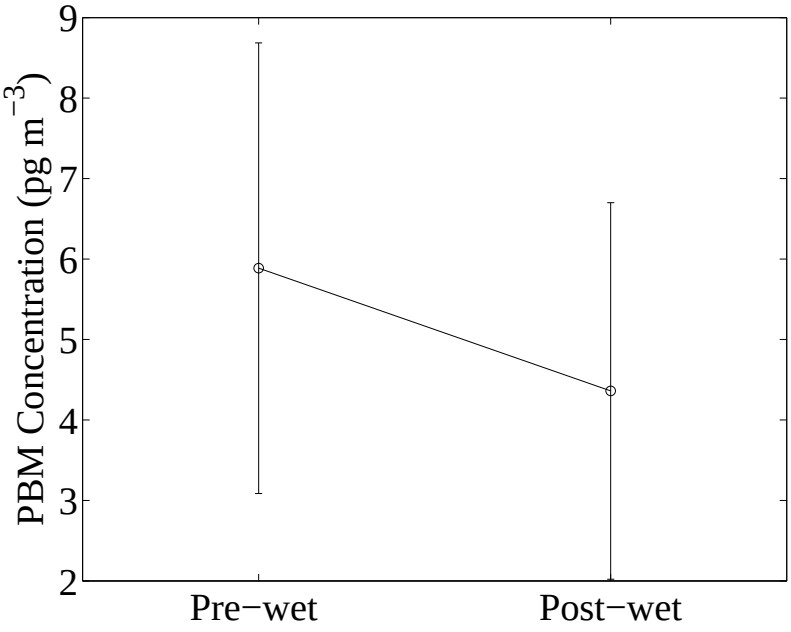

Figure 4.8: PBM precipitation scavenging for 56 separate precipitation events (24-hour timescale). Before-wet represents the median of the population of data points collected during the 24 hours preceding all of the qualifying precipitation events (425 data points). (See Section 4.1.2.) After-wet represents the median of the population of data points collected during and for 24 hours after the onset of all qualifying precipitation events (426 data points). Error bars are MADs.

3-hour time period to address serial correlation. Table 4.3 shows the basic statistics for dry and wet GEM using both pruned and unpruned data. Pruning the data shifted the quartiles surprisingly little, suggesting that pruning did not alter the distribution significantly. The time series of the wet and dry pruned GEM is shown in Figure 4.9a. There is little difference between the pruned and unpruned median wet and dry GEM (Fig. 4.9b). However, the results of the Wilcoxon test on the pruned and unpruned data sets are different. Without pruning, the Wilcoxon test showed that dry and wet GEM are statistically different. After pruning, which addresses the problem of serial correlation, the wet GEM is statistically the same as dry GEM (2-sided Wilcoxon test, 95%). The GEM scavenging efficiency for precipitation on a 2-hour timescale is, therefore, 0.0.

If precipitation had no effect on GEM concentrations, then approximately 10% of the (pruned) dry and wet GEM subsets should be below the overall lowest decile of unpruned GEM (1.31 $\mathrm{ng\ m^{-3}}$). Approximately 11% of dry GEM is below the overall decile while only 5% of the wet GEM is below the decile. Both this test and the Wilcoxon test support the hypothesis that GEM is not scavenged by precipitation. Indeed, these results suggest that if precipitation has any effect on GEM, precipitation increases GEM slightly. Perhaps precipitation suppresses the typical (assumed here) conversion from GEM to GOM. It is also possible that precipitation could drive mercury from the soil, thereby increasing atmospheric GEM (e.g., Lindberg et al., 1999).

The 2-hour Wilcoxon test results were extended to seasonal time periods to determine

Table 4.3: Statistical summary of dry and wet GEM on a 2-hour timescale with and without pruning. ($\mathrm{ng\ m^{-3}}$, except # data points).

GEM	Unpruned Dry	Unpruned Wet	Pruned Dry	Pruned Wet
# Data Points	66553	7396	3097	330
Minimum	0.25	1.00	0.73	1.14
Maximum	13.18	4.39	3.95	3.57
Lower Quartile ($q_{0.25}$)	1.43	1.49	1.43	1.47
Median ($q_{0.5}$)	1.57	1.60	1.57	1.60
Upper Quartile ($q_{0.75}$)	1.74	1.74	1.74	1.72
MAD	0.15	0.12	0.15	0.13

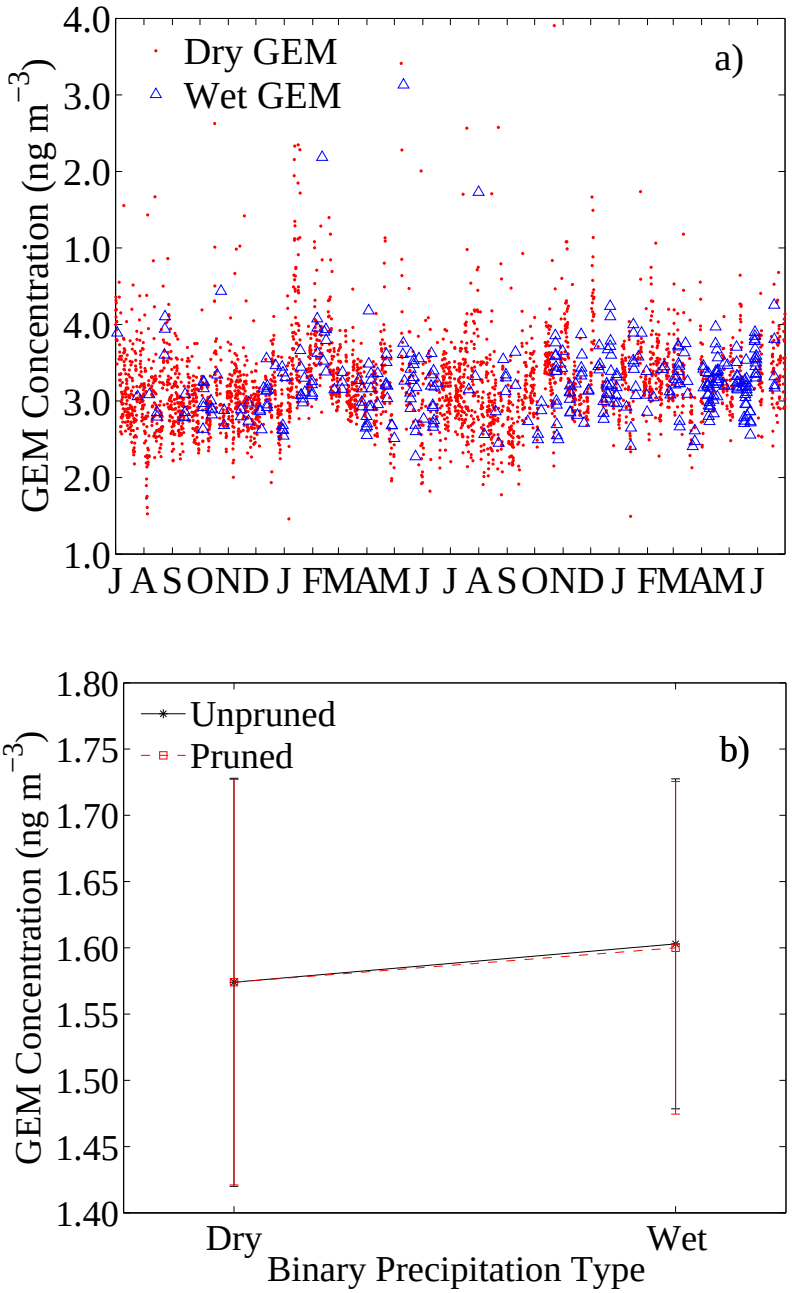

Figure 4.9: Dry and wet GEM (2-hour timescale) from 1 July 2009 to 30 June 2011: a) pruned time series, and b) pruned and unpruned medians with MAD error bars.

the robustness of the results (Figure 4.10). This analysis revealed that wet and dry GEM are statistically the same for all seasons, therefore, the scavenging efficiency for each season is 0.0.

The before-wet and after-wet GEM data are statistically the same (Fig. 4.11), suggesting that precipitation does not affect GEM on a 24-hour timescale (two-sided Wilcoxon test, 95%). The scavenging efficiency, defined in Equation 4.1, is 0.0, suggesting that precipitation does not scavenge nor promote GEM on a 24-hour timescale.

4.2 Hypothesis #2: Precipitation Intensity

The precipitation intensity analysis was conducted by including distinctions about the amount of precipitation that fell during the 2 hours preceding the time stamp on each wet data point. The designation for dry was the same as in Section 4.1, but wet events were sorted into "damp" and "soggy" categories. Damp data had total accumulated precipitation of more than 0 cm but less than or equal to the "soggy threshold." The soggy threshold

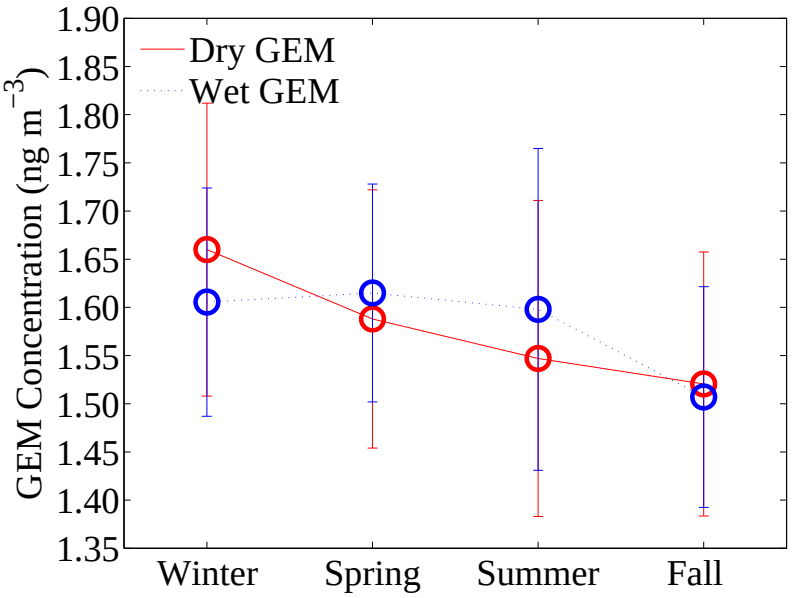

Figure 4.10: Dry and wet GEM medians by season. Seasons in which the dry and wet PBM were statistically different are marked with an X, and an O if they were statistically the same (Wilcoxon test). Error bars are MADs.

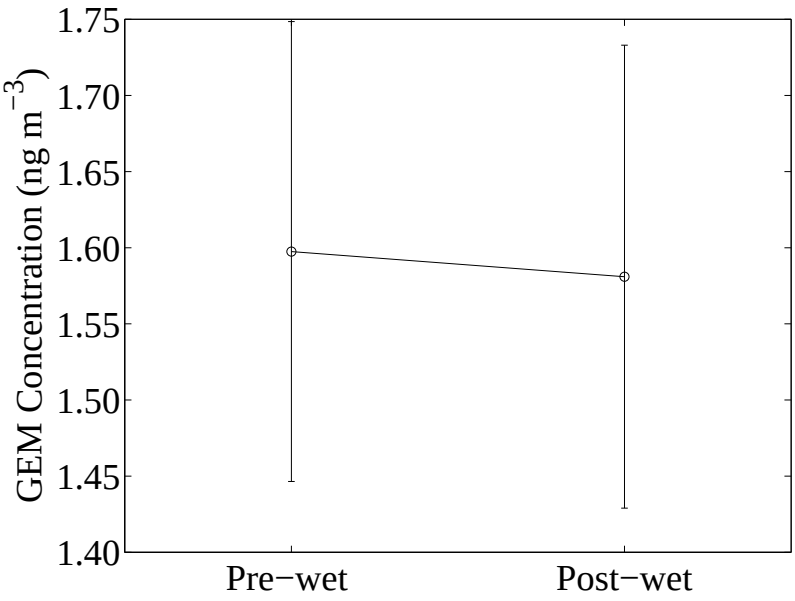

Figure 4.11: GEM precipitation scavenging for 82 separate precipitation events (24-hour timescale). Before-wet represents the median of the population of data points collected during the 24 hours preceding all of the qualifying precipitation events (654 data points). (See Section 4.1.2.) After-wet represents the median of the population of data points collected during and for 24 hours after the onset of all qualifying precipitation events (635 data points). Error bars are MADs.

was set to 0.09 cm, which produced damp and soggy data sets of similar size. For "soggy" data, there was an accumulation of precipitation in the preceding time window greater than the soggy threshold. Similar to Section 4.1, the Wilcoxon test, scavenging efficiencies, decile/MDL test, and seasonal analysis were all calculated on the dry, damp, and soggy data. Tables with results are presented in the corresponding test sections.

The post-pre (24-hour timescale) analysis was also extended to the precipitation intensity analysis. The wet events found in the previous analysis were separated into damp and soggy events. The total accumulated precipitation measured at KHIF between the beginning of the adsorption period (two hours before the time stamp on the event datum) and 24 hours after the time stamp on the event datum (a 26-hour period) was used to distinguish between damp and soggy events. If the 26-hour total accumulated precipitation was less than the chosen 26-hour soggy threshold, then the event was designated as "damp." Similarly, if the 26-hour total accumulated precipitation was more than the 26-hour soggy threshold, the event was designated as "soggy." The 26-hour soggy threshold was set to approximately the median of the 26-hour total accumulated precipitation for all events (0.25 cm). This threshold leads to approximately equal numbers of damp and soggy events.

4.2.1 Precipitation Intensity Scavenging Results for GOM

Damp and soggy GOM are both statistically lower than dry GOM (KW test, 95%). Damp and soggy GOM could not be statistically compared to each other because the median of each is below the MDL. Figure 4.12 shows the time series as well as the median dry, damp, and soggy GOM. Table 4.4 shows the basic statistics for dry, damp, and soggy GOM. The GOM scavenging efficiency for light precipitation (damp) on a 2-hour timescale is 0.6. The GOM scavenging efficiency for heavy precipitation (soggy) on a 2-hour timescale is 0.8 meaning that most GOM is removed from the atmosphere during heavy precipitation.

Approximately 37% of the entire GOM data set is below the MDL (1.5 $\mathrm{pg\,m^{-3}}$). If precipitation had no effect on GOM concentrations, then ~37% of each of the dry, damp,

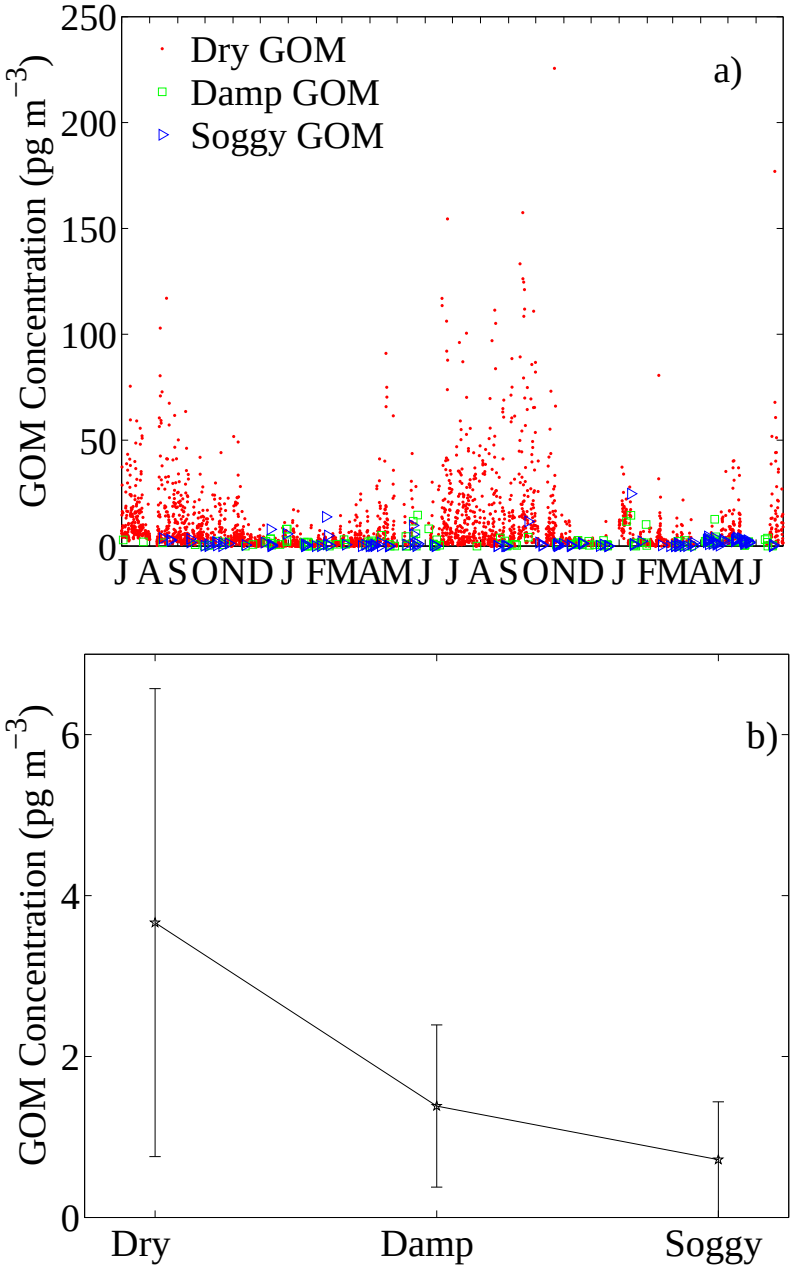

Figure 4.12: GOM concentrations under dry, damp, and soggy conditions from 1 July 2009 to 30 June 2011: a) time series, and b) medians with MAD error bars.

Table 4.4: Statistical summary of dry, damp, and soggy GOM on a 2-hour timescale ($\mathrm{pg\ m^{-3}}$, except # data points).

GOM	Dry	Damp	Soggy
# Data Points	2960	164	146
Minimum	0.0	0.0	0.0
Maximum	225.6	14.6	24.7
Lower Quartile	1.3	0.4	0.0
Median	3.7	1.4	0.7
Upper Quartile	10.1	2.5	2.0
MAD	2.9	1.0	0.7

and soggy GOM data subsets should be below the MDL. Only 28% of the dry data set is below the MDL, while 53% and 65% of the damp and soggy GOM are below the MDL, respectively. This result supports the hypothesis that GOM is scavenged more efficiently as precipitation intensity increases.

During all seasons (Fig. 4.13), dry GOM is statistically higher than damp and soggy GOM with scavenging efficiencies ranging between 0.3 and 1.0 (KW test, 95%). Damp and soggy GOM are statistically the same during all seasons at the 95% confidence levels. However, spring damp and soggy GOM are statistically different at the 90% confidence level, while winter damp and soggy GOM are statistically different at the 70% confidence level. For summer and fall, the damp and soggy GOM are both below the MDL and cannot be distinguished statistically. The soggy scavenging efficiency is greater than the damp scavenging efficiency for every season, consistent with the hypothesis that heavy precipitation will scavenge GOM more efficiently than light precipitation (Fig. 4.14).

The events in the pre-post (24-hour timescale) analysis of Section 4.1.3 were also subdivided into damp and soggy categories (Fig. 4.15). The before-damp and after-damp data are statistically different (two-sided Wilcoxon test, 95%) with a scavenging efficiency (Eq. 4.1) of 0.4. In addition, the before-soggy and after-soggy data are statistically different with a scavenging efficiency of 0.7. These results suggest that scavenging increases as precipitation increases on a 24-hour timescale.

The results of this section suggest that both light and heavy precipitation scavenge

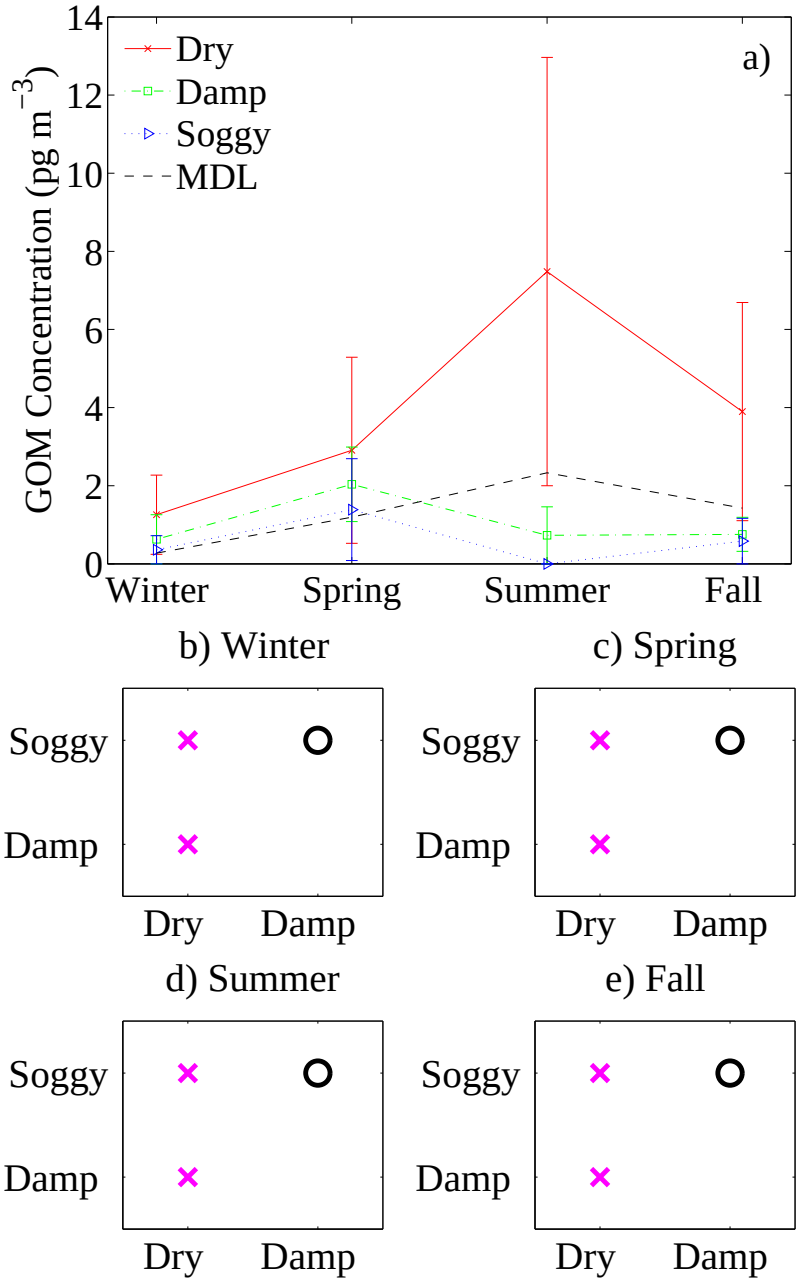

Figure 4.13: Seasonal pattern of GOM concentrations for dry, damp, and soggy conditions: a) Dry, damp, and soggy median GOM by season with MAD error bars, and results of KW test for b) winter, c) spring, d) summer, and e) fall. Comparison pairs that are statistically different are marked with an X, and an O if they are statistically the same.

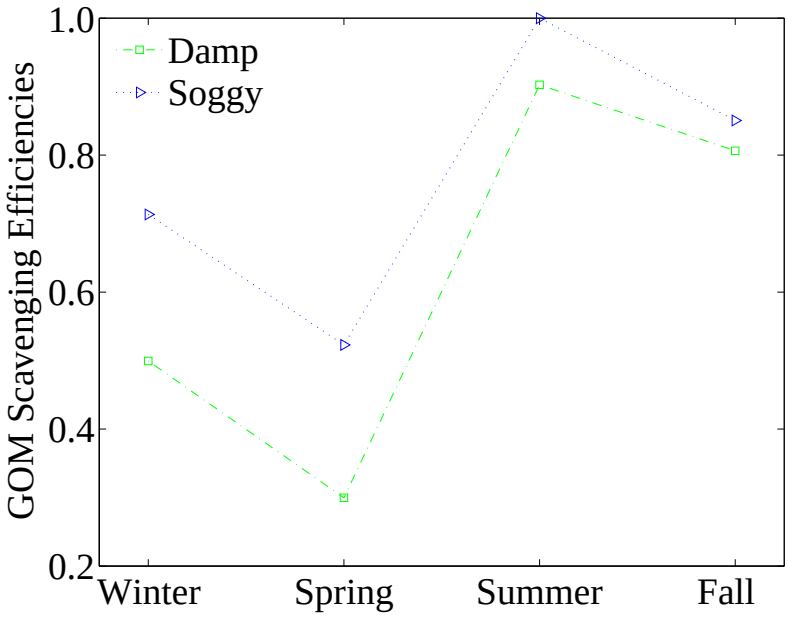

Figure 4.14: Seasonal pattern of scavenging efficiencies of GOM for damp, and soggy conditions.

GOM, and heavy precipitation scavenges GOM more efficiently than light precipitation on both 2-hour and 24-hour timescales.

4.2.2 Precipitation Intensity Scavenging Results for PBM

Dry, damp, and soggy PBM (Fig. 4.16) are all statistically different (KW test, 95%). The median PBM concentration decreases as the amount of precipitation increases. The time series of dry, damp, and soggy PBM is shown in Figure 4.17, with both full axes and truncated axes to allow the majority of data to be seen. Table 4.5 shows the PBM statistics for dry, damp, and soggy conditions. The PBM scavenging efficiency for light precipitation (damp) on a 2-hour timescale is 0.5. The PBM scavenging efficiency for heavy precipitation (soggy) on a 2-hour timescale is 0.7, meaning that the majority of PBM is removed from the atmosphere during heavy precipitation.

Approximately 7% of the entire PBM data set is below the MDL (1.5 $\mathrm{pg\,m^{-3}}$). If precipitation had no effect on PBM concentrations, then ~7% of each of the dry, damp, and soggy PBM data subsets should be below the MDL. Only 3% of the dry data set is

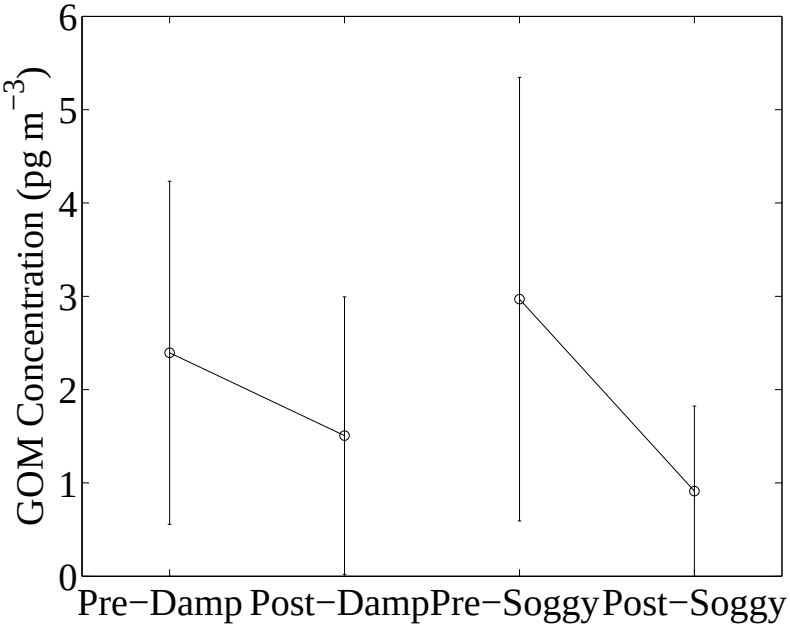

Figure 4.15: GOM precipitation scavenging for 26 separate light precipitation events and 29 separate heavy precipitation events (24-hour timescale). Before-damp represents the median of the population of data points collected during the 24 hours preceding the light precipitation events (197 data points). After-damp represents the median of the population of data points collected during and for 24 hours after the onset of the light precipitation events (201 data points). Likewise for the heavy precipitation events. Before-soggy and after-soggy data had 223 and 216 data points, respectively. Error bars are MADs.

Table 4.5: Statistical summary of dry, damp, and soggy PBM on a 2-hour timescale ($\mathrm{pg\ m^{-3}}$, except # data points).

PBM	Dry	Damp	Soggy
# Data Points	2906	171	157
Minimum	0.0	0.3	0.0
Maximum	343.9	77.0	803.2
Lower Quartile	4.1	2.0	1.2
Median	6.7	3.5	2.3
Upper Quartile	11.5	5.5	4.1
MAD	3.2	1.8	1.3

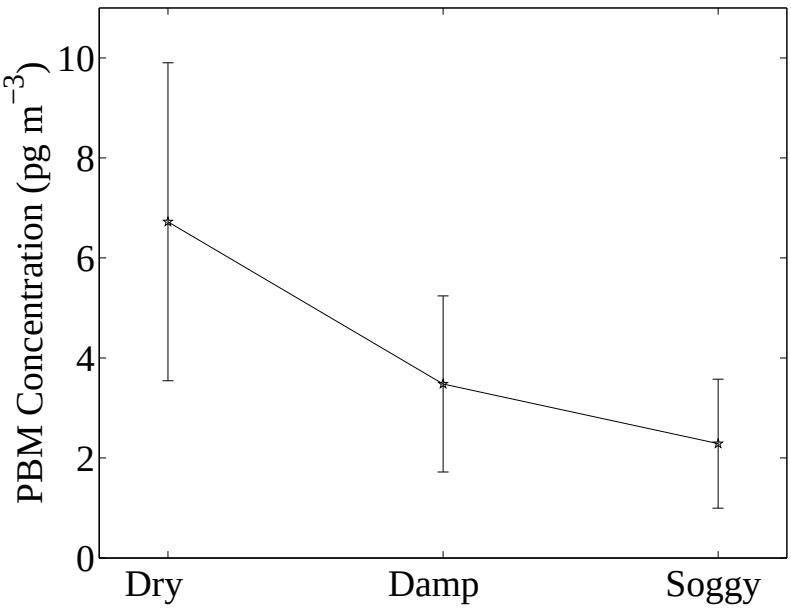

Figure 4.16: Median PBM concentrations with MAD error bars under dry, damp, and soggy conditions from 1 July 2009 to 30 June 2011.

below the MDL, while 14% and 32% of the damp and soggy PBM are below the MDL, respectively. This result supports the hypothesis that PBM is scavenged more efficiently as precipitation intensity increases.

During all seasons, dry PBM is statistically higher than damp and soggy PBM (Fig. 4.18). Fall and winter damp PBM are statistically higher than soggy PBM. Spring and summer damp and soggy PBM are statistically the same at the 95% confidence level (KW test). However, spring damp and soggy PBM are statistically different at the 75% confidence level. Damp PBM has a scavenging efficiency of 0.4-0.5 during all seasons, while soggy PBM has a scavenging efficiency of 0.4-0.8 (Fig. 4.19). The summer soggy PBM scavenging efficiency, in contrast the rest of the year, is only 0.4. The inconsistency during summer could be related to the small number of data points. For all other seasons, there are between 31 and 72 soggy PBM data points, but there are only 16 soggy PBM data points for summer.

The events in the pre-post (24-hour timescale) analysis of Section 4.1.4 were subdivided into damp and soggy categories. The before-damp and after-damp data are statistically dif-

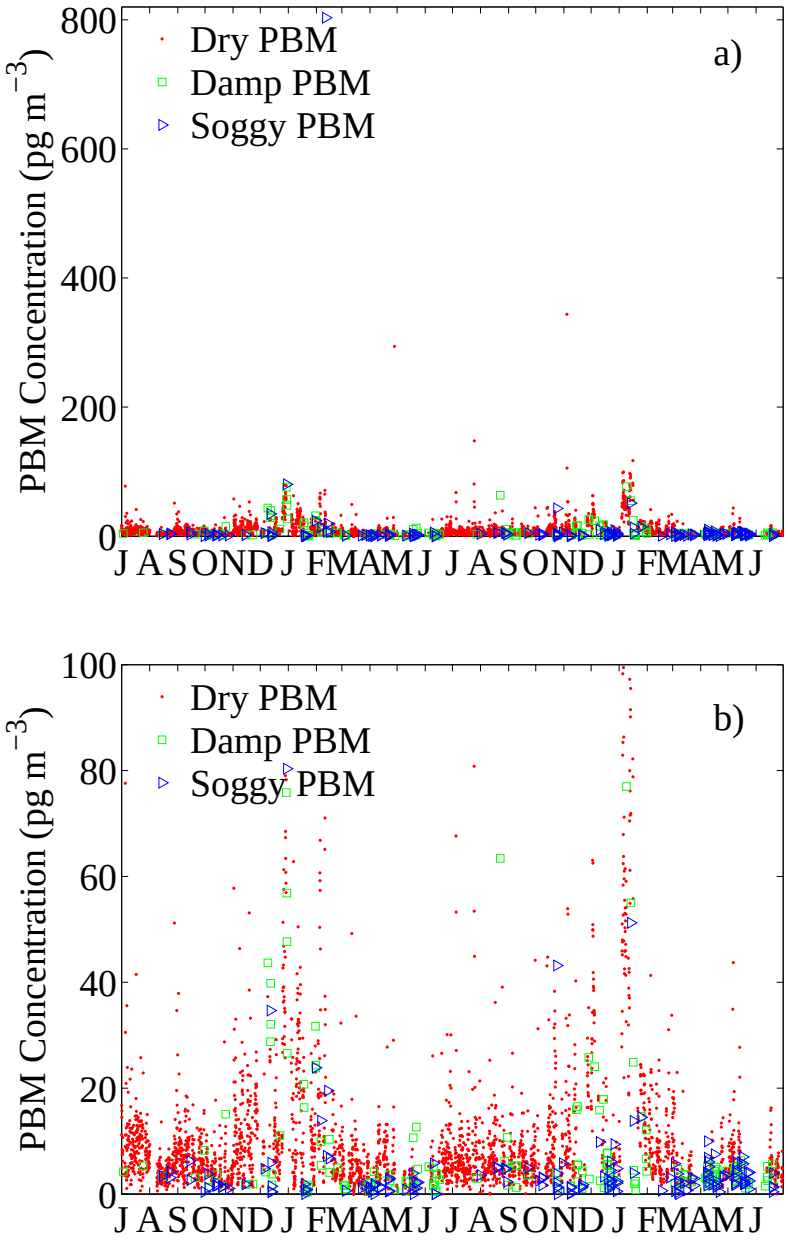

Figure 4.17: PBM concentration time series under dry, damp, and soggy conditions from 1 July 2009 to 30 June 2011 with: a) full, and b) truncated axes.

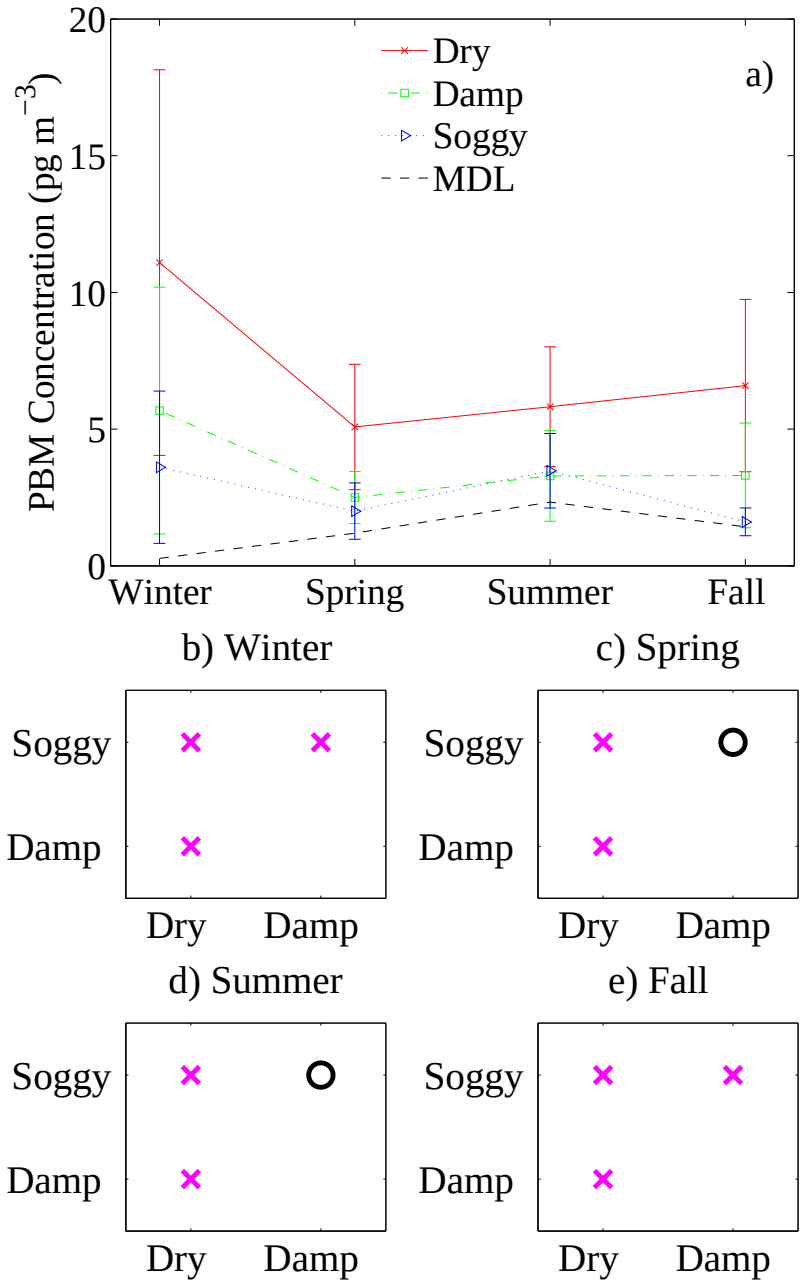

Figure 4.18: Seasonal pattern of PBM concentrations for dry, damp, and soggy conditions: a) dry, damp, and soggy median PBM by season with MAD error bars and results of KW test for b) winter, c) spring, d) summer, and e) fall. Comparison pairs that are statistically different are marked with an X, and an O if they are statistically the same.

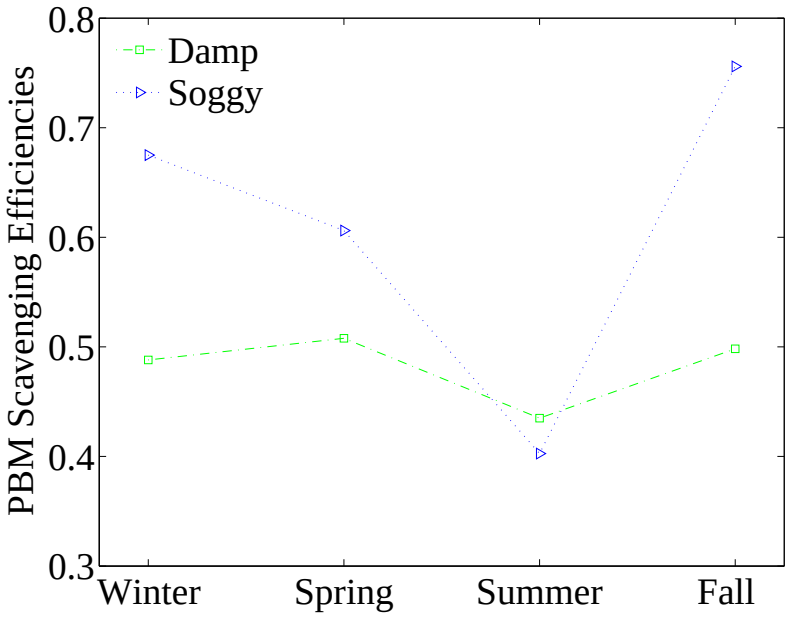

Figure 4.19: Seasonal pattern of scavenging efficiencies of PBM for damp and soggy conditions.

ferent (two-sided Wilcoxon test, 95%) on a 24-hour timescale as are the before-soggy and after-soggy data (Fig. 4.20). The scavenging efficiency, defined in Equation 4.1, is 0.2 for the damp case and 0.4 for the soggy case. This suggests that precipitation does scavenge PBM on a 24-hour timescale, but not a majority. It should be noted, however, that the Tekran 2537B only measures particles with aerodynamic diameters < ~2.7 μm. The scavenging efficiency will vary greatly depending on the underlying particle size distribution.

4.2.3 Precipitation Intensity Scavenging Results for GEM

Dry, damp, and soggy GEM are all statistically the same (KW test, 95%), which means that the scavenging efficiency is 0.0 (Fig. 4.21). Table 4.6 shows the basic statistics for dry, damp, and soggy GEM.

If precipitation had no effect on GEM concentrations, then approximately 10% of the (pruned) dry, damp, and soggy GEM subsets should be below the overall unpruned lowest decile of GEM (1.31 $\mathrm{ng\ m^{-3}}$). Approximately 11% of dry GEM is below the overall decile.

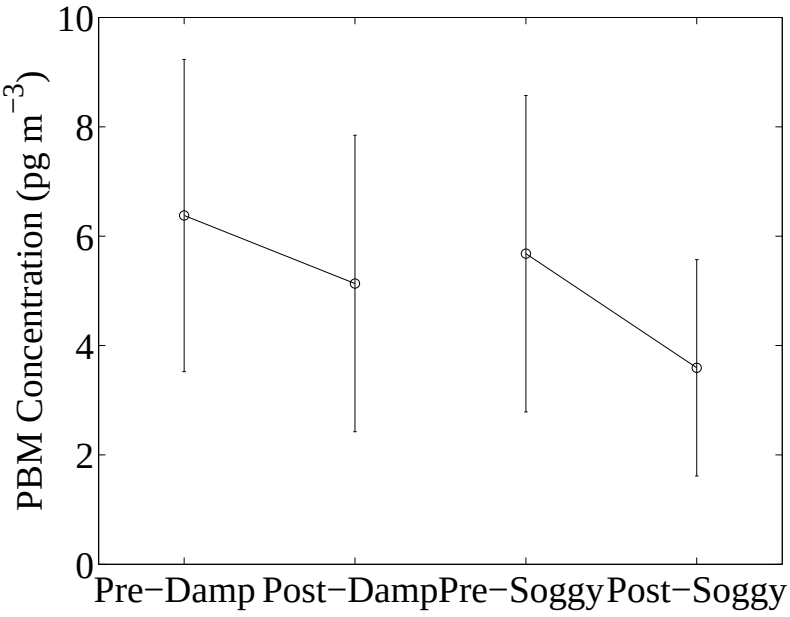

Figure 4.20: PBM precipitation scavenging for 28 separate light precipitation events and 28 separate heavy precipitation events (24-hour timescale). Before-damp represents the median of the population of data points collected during the 24 hours preceding the light precipitation events (209 data points). After-damp represents the median of the population of data points collected during and for 24 hours after the onset of the light precipitation events (220 data points). Likewise for the heavy precipitation events. Before-soggy and after-soggy data had 216 and 206 data points, respectively. Error bars are MADs.

Table 4.6: Statistical summary of dry, damp, and soggy GEM on a 2-hour timescale ($\mathrm{ng\ m^{-3}}$, except # data points).

GEM	Dry	Damp	Soggy
# Data Points	3097	172	158
Minimum	0.73	1.20	1.14
Maximum	3.95	3.57	3.09
Lower Quartile	1.43	1.46	1.49
Median	1.57	1.59	1.61
Upper Quartile	1.74	1.73	1.72
MAD	0.15	0.14	0.11

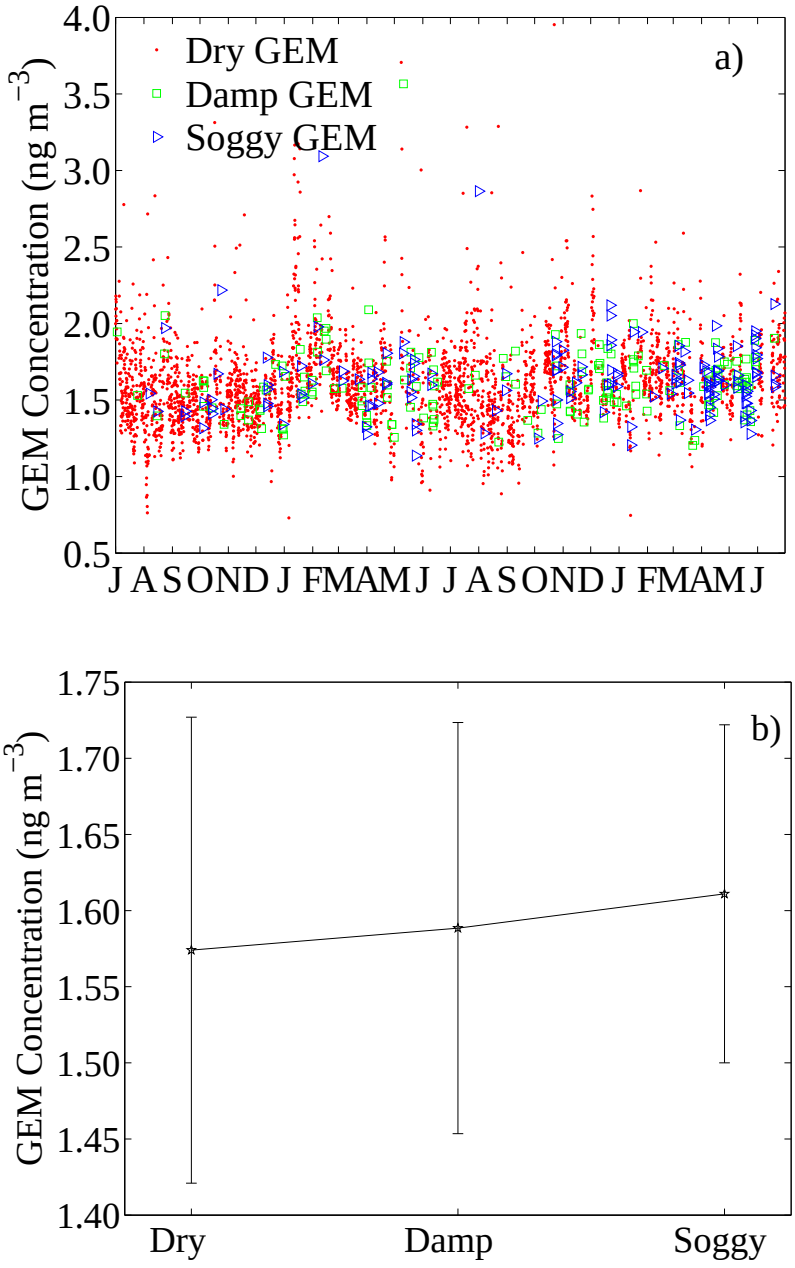

Figure 4.21: GEM concentrations under dry, damp, and soggy conditions from 1 July 2009 to 30 June 2011: a) time series, and b) medians with MAD error bars.

Meanwhile, only 5% of the damp GEM and only 6% of the soggy GEM is below the decile. These results suggest that if precipitation has any effect on GEM, GEM increases as the amount of precipitation increases. This apparent increase in GEM could be due to a reduction in the photochemical conversion of GEM to GOM during the cloudy and cold conditions that tend to accompany precipitation. It could also result from an increased emission from the soil (e.g., Lindberg et al., 1999).

Dry, damp, and soggy GEM (Fig. 4.22) are also all statistically the same for all seasons (KW test, 95%) yielding a scavenging efficiency of 0.0 for both damp and soggy GEM for every season.

The before-damp and after-damp data (Fig. 4.23) are statistically the same as are the before-soggy and after-soggy data (two-sided Wilcoxon test, 95%) on a 24-hour timescale. The scavenging efficiency, defined in Equation 4.1, is 0.0 for both the damp and soggy cases (i.e., precipitation does not scavenge GEM regardless of the amount of precipitation).

4.3 Hypothesis #3: Precipitation Type

This section will use the textual weather descriptions attached to the KHIF data to separate the data by precipitation type (i.e., rain, snow, or mixed). The raw KHIF data (mostly temperature and weather descriptions such as "rain" or "snow") were used to assign flags to the 1-hour precipitation data (Table 4.7).

The post-pre (24-hour timescale) analysis was extended to the precipitation type analysis. The events found in the post-pre analysis were separated into rain, snow and mixed events based on all KHIF observations made during the 26-hour period from the begin-

Table 4.7: Precipitation flags for the KHIF data.

Precipitation Type Flag	Meaning
0	No Measurable Precipitation
1	Rain
2	Snow
3	Mixed Rain and Snow or Uncertain Type (near 0°C)

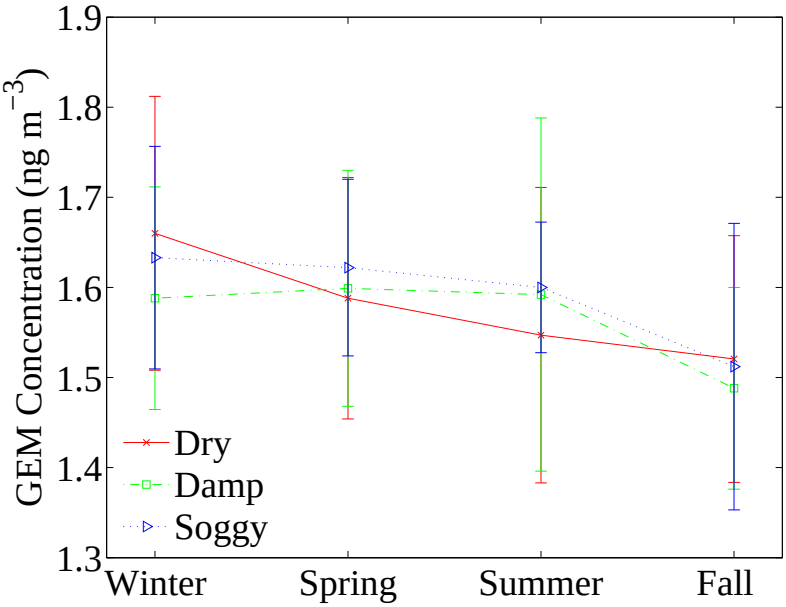

Figure 4.22: Dry, damp, and soggy median GEM by season with MAD error bars.

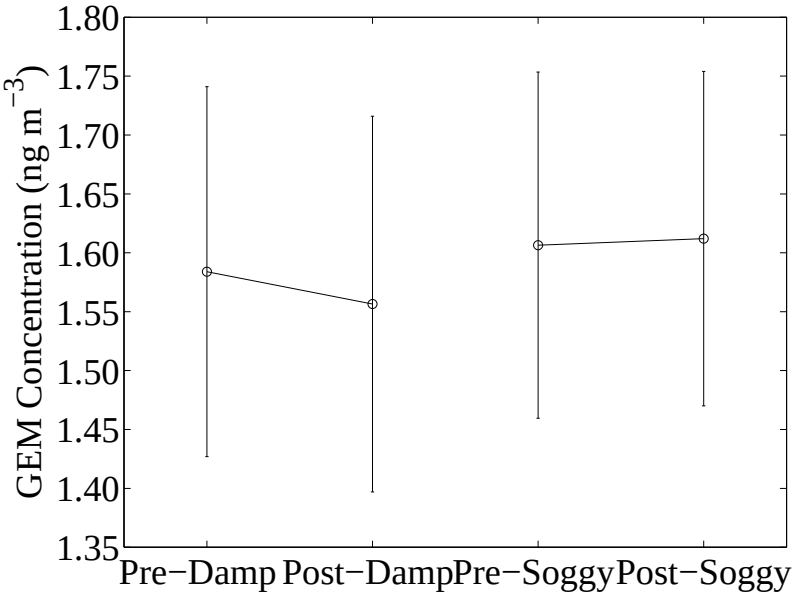

Figure 4.23: GEM precipitation scavenging for 41 separate light precipitation events and 41 separate heavy precipitation events (24-hour timescale). Before-damp represents the median of the population of data points collected during the 24 hours preceding the light precipitation events (332 data points). After-damp represents the median of the population of data points collected during and for 24 hours after the onset of the light precipitation events (324 data points). Likewise for the heavy precipitation events. Before-soggy and after-soggy data had 322 and 311 data points, respectively. Error bars are MADs.

ning of adsorption to 24 hours after the event datum time stamp. During rain events, only liquid precipitation was observed at KHIF. Likewise, during snow events, only frozen precipitation was observed at KHIF. Mixed events include times when both frozen and liquid precipitation occurred or when the precipitation type was unclear in the KHIF data.

The rain events were subsequently separated into light rain and heavy rain events based on the soggy definition (Section 4.2). Snow and mixed-phase precipitation events were similarly separated when there were enough events to do so.

4.3.1 Precipitation Type Effects on Scavenging of GOM

Dry GOM is statistically higher than rain, snow, and mixed GOM on a 2-hour timescale (Fig. 4.24). Meanwhile, rain, snow, and mixed GOM are all statistically the same as the median of each is below the MDL. The scavenging efficiency for both rain and snow is 0.7, while the scavenging efficiency for mixed precipitation is 0.8. These results suggest that all three forms of precipitation are quite effective at scavenging GOM. The time series of dry, rain, snow, and mixed GOM are shown in Figure 4.25. The statistical summary of the precipitation type analysis for GOM is given in Table 4.8. In addition to the medians and MADs demonstrating that the dry and precipitation subsets exhibit different distributions, the upper quartiles also show this quite clearly. The upper quartile for the dry GOM subset is 10.1 $\mathrm{pg\ m^{-3}}$, while none of the upper quartiles for any of the precipitation GOM subsets is above 2.5 $\mathrm{pg\ m^{-3}}$.

Table 4.8: Statistical summary of dry, rain, snow, and mixed GOM on a 2-hour timescale ($\mathrm{pg\ m^{-3}}$, except # data points).

GOM	Dry	Rain	Snow	Mixed
# Data Points	2960	177	85	48
Minimum	0.0	0.0	0.0	0.0
Maximum	225.6	14.6	24.7	14.5
Lower Quartile	1.3	0.2	0.3	0.0
Median	3.7	1.1	0.9	0.6
Upper Quartile	10.1	2.5	2.3	1.9
MAD	2.9	1.1	0.9	0.6

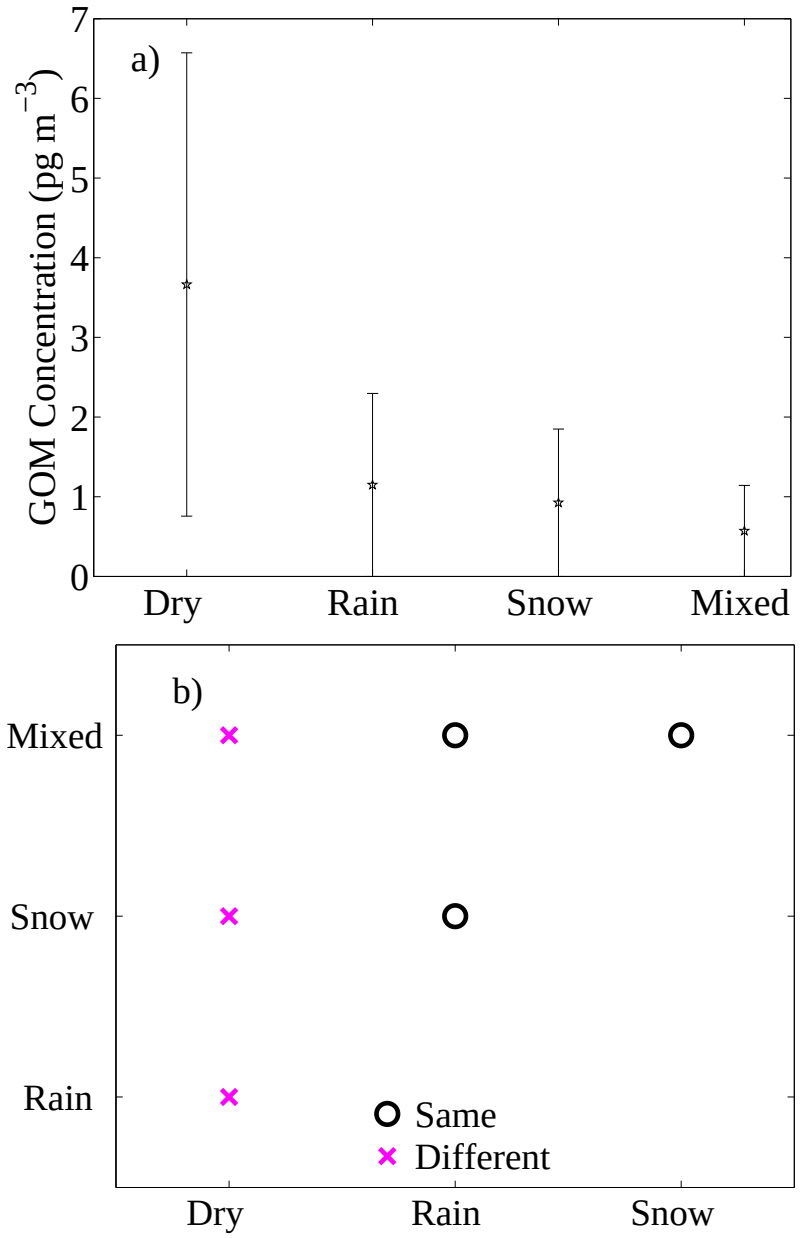

Figure 4.24: Dry, rain, snow, and mixed GOM: a) medians, error bars are MADs, and b) KW test results for comparison pairs.

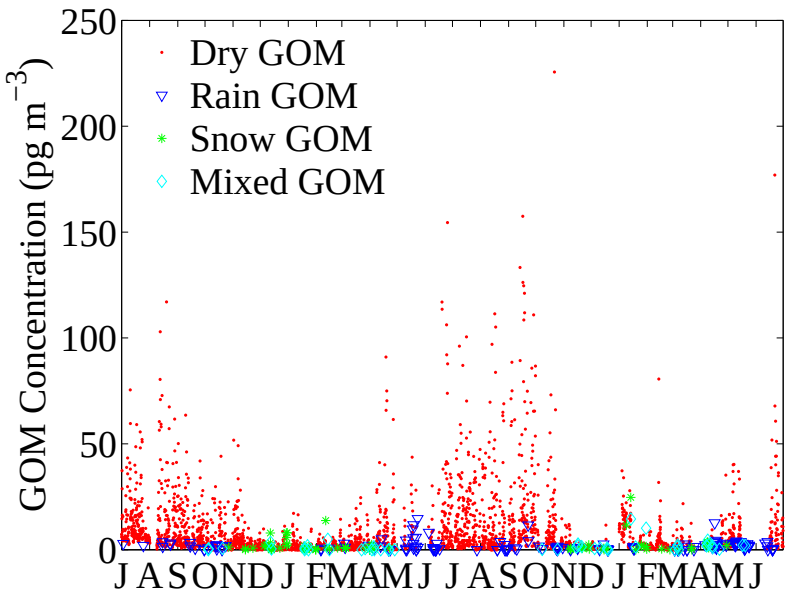

Figure 4.25: Dry, rain, snow, and mixed GOM time series from 1 July 2009 to 30 June 2011.

Approximately 37% of the entire GOM data set is below the MDL (1.5 $\mathrm{pg\ m^{-3}}$). If precipitation had no effect on GOM concentrations, then ~37% of each of the dry, rain, and snow GOM data subsets should be below the MDL. Only 28% of the dry data set is below the MDL, while 54%, 62%, and 68% of the rain, snow and mixed GOM are below the MDL, respectively. This result supports the hypothesis that GOM is scavenged by all forms of precipitation, and indicates mixed precipitation scavenges GOM most efficiently.

The seasonality of dry, rain, snow, and mixed GOM concentrations is shown in Figure 4.26. Only some types of precipitation could be included in the KW test for some seasons because of small sample sizes (i.e., at least 10 data points were required for statistical tests). During winter, dry, snow, and mixed GOM are statistically the same. Wintertime rain GOM is statistically lower than dry GOM with a scavenging efficiency of 0.7. During the spring, rain and snow GOM are statistically the same and are lower than dry GOM. The springtime scavenging efficiencies of GOM for rain and snow are 0.3 and 0.4, respectively. During the summer, dry GOM is higher than rain GOM with a scavenging efficiency of 0.9. In fall, dry

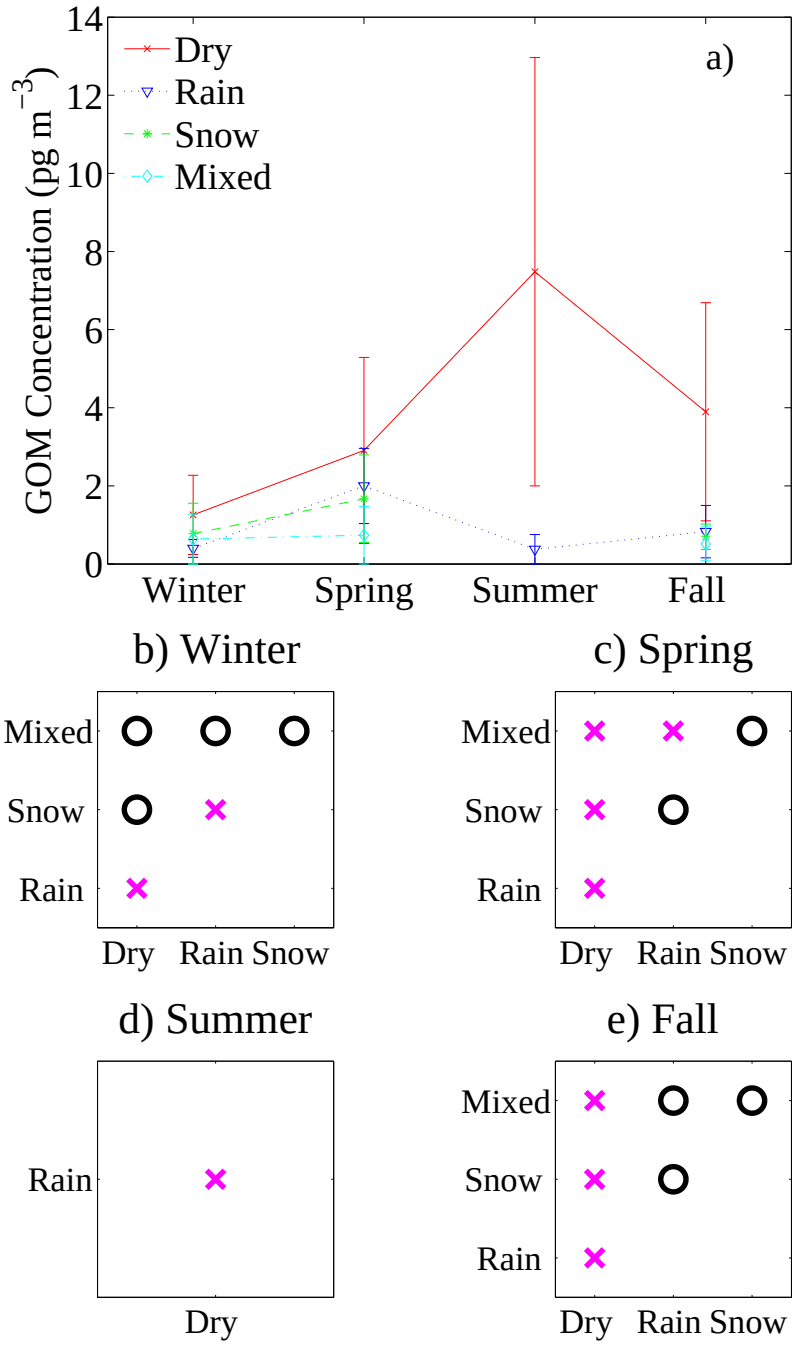

Figure 4.26: Dry, rain, snow, and mixed GOM: a) medians by season and results of the KW test for b) winter, c) spring, d) summer, and e) fall. Error bars are MADs.

GOM is statistically higher than rain, snow, and mixed GOM. The three GOM precipitation subsets are all statistically the same for fall because the medians are all below the MDL. The autumn scavenging efficiencies of GOM for rain, snow, and mixed precipitation are 0.8, 0.8 and 0.9, respectively. These results are consistent with the hypothesis that all forms of precipitation scavenge GOM.

The events in the pre-post (24-hour timescale) analysis were subdivided into rain, snow, and mixed categories (Fig. 4.27). The before-rain and after-rain data are statistically different (28 events), and the scavenging efficiency is 0.5. The before-snow and after-snow data are also statistically different (11 events) with a scavenging efficiency for snow of 0.6. The before-mixed and after-mixed data are statistically different (16 events), with a scavenging efficiency of 0.7.

When the rain events are separated into light rain and heavy rain events (using the soggy definition), pre- and post- light rain were statistically the same while pre- and post- heavy rain events were statistically different. This suggests that rain does scavenge GOM, but how well rain scavenges GOM depends on the amount of rain. The scavenging efficiency for heavy rain is 0.6. Only three of the eight snow events qualify as soggy, so no determination can be made about how well heavy snow events scavenge GOM compared to light snow events. Pre- and post- heavy mixed precipitation events were statistically different with a scavenging efficiency of 0.8. Only five of the 16 mixed events are light events, so it is not possible to use this data set to determine the scavenging efficiency of light mixed events.

4.3.2 Precipitation Type Effects on Scavenging of PBM

Dry PBM is statistically higher than rain, snow, and mixed (Fig. 4.28). Snow PBM is higher than both rain and mixed (KW test, 5%). The scavenging efficiencies for rain, snow, and mixed precipitation are 0.6, 0.5, and 0.7, respectively. Thus, mixed precipitation scavenges PBM more efficiently than other forms of precipitation. The time series of dry, rain, snow, and mixed PBM are shown in Figure 4.29. The statistical summary of the pre-

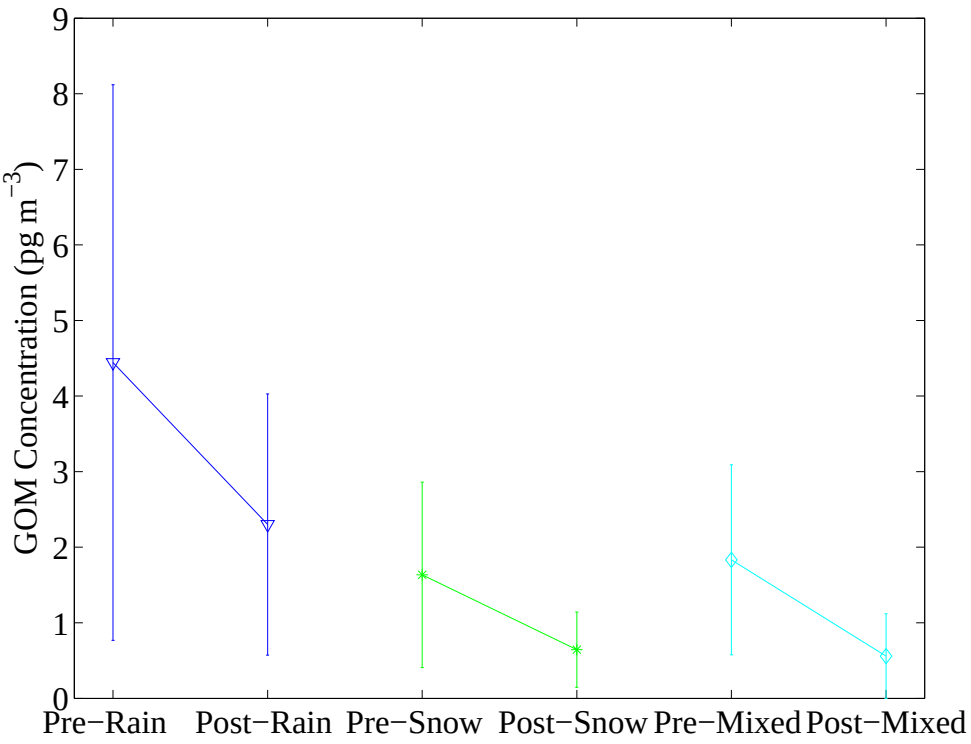

Figure 4.27: GOM precipitation scavenging for 28 separate rain events, 11 separate snow events, and 16 mixed events (24-hour timescale). Before-rain represents the median of the population of data points collected during the 24 hours preceding the rain events (212 data points). After-rain represents the median of the population of data points collected during and for 24 hours after the onset of the rain events (205 data points). Likewise for the snow and mixed events. Before-snow and after-snow data had 88 and 86 data points, respectively. Before-mixed and after-mixed data had 120 and 126 data points, respectively. Error bars are MADs.

Table 4.9: Statistical summary of dry, rain, snow, and mixed PBM on a 2-hour timescale ($\mathrm{pg\ m^{-3}}$, except # data points).

PBM	Dry	Rain	Snow	Mixed
# Data Points	2906	186	92	50
Minimum	0	0	0	0
Maximum	343.9	63.4	803.2	55.0
Lower Quartile ($q_{0.25}$)	4.1	1.8	1.4	1.2
Median ($q_{0.5}$)	6.7	2.8	3.4	2.3
Upper Quartile ($q_{0.75}$)	11.5	4.8	10.2	4.7
MAD	3.2	1.2	2.4	1.5

cipitation type analysis for PBM is given in Table 4.9. Every statistic for rain and mixed PBM demonstrate a lower distribution compared to dry PBM. Snow PBM, however, has some outliers of very high concentration. While the median snow PBM is well below the median dry PBM, the snow PBM upper quartile is above that for dry PBM. The scavenging efficiency for snow likely depends on the size distribution of snowflakes, about which no information is available for this data set. In addition, this analysis describes the scavenging efficiency of PBM of particles smaller than ~2.7 $\mu\mathrm{m}$ aerodynamic diameter, and the scavenging efficiency would likely be higher for larger particles.

Approximately 7% of the entire PBM data set is below the MDL (1.5 $\mathrm{pg\ m^{-3}}$). If precipitation had no effect on PBM concentrations, then ~7% of each of the dry, rain, and snow PBM data subsets should be below the MDL. Only 3% of the dry data set is below the MDL, while 17%, 27% and 36% of the rain, snow and mixed PBM are below the MDL, respectively. This result supports the hypothesis that PBM is scavenged by all forms of precipitation, and indicates mixed precipitation scavenges PBM most efficiently.

Figure 4.30 shows the dry, rain, snow, and mixed subcategories by season. A population is not included in the KW test if there are less than ten data points in a population for a given season. Accordingly, there are no KW results included for some types of precipitation during some seasons. The results in Figure 4.30 suggest that rain scavenges precipitation because rain PBM is statistically lower than dry PBM during all four seasons. The scavenging efficiency of rain for PBM varies between 0.4 and 0.6. Snow PBM was lower than

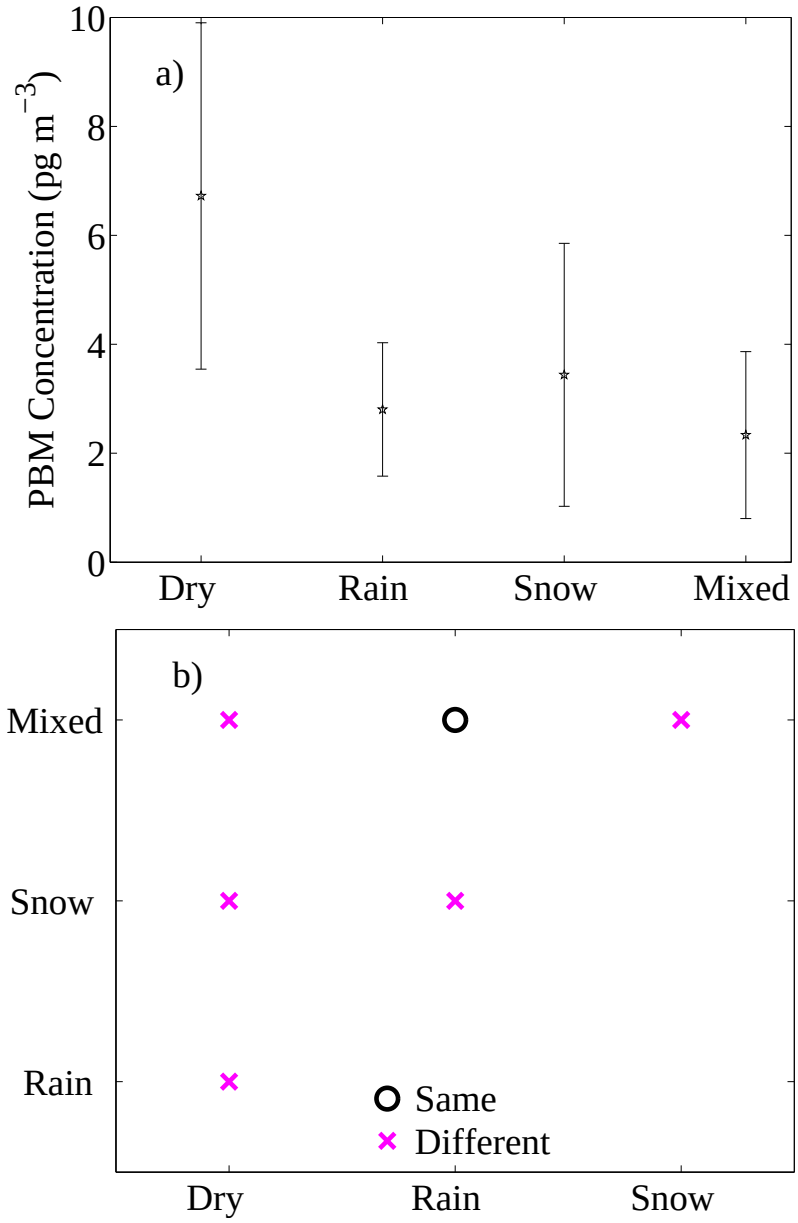

Figure 4.28: Dry, rain, snow, and mixed PBM: a) medians, error bars are MADs, and b) KW test results for comparison pairs.

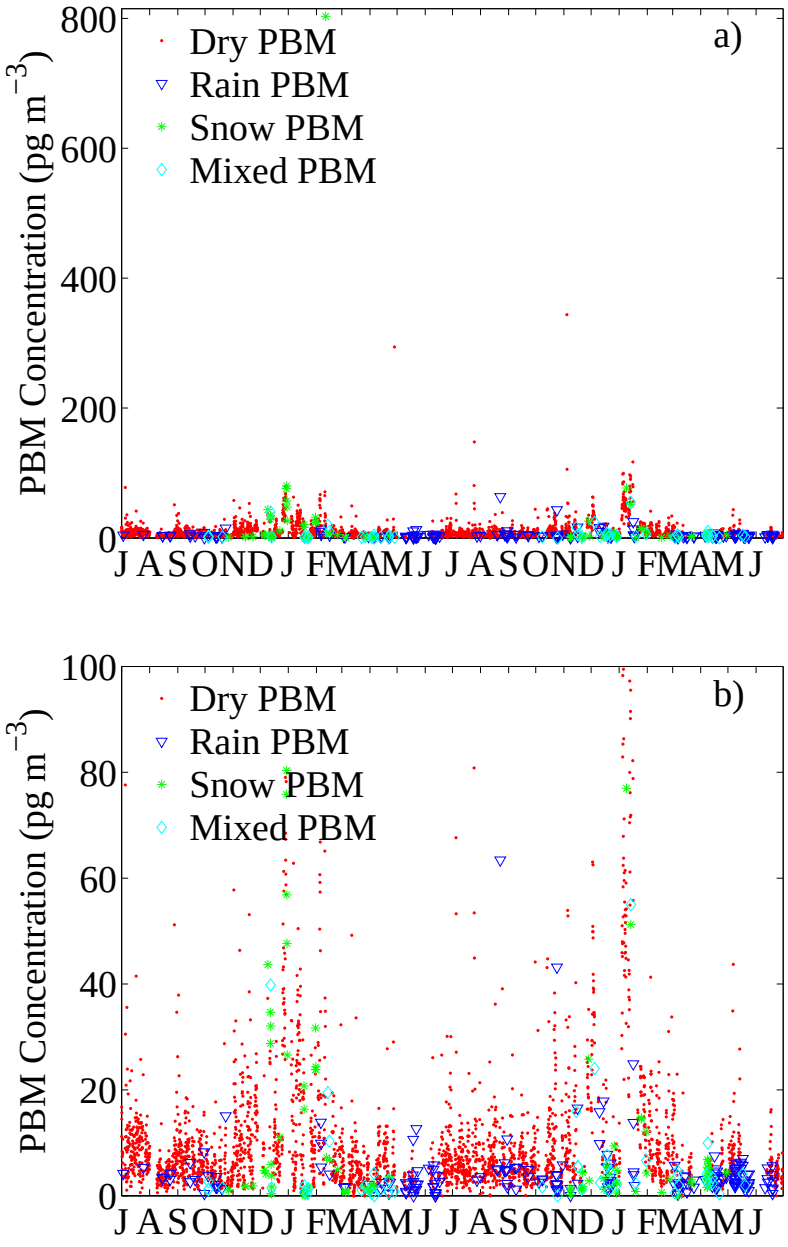

Figure 4.29: Dry, rain, snow, and mixed PBM time series from 1 July 2009 to 30 June 2011 with both: a) full axes to allow the outliers to be seen, and b) truncated axes to allow a view of the majority of data.

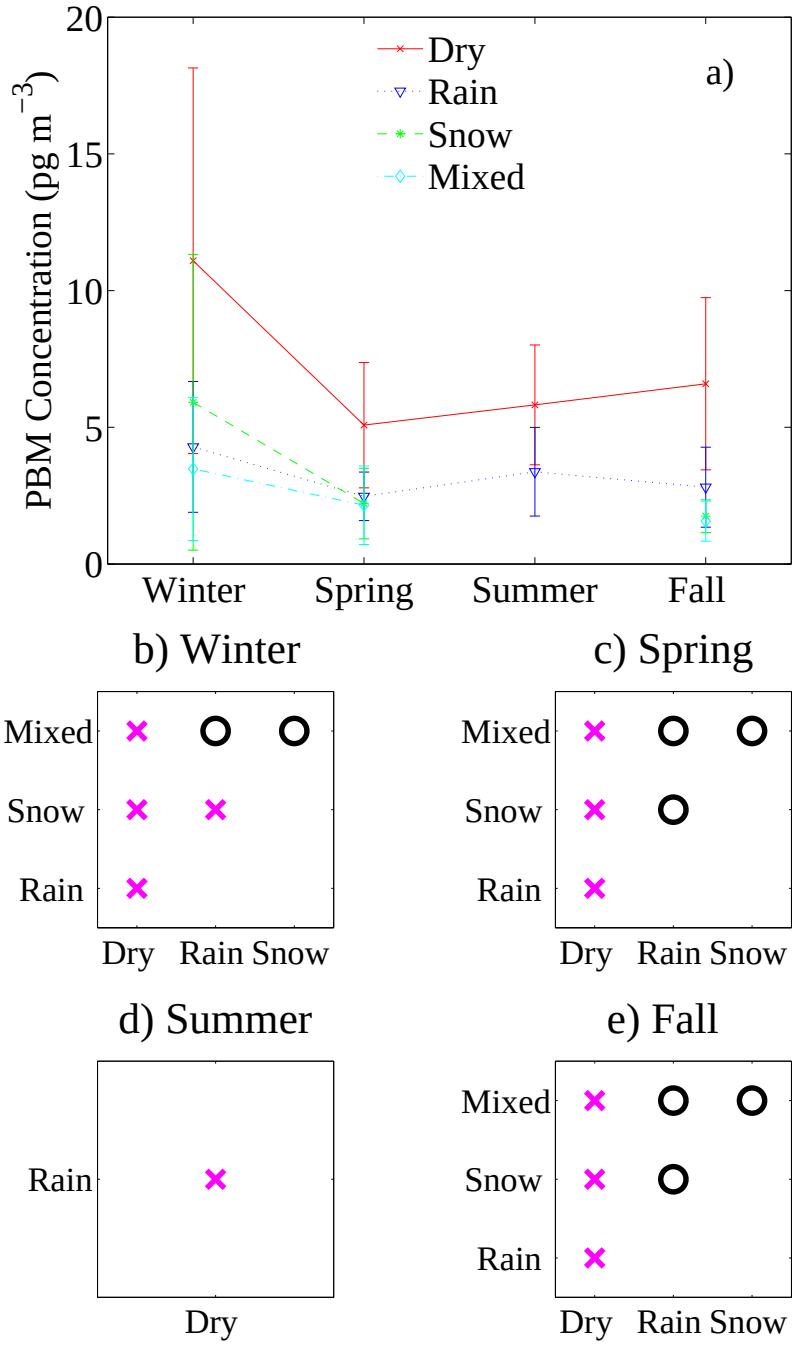

Figure 4.30: Dry, rain, snow, and mixed PBM: a) medians by season and results of the KW test for b) winter, c) spring, d) summer, and e) fall. Error bars are MADs.

dry PBM during fall through spring (the seasons that had snow), and the scavenging efficiencies varied between 0.5 and 0.7. Mixed PBM was lower than dry PBM during fall through spring (the seasons that had mixed precipitation), and the scavenging efficiencies varied between 0.6 and 0.8.

The events in the pre-post (24-hour timescale) analysis of Section 4.1.4 were subdivided into rain, snow, and mixed categories. The before-rain and after-rain data are statistically different (Fig. 4.31). The scavenging efficiency, defined in Equation 4.1, for rain is 0.1. The before-snow and after-snow data are statistically different with a scavenging efficiency of 0.3. In addition, the before-mixed and after-mixed data are statistically different (two-sided Wilcoxon test, 95%). The scavenging efficiency for mixed-phase precipitation is 0.4, suggesting that mixed-phase precipitation scavenges PBM better than either rain or snow alone.

When the rain events are separated into light rain and heavy rain events (using the soggy definition), pre- and post- light rain were statistically the same while pre- and post- heavy rain events were statistically different. The scavenging efficiency for heavy rain is 0.2. Only 3 of the 12 snow events qualify as soggy, so no determination can be made about how well heavy snow events scavenge PBM compared to light snow events. Five of the 15 mixed events are heavy events, so it is not possible to use this data set to determine what the scavenging efficiency of light mixed events might be. Pre- and post- heavy mixed-phase precipitation are statistically different with a scavenging efficiency of 0.5.

4.3.3 Precipitation Type Effects on Scavenging of GEM

Rain GEM is statistically higher than dry GEM on a 2-hour timescale (Fig. 4.32). Snow GEM is statistically lower than both dry GEM and rain GEM. Mixed GEM is statistically the same as dry, rain, and snow GEM which implies that rain GEM and snow GEM barely passed the statistical significance test. These results suggest that rain may act to promote higher GEM concentrations. The scavenging efficiency of rain is -0.04, indicating that rain

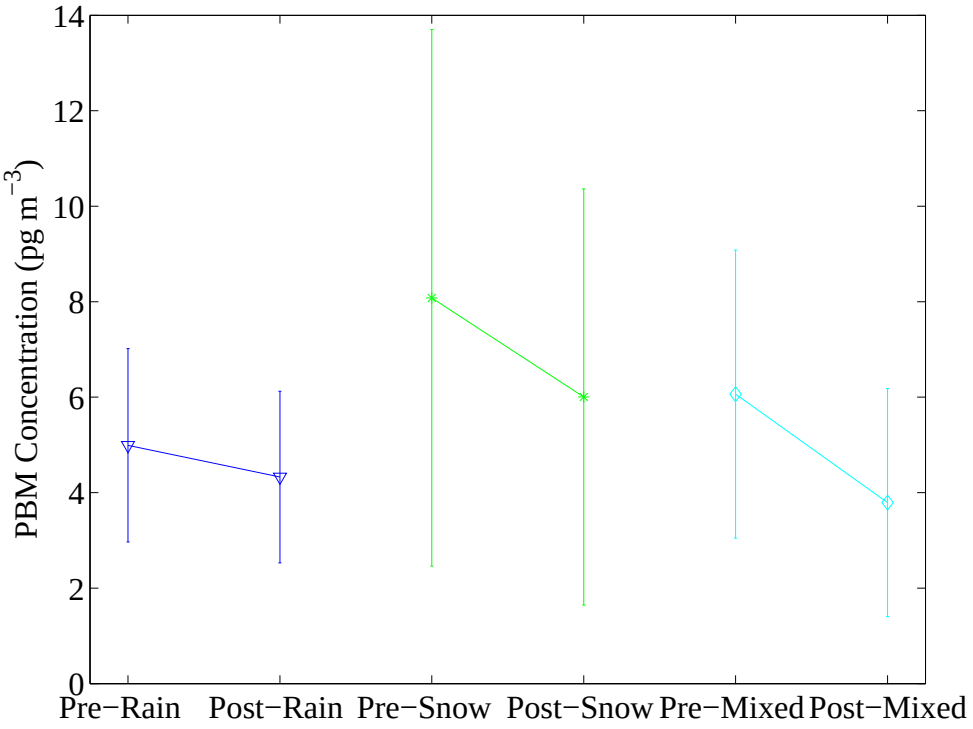

Figure 4.31: PBM precipitation scavenging for 29 rain, 12 snow, and 15 mixed precipitation events (24-hour timescale). Before-rain represents the median of the population of data points collected during the 24 hours preceding the rain events (216 data points). After-rain represents the median of the population of data points collected during and for 24 hours after the onset of the rain events (214 data points). Likewise for the snow and mixed precipitation events. Before-snow and after-snow PBM data had 96 and 94 data points, respectively. Before-mixed and after-mixed PBM data had 113 and 118 data points, respectively. Error bars are MADs.

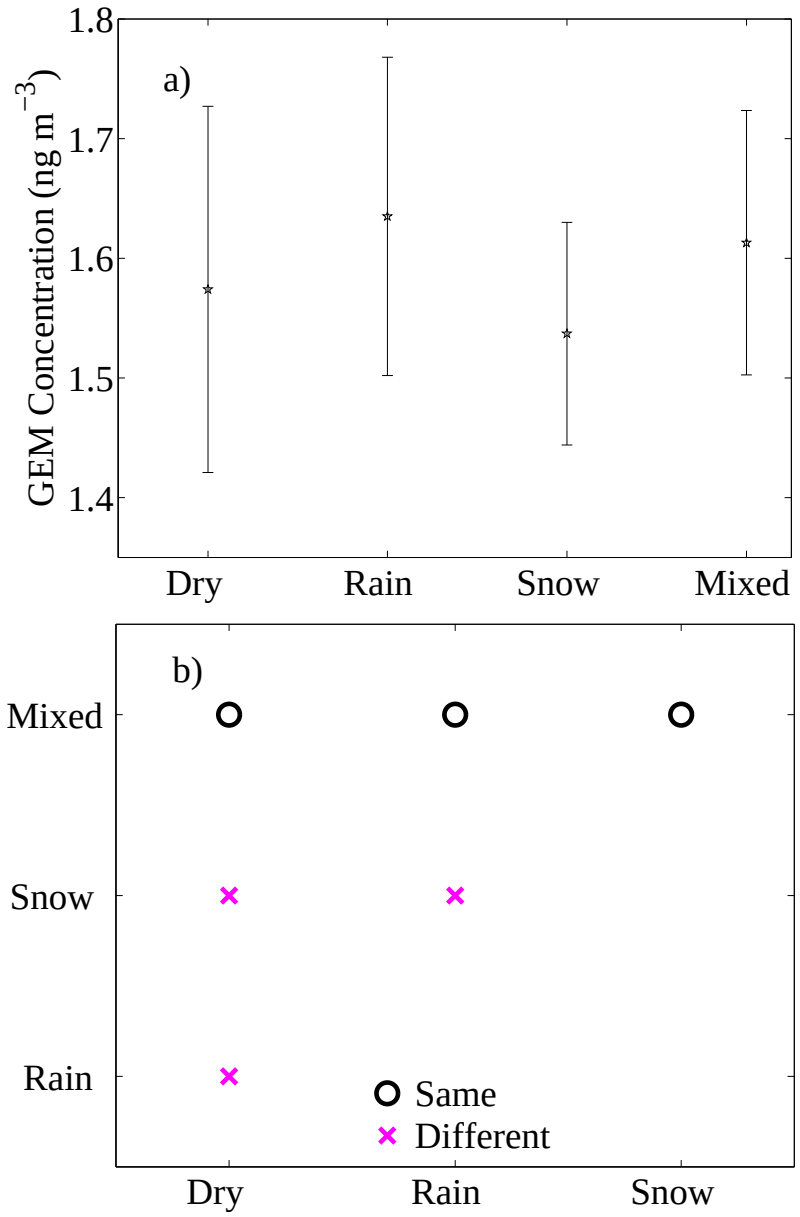

Figure 4.32: Dry, rain, snow, and mixed GEM: a) medians, error bars are MADs, and b) KW test results for comparison pairs.

may promote very slightly higher GEM concentrations compared to dry conditions. Weiss-Penzias et al. (2009) observed GEM enhancement events associated with rain near their detector. Snow GEM is statistically lower than dry GEM, suggesting that the presence of snow promotes lower concentrations of GEM. Scavenging seems an unlikely explanation as GEM is not water soluble and rain clearly does not scavenge GEM. A possible explanation is that snow covering the ground prevents soil emissions of GEM. The scavenging efficiency for snow is 0.02, indicating that while the snow GEM and dry GEM are statistically different, the effect of snow is quite small. As dry GEM and mixed GEM are statistically the same, the scavenging efficiency is 0.0. The time series of dry, rain, snow, and mixed GEM are shown in Figure 4.33. The statistical summary of the precipitation type analysis for GEM is given in Table 4.10.

The 2-hour precipitation type analysis for GEM is consistent with Lindberg et al. (1999) who observed emissions of mercury following wetting soil either by rainfall or irrigation using flux chambers. Perhaps the liquid precipitation promotes mercury emissions from the soil as, Lindberg et al. (1999) suggested, because liquid precipitation goes down into the soil. Meanwhile, snow will form a layer on top of the soil preventing emission. Mixed precipitation could go either way depending on whether it is more like rain or more like snow.

The results of the lowest 10% test for dry, rain, snow, and mixed GEM are shown in Table 4.11. The results are not consistent with the hypothesis that precipitation scavenges GEM. The results suggest that if precipitation has any affect on GEM, precipitation promotes higher GEM. Unlike the results for GOM and PBM, the dry GEM subset has slightly more than 10% of its population below the overall decile of 1.31 $\mathrm{ng\ m^{-3}}$ and less than 10% of each precipitation data subset is below the overall decile.

Seasonality of dry, rain, snow, and mixed GEM concentrations is shown in Figure 4.34. Only some types of precipitation could be included in the KW test for some seasons because of small sample sizes. During winter and spring, snow GEM is statistically lower than dry

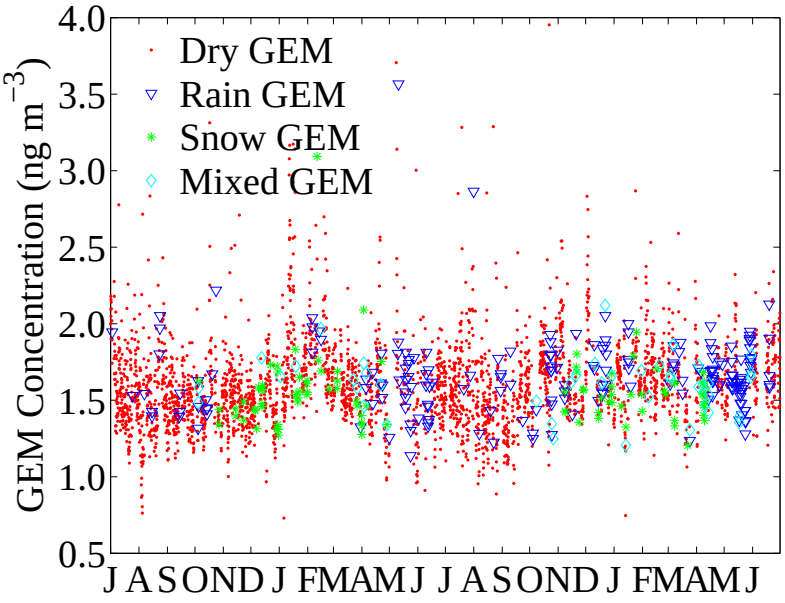

Figure 4.33: Dry , rain, snow, and mixed GOM time series from 1 July 2009 to 30 June 2011.

Table 4.10: Statistical summary of dry, rain, snow, and mixed GEM on a 2-hour timescale (ng m^{-3}, except # data points).

GEM	Dry	Rain	Snow	Mixed
# Data Points	3097	193	95	42
Minimum	0.73	1.14	1.20	1.21
Maximum	3.95	3.57	3.09	2.12
Lower Quartile	1.43	1.52	1.43	1.49
Median	1.57	1.64	1.54	1.61
Upper Quartile	1.74	1.78	1.62	1.69
MAD	0.15	0.13	0.09	0.11

GEM, which is lower than rain GEM. During the summer, dry and rain GEM are the same. During fall, dry, snow and rain GEM are all statistically the same. These results suggest that rain promotes higher concentrations of GEM and snow promotes lower concentrations of GEM, though these observations are only statistically significant for two of the four seasons.

The events in the pre-post (24-hour timescale) analysis were subdivided into rain, snow, and mixed categories (Fig. 4.35). The before-rain and after-rain data are statistically the same (37 events), with a scavenging efficiency of 0.0. When the rain events are separated into light rain and heavy rain events (using the soggy definition), pre- and post- light rain are the statistically the same (18 events). The pre- and post- heavy rain are also statistically the same (19 events).

The before-snow and after-snow data are statistically the same, so the scavenging efficiency is 0.0. Fourteen of the 19 snow events were light events, and pre- and post- light snow events are also statistically the same.

The before-mixed and after-mixed GEM data are statistically the same (two-sided Wilcoxon test, 95%), with a scavenging efficiency of 0.0. Seventeen of the 26 mixed events are heavy events, and pre- and post- heavy mixed events were statistically the same. Figure 4.35 shows the medians and MADs for the pre-post rain/snow/mixed analysis.

Table 4.11: Dry, rain, snow and mixed GEM below lowest decile (2-hour timescale).

GEM	Value	# Data Points
Overall Lowest Decile	1.31 $\mathrm{ng\ m^{-3}}$	111674
Dry Below Decile	11 %	3097
Rain Below Decile	5 %	193
Snow Below Decile	4 %	95
Mixed Below Decile	7 %	42

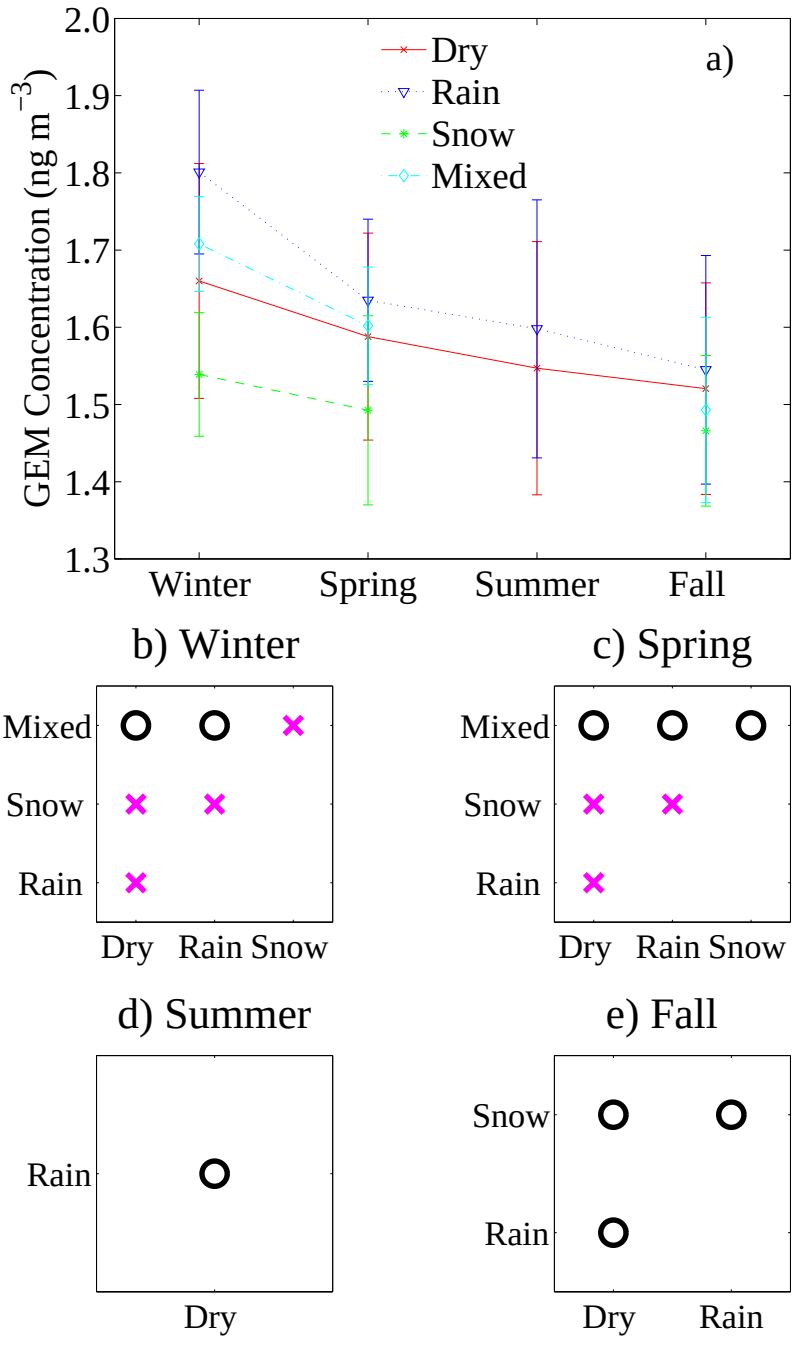

Figure 4.34: Dry, rain, snow, and mixed GEM: a) medians by season and results of the KW test for b) winter, c) spring, d) summer, and e) fall. Error bars are MADs.

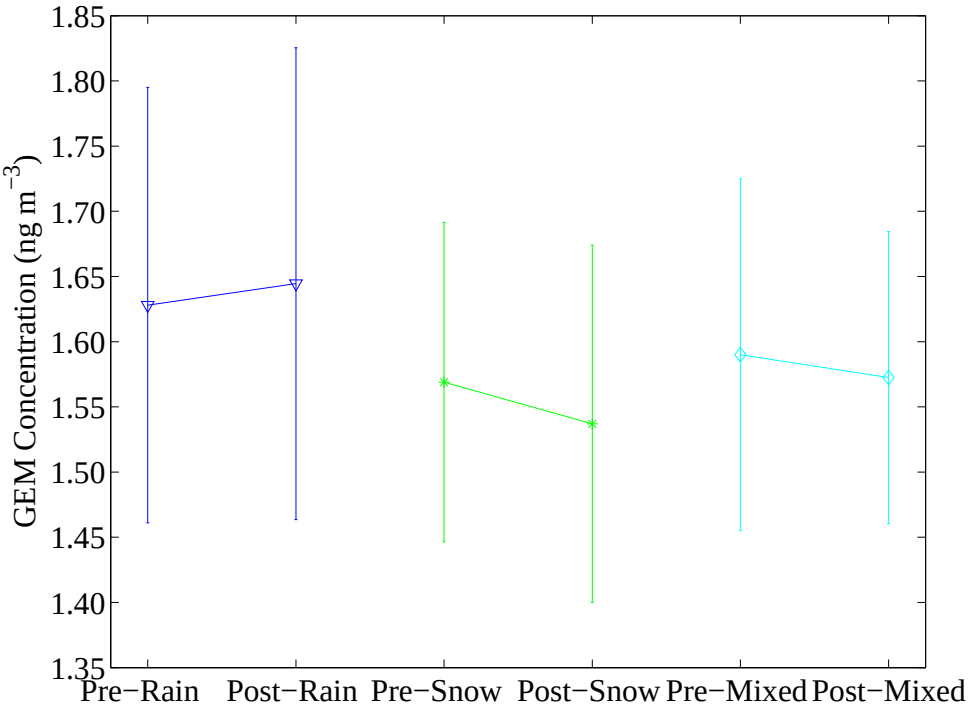

Figure 4.35: GEM precipitation scavenging for 37 separate rain events, 19 separate snow events, and 26 mixed events (24-hour timescale). Before-rain represents the median of the population of data points collected during the 24 hours preceding the rain events (301 data points). After-rain represents the median of the population of data points collected during and for 24 hours after the onset of the rain events (280 data points). Likewise for the snow and mixed events. Before-snow and after-snow data had 158 and 151 data points, respectively. Before-mixed and after-mixed data had 195 and 204 data points, respectively. Error bars are MADs.

CHAPTER 5

CONCLUSIONS

The UT96 site has the only speciated atmospheric mercury detector in continuous operation in Utah with two years of data (July 2009 – June 2011), and is, therefore, an invaluable tool for understanding mercury contamination in the region.

5.1 Temporal Variations in Mercury Concentrations

All three species of atmospheric mercury (GEM, PBM, and GOM) exhibit non-Gaussian distributions and vary over multiple orders of magnitude. Consequently, non-parametric statistics are needed to analyze the data. GEM is the dominant species, comprising 99.48% of total atmospheric mercury observed at UT96. Meanwhile, PBM and GOM comprise 0.36% and 0.16% of total atmospheric mercury, respectively. The medians (ranges) of GEM, PBM, and GOM are 1.58 $\mathrm{ng\ m^{-3}}$ (0.25-64.47 $\mathrm{ng\ m^{-3}}$), 5.7 $\mathrm{pg\ m^{-3}}$ (0.0-803.2 $\mathrm{pg\ m^{-3}}$), and 2.6 $\mathrm{pg\ m^{-3}}$ (0.0-225.6 $\mathrm{pg\ m^{-3}}$), respectively. Approximately 7% of the PBM data and ~37% of the GOM data are below the MDL. In comparison to rural Dexter, MI and urban Detroit, MI (Liu et al., 2010), UT96 can be characterized as moderately urban. UT96 is influenced by local/regional urban and industrial activities. UT96 could not be used to find background concentrations without careful consideration of wind direction and back-trajectories. Air parcels from the northeast could probably be considered background.

GEM and PBM concentrations are highest during winter, while GOM concentrations are highest during summer. High wintertime PBM could represent temperature-dependent adsorption or condensation of GEM or GOM onto atmospheric particles. It could also be re-

lated to heating activities. Wintertime temperature inversions may also trap GEM and PBM allowing mercury to accumulate. High summertime GOM could be due to photochemistry, entrainment of free tropospheric air, or conversion in a halogen-rich environment.

The diurnal patterns provide evidence of very dynamic, short-timescale processes and that all three species are impacted by meteorological variables. Both GEM and PBM concentrations tend to dip during the afternoon, while peak GOM concentrations are generally observed during the afternoon. The afternoon dips in both GEM and PBM could be due to conversions to GOM or enhanced afternoon deposition. In addition to conversion, the afternoon peaks in GOM could be due to entrainment of free tropospheric air into the boundary layer or air-surface exchange.

All three species exhibit the largest amplitude in diurnal variation during summer. GOM exhibits the weakest diurnal pattern during winter, while GEM and PBM exhibit no diurnal pattern during winter. These findings suggest that the processes that drive high winter GEM and PBM concentrations are not related to the processes that drive their diurnal patterns. Meanwhile, it is plausible that the processes that drive the seasonal and diurnal variations in GOM concentration are the same.

GEM and PBM both exhibit sporadic extremely high events suggesting the events are from local/regional sources. GOM, in contrast, exhibits extremely high events with an obvious seasonality suggesting a relationship among GOM concentrations and meteorological variables. High and low (top and bottom 0.5% of data) GEM events occur throughout the year, and occasionally within close temporal proximity. High GEM events occur throughout the day, but are least common during the afternoon, which is when low GEM events are most common. High GEM events are thought to be predominantly related to local/regional anthropogenic sources. Low GEM events are thought to be wintertime conversion of GEM to PBM and summertime conversion to GOM and subsequent deposition. Studying mercury depletion events could provide information on how mercury enters the local ecosystem where it can be methylated.

High PBM events are generally thought to be related to local/regional industrial/urban emission sources, though concentrations may also be influenced by RH. Perhaps high RH promotes adsorption of GEM and GOM onto aerosols to form PBM. More than half of all high PBM events occurred during January 2011. Perhaps this is due to inversions trapping local emissions, cold-temperature conversion of GEM and GOM to PBM, and/or an increase in local urban/industrial emissions. The high PBM event on 25 July 2011 and other elevated PBM concentration events observed following July holidays (Independence Day and Pioneer Day) are most likely due to fireworks. High GEM and PBM events may have at least some common sources. For example, four of the 14 high PBM events occurred concurrently with high GEM events, and a fifth occurred on the same day, but not concurrently.

All high GOM events occurred between May and October. Six of the 19 high GOM events occurred concurrently with low GEM events. All high GOM events were adsorbed between late morning and late afternoon (i.e., 1000 and 2000 MST). No high GOM events occurred while the RH was above 44%, and most occurred while the RH was below 30%. High GOM concentrations appear to be strongly influenced by meteorological conditions.

5.2 Effects of Precipitation on Airborne Mercury Species

GOM is scavenged by precipitation on both 2-hour and 24-hour timescales and for the data set as a whole and by season. GOM is scavenged under both damp and soggy conditions (Table 5.1). Median GOM concentrations during both damp and soggy conditions were either statistically the same or below the MDL and could not be distinguished. Similarly, GOM concentrations during different types of precipitation (rain, snow, and mixed) could not be distinguished statistically. Overall, GOM is generally well scavenged by any measurable amount of precipitation of any type, which is important because wet deposition of GOM is a pathway for atmospheric mercury to enter ecosystems where it can become methylated and cause harm.

Table 5.1: Precipitation scavenging efficiencies for atmospheric mercury.

	2-hr GOM	24-hr GOM	2-hr PBM	24-hr PBM	2-hr GEM	24-hr GEM
wet	0.7	0.6	0.6	0.3	0.0	0.0
damp	0.6	0.4	0.5	0.2	0.0	0.0
soggy	0.8	0.7	0.7	0.4	0.0	0.0
rain	0.7	0.5	0.6	0.1	-0.04	0.0
snow	0.7	0.6	0.5	0.3	0.02	0.0
mixed	0.8	0.7	0.7	0.4	0.0	0.0

PBM is scavenged by precipitation on both 2-hour and 24-hour timescales for the data set as a whole and by season. However, PBM is not scavenged as well as GOM. Scavenging of PBM increases as precipitation amount increases on both 2-hour and 24-hour timescales. Damp and soggy PBM are not scavenged as well as damp and soggy GOM, especially on 24-hour timescales (Table 5.1). While all forms of precipitation do scavenge PBM, mixed precipitation scavenges PBM most efficiently. Overall, while PBM is not scavenged by precipitation as well as GOM, wet deposition of PBM still represents an important pathway for atmospheric mercury to enter ecosystems, where it can become methylated and cause harm.

On a 2-hour timescale including two years of data, rain promotes slightly higher concentrations of GEM, while snow promotes slightly lower concentrations of GEM. This pattern also holds during winter and spring. Lindberg et al. (1999) also observed higher concentrations of GEM following a rain event and irrigation and concluded that liquid precipitation promotes mercury emissions from the soil. By the same token, perhaps snow-covered ground could inhibit emissions from soil, promoting slightly lower concentrations of GEM. Also, perhaps the cold and cloudy weather associated with rain suppresses the (assumed) GEM to GOM conversion.

5.3 Future Work

The large temporal variations in concentrations for each species suggest that all three types of mercury undergo interesting dynamics that warrant further study. This work could

be extended by analyzing GEM and PBM concentrations as functions of atmospheric stability to investigate whether high GEM and PBM concentrations are related to inversions. More generally, an in-depth analysis of the potential relationships between meteorological conditions and mercury concentrations may provide a great deal of insight into atmospheric mercury dynamics. Mercury concentrations could also be compared to concentrations of other pollutants such as particulate matter and ozone.

The analysis of diurnal patterns could be extended by analysis of the derivatives of concentrations (i.e., how the magnitude of the change in GOM concentration compares to the change in GEM and PBM concentrations). The hypothetical deposition rates that would be required to bring mass balance could be calculated, and these deposition rates could be compared to results from existing dry deposition models. Several low GEM events occurred concurrently with high GOM events. It may be worthwhile to do a more in-depth statistical analysis of GEM concentrations during elevated GOM concentrations. Two Tekran systems set up at two different elevations on a tower (i.e., 4 m and 10 m) could measure the net flux of speciated mercury to the surface. It would also be worthwhile to analyze the GOM concentrations in relation to observed entrainment rates to determine the potential significance of the free troposphere as a source of GOM to the boundary layer.

The precipitation analysis could be extended fairly easily to other locations with long-running Tekran systems as long as there is a rain gauge in close proximity. It would be interesting to break down the dry-damp-soggy analysis for PBM into finer precipitation bins and simultaneously segregate the data by precipitation type to plot scavenging efficiency as a function of precipitation amount and type. This would require a location with more precipitation than UT96 and/or a data set much longer than 2 years. It might also be interesting to combine data from different locations and calculate aggregate scavenging efficiencies, which should be quite similar to those calculated for individual locations. The precipitation analysis at UT96 could also be improved by putting a rain gauge on-site.

It may be possible to use information such as cloud height, precipitation amounts, and

scavenging efficiencies to estimate wet deposition for individual precipitation events and subsequently extend to an annual deposition. This could be compared to wet deposition measurements where Tekran systems are co-located with wet deposition measurements. This would be useful because the amount of mercury wet deposition due to GOM versus PBM could be estimated. It would also allow estimates of wet deposition in locations that have Tekran systems and no wet deposition measurements. This information could be useful for policy decisions regarding mercury emissions. In addition, this method would provide much higher temporal resolution than typical wet deposition measurements, and a net flux of mercury to the soil could be estimated for rain events.

REFERENCES

Abbott, M. L., C. J. Lin, P. Martian, and J. J. Einerson, 2008: Atmospheric mercury near Salmon Falls Creek Reservoir in southern Idaho. *Appl. Geochem.*, **23**, 438–453.

AMNet, 2011a: Amnet Standard Operating Procedures (SOPs).
URL http://nadp.sws.uiuc.edu/amn/docs.aspx

— 2011b: Map of AMNet sites.
URL http://nadp.sws.uiuc.edu/amn/

Caldwell, C. A., P. Swartzndruber, and E. Prestbo, 2006: Concentration and dry deposition of mercury species in arid south central New Mexico (2001-2002). *Environ. Sci. Technol.*, **40**, 7535–7540.

Conover, W. J., 1980: *Practical Nonparametric Statistics*. John Wiley and Sons, Inc., 2nd edition, 493 pp.

Converse, A. D., A. L. Riscassi, and T. M. Scanlon, 2010: Seasonal variability in gaseous mercury fluxes measured in a high-elevation meadow. *Atmos. Environ.*, **44**, 2176–2185, 10.1016/j.atmosenv.2010.03.024.

Engle, M. A., M. S. Gustin, F. Goff, D. A. Counce, C. J. Janik, D. Bergfeld, and J. J. Rytuba, 2006: Amospheric mercury emissions from substrates and fumaroles associated with three hydrothermal systems in the western United States. *J. Geophys. Res.*, **111**, D17304, 10.1029/2005JD006563.

Engle, M. A., M. S. Gustin, S. E. Lindberg, A. W. Gertler, and P. A. Ariya, 2005: The influence of ozone on atmospheric emissions of gaseous elemental mercury and reactive gaseous mercury from substrates. *Atmos. Environ.*, **39**, 7506–7517.

Engle, M. A., M. S. Gustin, and H. Zhang, 2001: Quantifying natural source mercury emissions from the Ivanhoe Mining Destrict, north-central Nevada, USA. *Atmos. Environ.*, **35**, 3987–3997.

EPA, 1997a: Mercury study report to Congress Volume I: Executive summary.
URL http://www.epa.gov/ttn/atw/112nmerc/volume1.pdf

— 1997b: Mercury study report to Congress Volume II: An inventory of anthropogenic mercury emissions in the United States.
URL http://www.epa.gov/ttn/oarpg/t3/reports/volume2.pdf

— 1997c: Mercury study report to Congress Volume III: Fate and transport of mercury in the environment.
URL http://www.epa.gov/ttn/atw/112nmerc/volume3.pdf

— 1997d: Mercury study report to Congress Volume VII: Characterization of human health and wildlife risks from mercury exposure in the United States.
URL http://www.epa.gov/ttn/oarpg/t3/reports/volume7.pdf

— 2011a: 2010 Advisory Listing.
URL http://water.epa.gov/scitech/swguidance/fishshellfish/fishadvisories/upload/nlfa_slides_2011.pdf

— 2011b: Controlling power plant emissions: Emissions progress. URL http://www.epa.gov/mercury/control_emissions/emissions.htm

— 2011c: TRI explorer, releases: Facility report for chlorine (Utah). URL http://www.epa.gov/tri

Ericksen, J. A., M. S. Gustin, D. E. Schorran, D. W. Johnson, S. E. Lindberg, and J. S. Coleman, 2003: Accumulation of atmospheric mercury in forest foliage. *Atmos. Environ.*, **37**, 1613–1622.

Fain, X., D. Obrist, A. G. Hallar, I. Mccubbin, and T. Rahn, 2009: High levels of reactive gaseous mercury observed at a high elevation research laboratory in the Rocky Mountains. *Atmos. Chem. Phys.*, **9**, 8049–8060.

Fitzgerald, W. F., D. R. Engstrom, R. P. Mason, and E. A. Nater, 1998: The case for atmospheric mercury contaminationin remote areas. *Environ. Sci. Technol.*, **32**, 1–7.

Friedli, H. R., L. F. Radke, J. Y. Lu, C. M. Banic, W. R. Leaitch, and J. I. MacPherson, 2003: Mercury emissions from burning biomass from temperate North American forests: laboratory and airborne measurements. *Atmos. Environ.*, **37**, 253–267.

Furl, C. V., J. A. Colman, and M. H. Bothner, 2010: Mercury sources to Lake Ozette and Lake Dickey: Highly contaminated remote coastal lakes, Washington State, USA. *Water Air Soil Pollut.*, **208**, 1–4, 10.1007/s11270-009-0165-y.

Gratz, L. E., G. J. Keeler, and E. K. Miller, 2009: Long-term relationships between mercury wet deposition and meteorology. *Atmos. Environ.*, **43**, 6218–6229.

Guentzel, J. L., W. M. Landing, G. A. Gill, and C. D. Pollman, 2001: Processes influencing rainfall deposition of mercury in florida. *Environ. Sci. Technol.*, **35**, 863–873, 10.1021/es001523.

Gustin, M. S., S. E. Lindberg, K. Austin, M. Coolbaugh, A. Vette, and H. Zhang, 2000: Assessing the contribution of natural sources to regional atmospheric mercury budgets. *Sci. Total Environ.*, **259**, 61–71.

Hájek, J., Z. Sidák, and P. Sen, 1999: *Theory of Rank Tests*. Academic Press, 2nd edition, 435 pp.

Horel, J., M. Splitt, L. Dunn, J. Pechmann, B. White, C. Ciliberti, S. Lazarus, J. Slemmer, D. Zaff, and J. Burks, 2002: MesoWest: Cooperative mesonets in the western United States. *Bull. Amer. Meteorol. Soc.*, **83**, 211–225.

Lin, C.-J., P. Pongprueska, S. E. Lindberg, S. O. Pehkonen, D. Byun, and C. Jang, 2006: Scientific uncertainties in atmospheric mercury models I: Model science evaluation. *Atmos. Environ.*, **40**, 2911–2928.

Lindberg, S., R. Bullock, R. Ebinghaus, D. Engstrom, X. Feng, W. Fitzgerald, N. Pirrone, E. Prestbo, and C. Seigneur, 2007: A synthesis of progress and uncertainties in attributing the sources of mercury in deposition. *Ambio*, **36**, 19–33.

Lindberg, S. E., H. Zhang, M. Gustin, A. Vette, F. Marsik, J. Owens, A. Casimir, R. Ebinghaus, G. Edwards, C. Fitzgerald, J. Kemp, H. H. Kock, J. London, M. Majewiski, L. Poissant, M. Pilote, P. Rasmussen, F. Schaedlich, D. Schneeberger, J. Sommar, R. Turner, D. Wallschlager, and Z. Xiao, 1999: Increases in mercury emissions from desert soils in response to rainfall and irrigation. *J. Geophys. Res.*, **104**, 21,879–21,888.

Liu, B., G. J. Keeler, J. T. Dvonch, J. A. Barres, M. M. Lynam, F. J. Marsik, and J. T. Morgan, 2010: Urban-rural differences in atmospheric mercury speciation. *Atmos. Environ.*, **44**, 2013–2023, 10.1016/j.atmosenv.2010.02.012.

Lu, J. Y. and W. H. Schroeder, 2004: Annual time-series of total filterable atmospheric mercury concentrations in the Arctic. *Tellus*, **56B**, 213–222.

Lynam, M. M. and G. J. Keeler, 2005: Automated speciated mercury measurements in Michigan. *Environ. Sci. Technol.*, **39**, 9253–9262, 10.1021/es040458r.

Mason, R. P., N. M. Lawson, and K. A. Sullivan, 1997: The concentration, speciation and sources of mercury in Chesapeake Bay precipitation. *Atmos. Environ.*, **31**, 3541–3550.

Mason, R. P. and G.-R. Sheu, 2002: Role of the ocean in the global mercury cycle. *Global Biogeochem. Cycles*, **16(4)**, 40.

MDN, 2011: Mercury Deposition Network (MDN) description.
URL `http://nadp.sws.uiuc.edu/mdn/`

Murphy, D. M., P. K. Hudson, D. S. Thomson, P. J. Sheridan, and J. C. Wilson, 2006: Observations of mercury-containing aerosols. *Environ. Sci. Technol.*, **40**, 3163–3167.

Obrist, D., E. Tas, M. Peleg, V. Matveev, X. Fain, D. Asaf, and M. Luria, 2010: Bromine-induced oxidation of mercury in the mid-latitude atmosphere. *Nature Geosci*, **4**, 22–26, 10.1038/NGEO1018.

Poissant, L., M. Pilote, C. Beauvais, P. Constant, and H. H. Zhang, 2005: A year of continuous measurements of three atmospheric mercury species (GEM, RGM and Hg_p) in southern Québec, Canada. *Atmos. Environ.*, **39**, 1275–1287.

Rasmussen, P. E., 1994: Current methods of estimating atmospheric mercury fluxes in remote areas. *Environ. Sci. Technol.*, **28**, 2233–2241.

Sakata, M. and K. Asakura, 2007: Estimating contribution of precipitation scavenging of atmospheric particulate mercury to mercury wet deposition in Japan. *Atmos. Environ.*, **41**, 1669–1680.

Schroeder, W. H. and J. Munthe, 1998: Atmospheric mercury - an overview. *Atmos. Environ.*, **32**, 809–822.

Schuster, P. F., D. P. Krabbenhoft, D. L. Naftz, L. D. Cecil, M. L. Olson, J. F. Dewild, D. D. Susong, J. R. Green, and M. L. Abbott, 2002: Atmospheric mercury deposition during the last 270 years: A glacial ice core record of natural and anthropogenic sources. *Environ. Sci. Technol.*, **36**, 2303–2310.

Seinfeld, J. H., 1986: *Atmospheric Chemistry and Physics of Air Pollution*. John Wiley and Sons, Inc., 738 pp.

Seinfeld, J. H. and S. N. Pandis, 1998: *Atmospheric Chemistry and Physics From Air Pollution to Climate Change*. John Wiley & Sons, Inc., 1326 pp.

Selin, N. E. and D. J. Jacob, 2008: Seasonal and spatial patterns of mercury wet deposition in the United States: Constraints on the contribution from North American anthropogenic sources. *Atmos. Environ.*, **42**, 5193–5204.

Selin, N. E., D. J. Jacob, R. J. Park, R. M. Yantosca, S. Strode, L. Jaegle, and D. Jaffe, 2007: Chemical cycling and deposition of atmospheric mercury: Global constraints from observations. *J. Geophys. Res.*, **112**, D02308, 10.1029/2006JD007450.

Sillman, S., F. J. Marsik, K. I. Al-Wali, G. J. Keeler, and M. S. Landis, 2007: Reactive mercury in the troposphere: Model formation and results for Florida, the northeastern United States, and the Atlantic Ocean. *J. Geophys. Res.*, **112**, D23305, 10.1029/2006JD008227.

Song, X. and B. V. Heyst, 2005: Volatilization of mercury from soils in response to simulated precipitation. *Atmos. Environ.*, **39**, 7494–7505, 10.1016/j.atmosenv.2005.07.064.

Stamenkovic, J., S. Lyman, and M. S. Gustin, 2007: Seasonal and diel variation of atmospheric mercury concentrations in the Reno (Nevada, USA) airshed. *Atmos. Environ.*, **41**, 6662–6672, 10.1016/j.atmosenv.2007.04.015.

Stutz, J., R. Ackermann, J. D. Fast, and L. Barrie, 2002: Atmospheric reactive chlorine and bromine at the Great Salt Lake, Utah. *Geophys. Res. Lett.*, **29**, 18–1 18–4.

Swartzendruber, P. C., D. A. Jaffe, E. M. Prestbo, P. Weiss-Penzias, N. E. Selin, R. Park, D. J. Jacob, S. Strode, and L. Jaegle, 2006: Observations of reactive gaseous mercury in the free troposphere at the mount bachelor observatory. *J. Geophys. Res.*, **111**, D23401, 10.1029/2006JD007415.

Tekran, 2007: *Model 2537B Ambient Mercury Vapor Analyzer User Manual*. Tekran Instruments Corporation, Rev: 3.10, 144 pp.

UDEQ, 2009: Utah: Mercury sampling sites and consumption advisories.
URL `http://www.fishadvisories.utah.gov/docs/fishsampleadvisorymap.pdf`

USGS, 1984: USGS product-satellite image report 40111 e7-si-121. *USGS*.
URL `http://ut.water.usgs.gov/greatsaltlake/`

Valente, R. J., C. Shea, K. L. Humes, and R. L. Tanner, 2007: Atmospheric mercury in the Great Smoky Mountains compared to regional and global levels. *Atmos. Environ.*, **41**, 1861–1873.

von Storch, H.: 1995, Misuses of statistical analysis in climate research. *Analysis of Climate Variability*, H. von Storch and A. Navarra, eds., Springer, 11–26.

Wang, S. X., L. Zhang, G. H. Li, Y. Wu, J. M. Hao, N. Pirrone, F. Sprovieri, and M. P. Ancora, 2010: Mercury emissions and speciation of coal-fired power plants in China. *Atmos. Chem. Phys.*, **10**, 1183–1192.

Weiss-Penzias, P., M. S. Gustin, and S. N. Lyman, 2009: Observations of speciated atmospheric mercury at three sites in Nevada: Evidence for a free tropospheric source of reactive gaseous mercury. *J. Geophys. Res.*, **114**, D14302, 10.1029/2008JD011607.

Wilks, D. S., 2006: *Statistical Methods in the Atmospheric Sciences*. Academic Press, 2nd edition, 627 pp.

Xin, M. and M. S. Gustin, 2007: Gaseous elemental mercury exchange with low mercury containing soils: Investigation of controlling factors. *Appl. Geochem.*, **22**, 1451–1466.